A Geological and Hydrogeological Study of the Shu Shu Thermal Springs, KwaZulu-Natal

By: K.R. Gravelét-Blondin

Submitted in fulfilment of the academic requirements for the degree of Master of Science in the School of Agricultural, Earth and Environmental Sciences.

University of KwaZulu-Natal
Durban
4001
South Africa

December 2013

For my father

Abstract

The Shu Shu thermal springs are located in central KwaZulu-Natal in South Africa at an altitude of 250m above mean sea level at the bottom of the Tugela Valley. They have been investigated in an attempt to ascertain whether or not they possibly share a common origin with fifteen other springs which are located in a north-northwestern trending, 1000km long zone within the eastern interior of the country. They have also been studied to establish if they potentially represent a viable and sustainable geothermal energy resource that may be developed in the future.

Isotope ratios confirm that the thermal springs are meteoric in origin, and are likely recharged within a 130km long band located to the west toward the Great South African Escarpment. These waters then descend vertically to a depth of approximately 1827m – 2153m, at which point the fractures along which they move close due to escarpment-associated confining pressure. It is a reduction in this self-same confining pressure along the coastal plain, which occurs due to the continual removal of overburden, which forces the thermal water to migrate toward the east along ever-more opening fractures. Due to a slightly elevated geothermal gradient of 3.1°C / 100m at depth, this groundwater reaches a temperature of approximately 75°C – 85°C as it traverses toward the Shu Shu thermal springs over a time period of > 61 years (at present).

The geochemical signature of the Shu Shu thermal waters is derived through leaching from the basement rocks through which they pass, with elevated concentrations of Na, K, Ca, Mg, Fe, Al, Si, F, Sr and SO_4 detected. Once below the floor of the Tugela Valley, at a depth of approximately 990m, the thermal groundwater commences its ascent, likely along the west-southwest – east-northeast orientated thrusts and associated fractures of the Tugela Terrane of the Natal Metamorphic Province. However, the thermal waters abut against those brittle structures trending north-northwest – south-southeast, which are perpendicular to the axis of least principle compressive stress, and so are ultimately forced to rise within the Shu Shu thermal springs.

Prior to surfacing, the temperatures of these waters drop to approximately 67°C as a result of natural, conductive cooling processes. However intermixing with shallow, cold groundwater, which is discernible through geochemical and isotopic variations, and atmospheric impacts, further cool the thermal waters to a surfacing temperature of approximately 50°C. Nevertheless,

a binary cycle geothermal energy power plant remains a possibility. Although thermal efficiency and volume flow rate values are favourable, heat transfer values are low and require further investigation through exploratory drilling. Nevertheless, the establishment of a 400kW power plant, should it occur, will typically be sufficient to service 625 rural homes.

Table of Contents

Appendices

List of Figures

List of Tables

Units & Applicable Abbreviations

mm	-	millimetres
m	-	metres
km	-	kilometres
amsl	-	above mean sea level
°C	-	degrees Celsius
Ma	-	million years ago
Ga		billion years ago
^{2}H	-	hydrogen-2
^{3}H	-	hydrogen-3 (tritium)
^{14}C	-	carbon-14
^{16}O	-	oxygen-16
^{18}O	-	oxygen-18
^{13}C	-	carbon-13
D (^{2}H)	-	deuterium
δ	-	deviation away from known standard
‰	-	per mil
TU	-	tritium units
PDB	-	Pee Dee Belemnite
n.d.	-	not determined
n.a.	-	not applicable
ppm	-	parts per million
mg/l	-	milligrams per litre
mWm^{-2}	-	megaWatts per square metre
kW/hr	-	kilowatt hour
rpm	-	revolutions per minute
l/sec	-	litres per second
l/hr	-	litres per hour
BDL	-	below detection limit
LOI	-	loss on ignition

Chapter 1
Introduction

1.1 Background

According to Kent (1949), a thermal spring can be defined as one whose temperature exceeds 25°C the year round, with eighty-seven known to fulfil this criterion within South Africa. The Shu Shu thermal springs are situated 111km north of Durban and 19km northeast of Kranskop in central KwaZulu-Natal (KZN). Rising at an elevation of approximately 250m amsl, the thermal springs surface at the southern edge of a permanent, vegetated sand bar in the Tugela River. Of the twenty thermal springs located within the eastern interior of the county, the Shu Shu thermal springs constitute one of sixteen located within a north-northwest trending zone which stretches from central KZN in the south, to northern Limpopo Province in the north. This 1000km long zone, which has previously been recognized, is seen to occur at an approximately constant distance of 50km – 100km west of the Lebombo 'monocline', with a structural relationship between these two features noted by Gevers (1963). This mid- to late-Jurassic structure is dominated by complex faulting and block tilting which defines the eastern edge of the Archaean Kaapvaal Craton (Du Toit, 1929; Watkeys, 2002) (see Figure 1.1). Furthermore however, the southernmost six thermal springs located within the north-northwest trending zone surface approximately 100km – 150km east of the Great South African Escarpment (see Figure 1.1). This elevated topographical feature reaches a maximum altitude much greater than that of the lower-lying coastal regions within South Africa.

Worldwide, thermal springs are concentrated in regions of volcanic activity. However, the intrusion of a 'kimberlite' pipe in Brakfontein in the Namaqualand, which occurred ~54.1Ma (Davis, 1977), remains the youngest known volcanic event in southern Africa, aside from possible incipient volcanic activity observed in Lesotho in 1983 (Hartnady, 1985). Consequently, as is stated by several authors (Rindl, 1918; Gevers, 1942; Kent, 1949; Gevers, 1963; Kent, 1969; Olivier *et al.*, 2008), the local geothermal gradient is assumed to be the heat source responsible for the elevated temperatures measured across the various thermal springs in South Africa. This can be attributed to a lack of distinct thermal regions in South Africa, such that with few exceptions, thermal springs occur intermittently across the country where annual rainfall exceeds 254mm (Kent, 1969). However, such observations infer a possibly common origin of many of the thermal springs located within the eastern interior of South Africa, and as such their spatial relation to the Lebombo 'monocline' and the Great South African Escarpment

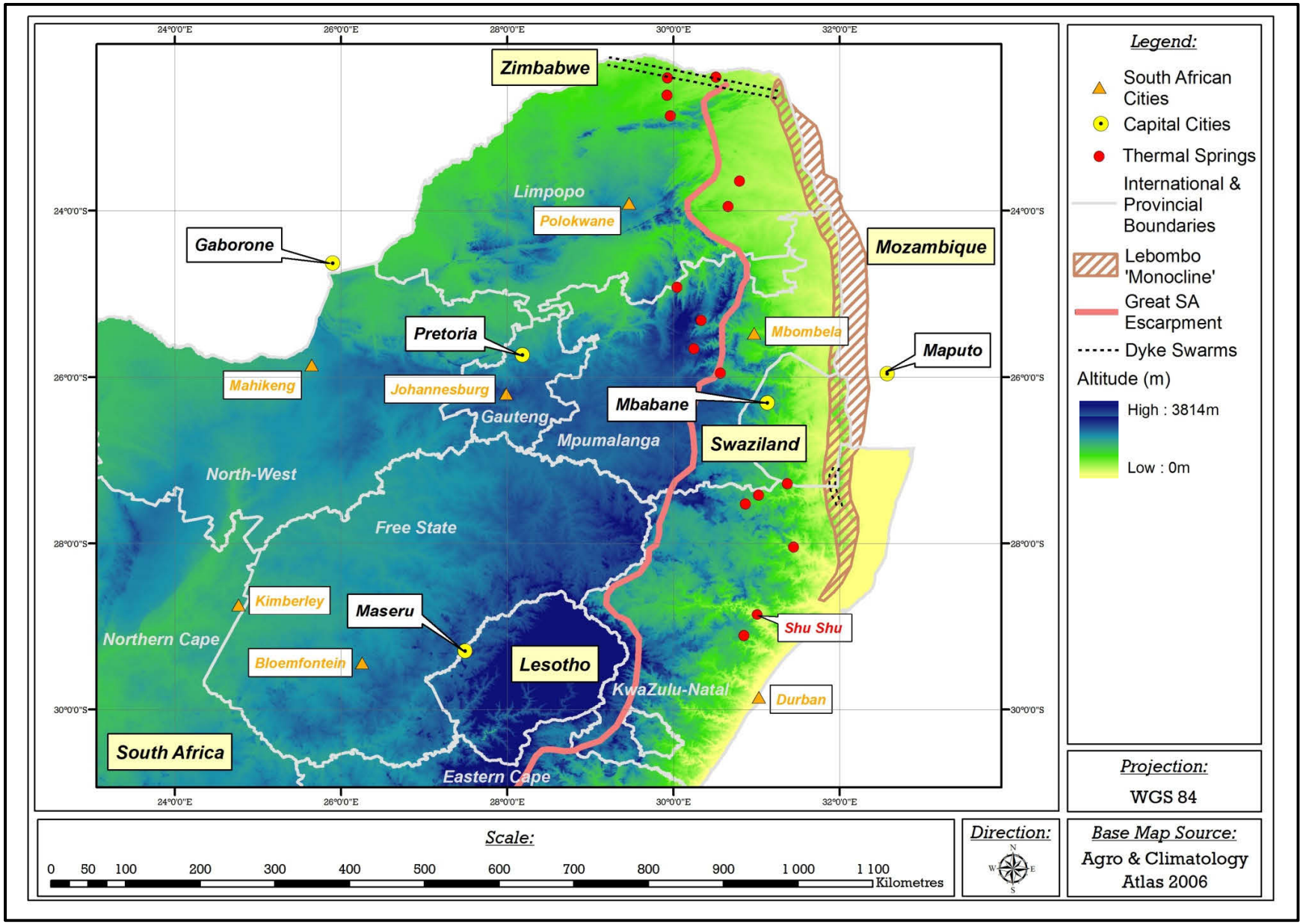

Figure 1.1: Eastern South African thermal spring localities in relation to the Lebombo 'monocline' and the Great South African Escarpment.

cannot be overlooked.

Further to their geological and hydrological importance, the commercial significance of thermal springs need also be studied, as they are natural resources that have the potential to make considerable contributions to the local and regional economy (Olivier *et al.*, 2008). According to Lund (2000), thermal springs are increasingly being employed for agriculture, aquaculture, industrial processing and rare element extraction, whilst many are already centres of hydrotherapy. However, as the supply of clean energy is a practice attaining ever-increasing importance throughout the world, continued research into thermal springs is crucial in understanding, and identifying, those areas that may potentially be exploited for geothermal energy in the future (Mock, 1993).

1.2 Objectives of Study

The main objective of this study was to explore the potential of the Shu Shu thermal springs as a viable geothermal resource that could be safely exploited in the future. This objective was accomplished through the geological and hydrogeological characterization of the thermal springs, as follows:

- Determine the pathways by which the thermal waters migrate.
- Determine the origin and hydrochemical signature of the thermal water.
- Determine the source and extent of the processes responsible for heating.
- Develop a conceptual model for the existence of the Shu Shu thermal springs.

This model needed to take into account the regional geology, including the Lebombo 'monocline' and the Great South African Escarpment.

1.3 Methodology

A summary of the measures undertaken to complete each phase of the investigation is given below, with a full description included at the end of this study in Appendix A: Methods of Investigation.

1.3.1 Desktop Study

The study commenced with the preparation of a literature review detailing the findings of an investigation into the available local geological, structural, hydrological, isotopic and geothermal

information from the Shu Shu thermal springs and the surrounding areas. The processes by which geothermal energy from continental areas can be safely exploited, were also investigated. Geological maps at scales of 1 : 250 000 and 1 : 125 000 were subsequently utilized to construct regional geological cross-sections depicting the likely orientation and location of structures and tectonic / petrological contacts beneath the Shu Shu thermal springs. The results of this analysis were used in conjunction with those of a photo-geological lineament interpretation exercise to aid in determining the principle pathways of groundwater movement beneath, and flow directions of groundwater toward, the thermal springs.

1.3.2 Geological Mapping and Geophysical Investigations

Field mapping was completed along a 1250m stretch of the Tugela River west and east of the Shu Shu thermal springs, where the underlying geological formations are best exposed. This included detailed structure mapping of selected pavements, with the results of this exercise assisting in the analysis of the brittle tectonic evolution of the region. Planar features were recorded as dip and strike using the 'right-hand rule', whereby when placing the hand on the plane, the thumb runs parallel to strike and the fingers are orientated in the direction of dip. A handheld Garmin etrex® GPS apparatus and ESRI® ArcMap™ 9.3.1 GIS software were utilized to produce a digital map of the area, depicting the location of the mapped pavements.

A geophysical investigation of the region surrounding the Shu Shu thermal springs was completed through the use of magnetic and electro-magnetic techniques. Numerous traverses were run in varying directions across the surrounding areas, with an analysis of the collected geophysical data resulting in the identification of some of the principle (water-bearing) structures in the region.

1.3.3 Water and Rock Sample Collection and Analysis

Surface water, groundwater and rainwater samples were collected from various sources surrounding / including the Shu Shu thermal springs for geochemical and environmental isotope analysis. However, the number of groundwater samples that could be collected within a 4km – 8km radius of the Shu Shu thermal springs was limited to two by the number of drilled boreholes that were equipped with operational handpumps (DWA, 2011). Physical water parameters were measured in the field using a Hanna® handheld HI9813-6 multiparameter portable meter and included the profile logging of a nearby 'thermal' borehole. This was completed through the collection of E.C. and temperature measurements every 1 m, utilising a Heron Conductivity Plµs

Level and Temperature Meter. Samples of the various rock units were collected for geochemical classification in the laboratory using major and minor oxide and trace element analysis. Furthermore, these samples were orientated in the field, thereby allowing for the preparation of orientated thin sections, and consequently the completion of a petrological analysis.

1.3.4 Report Compilation: Data Analysis and Interpretation

Measured joint readings were plotted in a structural software program, under lower hemisphere and equal area settings, whilst the collected geophysical data were plotted graphically and subsequently analysed. The results of these exercises were studied in conjunction with those of the cross-section drawings and the photo-geological lineament analysis in an attempt to investigate the tectonic events responsible for the formation of the main (groundwater-bearing) structures in the region. Together with the 'thermal' borehole profile logs, the petrological, water chemistry and environmental isotope analysis results were used to trace the horizontal and vertical movements of groundwater in the thermal spring system. These interpretations were integrated with existing data and information to produce a conceptual model explaining the origin of the Shu Shu thermal springs, and consequently an outline of the geothermal energy prospects for the future.

1.4 Previous Work

The Shu Shu thermal springs were primarily investigated by Gevers (1942) and Kent (1949), although numerous workers (Gevers, 1963; Kent, 1969; Mazor and Verhagen, 1983) have since referred to their data and interpretations. However, most information relating to Shu Shu is sought from indirect sources which detail the local geology and hydrology of the area. This is due to limited amounts of information in published literature pertaining not only to the Shu Shu thermal springs, but many thermal springs across southern Africa.

1.4.1 Local Geology

Gevers (1942) described the rocks surrounding the Shu Shu thermal springs as platy and foliated black amphibolites, composed chiefly of elongate green hornblende and plagioclase, which strike at 073° – 083° and dip at an average of 20° toward the south-southeast. Nearer the thermal springs however, a variation in fabric, metamorphic grade and mineralogy resulted in Gevers (1942) classifying the rock type as a biotite-hornblende gneiss, for which a magmatic origin was proposed. Although the prevailing lithostratigraphic nomenclature of the region has

varied since Du Toit (1931) originally classified these rocks as forming part of the Tugela Series, they are known to form part of the Mesoproterozoic Natal Metamorphic Province; a ~400km wide orogenic belt that occurs as a series of high-grade tectonometamorphic terranes (McCourt *et al.*, 2006). The location of the Shu Shu thermal springs is delineated within the river-bed by a well-developed breccia in-filled by white crystalline calcite. Gevers (1942) termed this rock type a crush-breccia, as it is composed predominantly of angular fragments of gneiss and amphibolites together with subordinate white and reddish aplite and biotite-rich granite.

Furthermore, there is evidence of mylonitisation, which is likely given that the various eyes of the Shu Shu thermal springs surface within an east-northeast trending fault which dips toward the north-northwest at a steep angle (cf. Gevers, 1942). Although the location of the springs is consistent with a mapped fault of considerable length, Gevers (1942) reported difficulty in tracing the fault zone either side of the Tugela River. However, the extent of the fault zone (which measures approximately 4.5m in width), coupled with significant amounts of crushing and mylonitisation, led Gevers (1942) to state that its formation was due to tectonic movements of considerable intensity, which resulted in this fault zone which is of substantial vertical and lateral extent.

1.4.2 Hydrology

Gevers (1942), and later Kent (1949), detail the chemical composition of the thermal waters being emitted at Shu Shu. At a reported surfacing temperature of 52°C – 53°C, and a pH of 8.2, the spring waters are dominated by the cations Na and Ca, and the anions Cl and SO_3 (SO_4) (Gevers, 1942). Furthermore, limited amounts of CO_2 and H_2S gas bubble up through the fault zone in the thermal waters. Utilising these data, Kent (1949) defines these waters as 'scalding', and characterizes the Shu Shu thermal springs as forming part of Class A according to the classification first proposed by Bond (1946). This class encompasses highly mineralised Cl–SO_4 waters, whereby TDS concentrations exceed 1000mg/l and Cl and SO_4 concentrations exceed 27% and 5% respectively thereof. Gevers (1942), and later Kent (1949), attribute the majority of the dissolved constituents in the Shu Shu thermal springs to the dissolution of various minerals in the amphibolites and gneisses through which the thermal waters move / surface. However, the dissemination of pyrite at depth is thought to account not only for the elevated levels of SO_4 in the thermal waters, but also the presence of the gases.

Gevers (1942) provides a short review of the possible source of the waters rising at Shu Shu, which he states as being meteoric. He considered rainfall falling during the summer months atop the adjacent plateau responsible for the waters which surface in the springs. This notion is partially furthered upon by Mazor and Verhagen (1983), who undertook a country-wide investigation into the stable and radiogenic isotope signatures, and the noble gas concentrations, of sixteen thermal springs. Although the Shu Shu thermal springs did not form part of this study, Mazor and Verhagen (1983) infer that their findings are representative of prevailing conditions in South Africa. Not only do noble gas concentrations suggest a clear dependence on climatic source factors, but stable isotope data indicate direct recharge. Further to this, there is no relationship in existence between the waters which rise in these thermal springs and the rivers adjacent to / in which they surface. Mazor and Verhagen (1983) finally conclude by stating that radiogenic isotope data define residence times in excess of 50 years, although the sub-recent admixture of recent waters occurs on occasion.

1.4.3 *Thermal Spring Origins*

Numerous authors (Rindl, 1918; Gevers, 1942, Kent, 1949; Gevers, 1963; Kent, 1969, Temperley, 1975; Hoffmann, 1979, Mazor and Verhagen, 1983; Olivier *et al.*, 2008 and others); attribute the origin of the thermal springs in southern Africa to the natural geothermal gradient, whereby depth descent of rainwater ultimately increases the temperature of the groundwater into either the warm (25°C – 37°C), hot (37°C – 50°C) or scalding (>50°C) classes as defined by Kent (1949). This theory was expanded upon by Gevers (1942), who calculated that rainwater descending through the sandstones of the Natal Group atop the adjacent plateau, and the underlying rocks of the Natal Metamorphic Province, ultimately reaches the temperatures measured in the Shu Shu thermal springs, as a result of the natural geothermal gradient. Although limited information exists on such a topic, Jones (1992a) did identify a slightly elevated heat flow anomaly to the north-west of Shu Shu, whilst in certain regions of southern Africa, areas of elevated heat flow are marked by a limited increase in the number of thermal springs.

Although the existence of the thermal spring zone, in relation to the Lebombo ‘monocline’, has been referred to by various workers, none are known to have investigated it further. Consequently, should a relationship exist between this feature and the Shu Shu thermal springs, possible details thereof remain unknown.

Chapter 2

Geological, Hydrogeological and Geothermal Setting

An assessment of published work detailing thermal spring systems across the World reveals that three principle components are required for thermal spring existence. These components typically differ when assessing the geological systems in which they surface, as is detailed graphically in Figure 2.1.

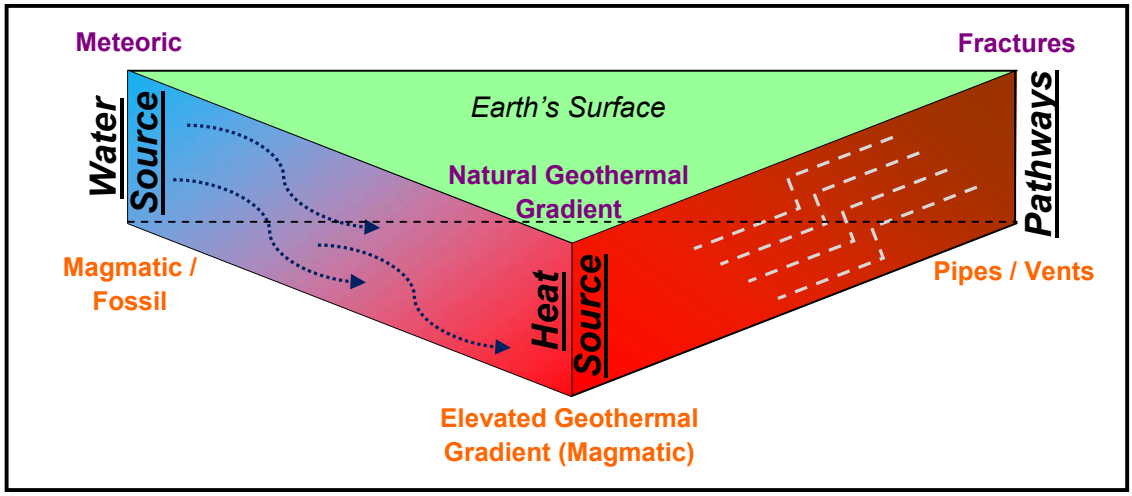

Figure 2.1: Conceptual model linking principle components of thermal springs (water source, heat source and pathways) in different geological systems.

However, the consistency of such geological systems is theoretical, as the majority of thermal springs cannot be defined as having a purely volcanic or meteoric origin, as is differentiated above. This is most commonly illustrated through an examination of continental rift thermal springs, as although a magmatic heat source may be in existence, water is sourced through precipitation, whilst various extensional structures provide a depth-to-surface flowpath.

A brief review of the geological, hydrogeological and geothermal setting of the Shu Shu thermal springs not only aides in identifying the various components which define this system, but furthermore allows for their detailed characterisation.

2.1 Geological Evolution

The geological and structural evolution of the region surrounding the Shu Shu thermal springs, according to published literature is detailed hereafter. Such an exercise typically allows for an

initial assessment of the possible groundwater quality at Shu Shu, and the pathways by which it surfaces.

2.1.1 Local Geology

The Natal Metamorphic Province lies adjacent to the south-eastern margin of the Kaapvaal Craton and embodies entirely juvenile crust which was extracted from the mantle after ~1.5 Ga (Eglington *et al.*, 1989). It is subdivided (from north to south) into the Tugela, Mzumbe and Margate Terranes, with the Shu Shu thermal springs situated in the former (Matthews and Charlesworth, 1981). The Tugela Terrane comprises rocks at amphibolite and greenschist facies and is divisible in four tectonostratigraphic packages: the Tugela, Mandleni, Madidima and Nkomo thrust sheets.

The Shu Shu thermal springs are located in rocks that together comprise the Mandleni thrust sheet (Matthews and Charlesworth, 1981) (see Figure 2.2). McCourt *et al*. (2006) state that there are four mappable units which comprise this tectonostratigraphic unit; the Dondwana gneiss unit, the Evuleka ultramafic unit, the Mtungweni granitoid unit and the Mambula Complex. The thermal springs are located within 'Wosi' amphibolite (as it has historically been known), which together with a feldspathic gneiss, comprise the Dondwana gneiss unit (Johnston *et al*., 2003). Three varieties of amphibolite are recognized: blue-green hornblende amphibolite, diopside amphibolite and epidote amphibolite (McCourt *et al*., 2006). Although the former is the most abundant, migmatite is commonly associated with the diopside amphibolite (Johnston *et al*., 2003). The felsic component of the Dondwana gneiss unit is a variably foliated, feldspar-rich, homogenous rock of quartz-monzonite to granodioritic composition (McCourt *et al*., 2006). It has been suggested that this feldspathitic gneiss is derived from an igneous protolith, and together with the 'Wosi' amphibolite unit, represents a deformed and metamorphosed bimodal magmatic series formed in an intraplate, oceanic island setting (Arima *et al*., 2001).

2.1.2 Tectonic Setting

The formation of the Natal Metamorphic Province represents the earliest possible tectonic / formation event that could have resulted in the structures evident in the region surrounding the Shu Shu thermal springs. McCourt *et al*. (2006) state that three distinct planar fabrics (S_{1-3}) have been indentified within the Tugela, Mandleni and Madidima thrust sheets. According to Johnston *et al*. (2003), these developed during progressive north-verging deformation and syn-

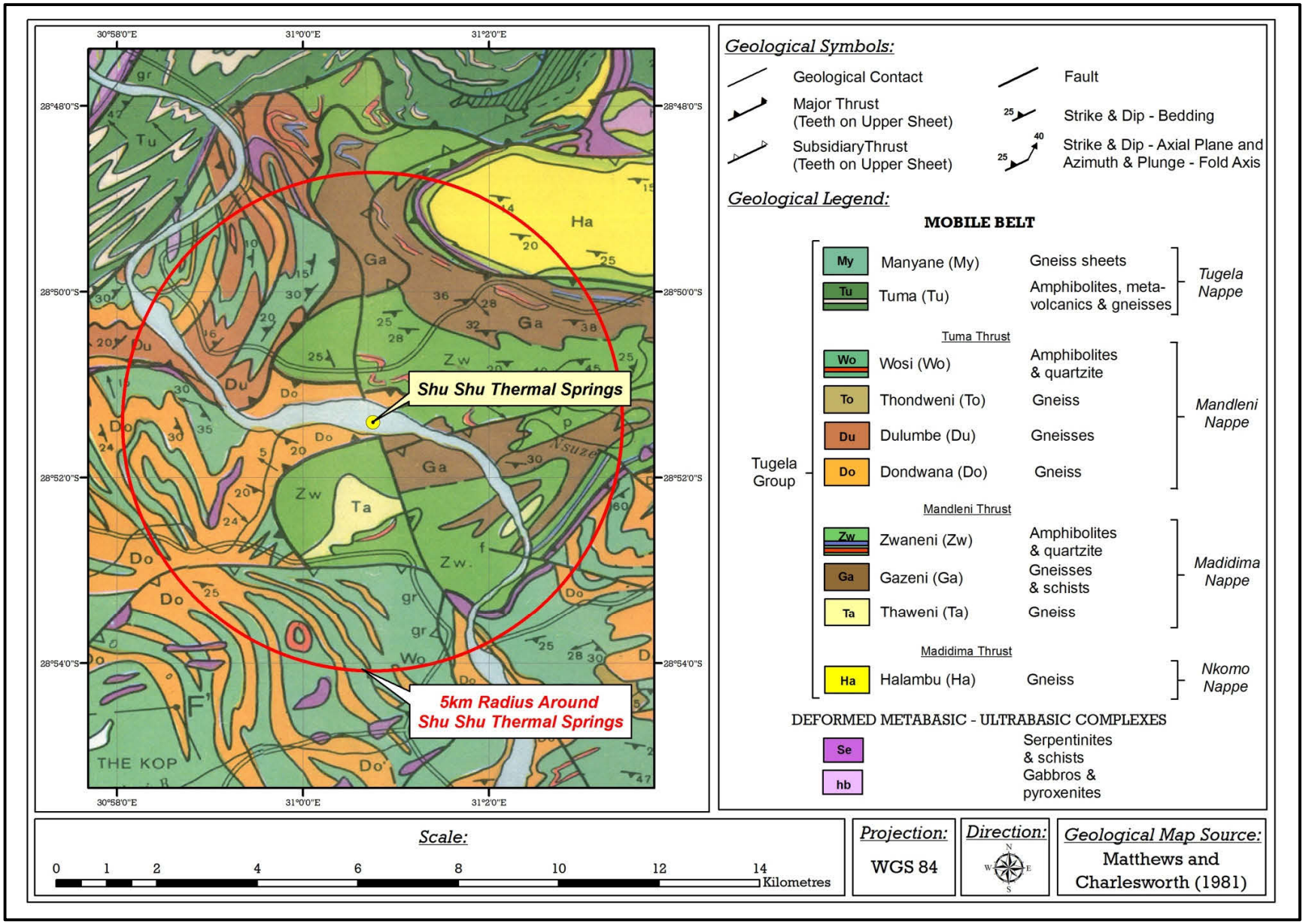

Figure 2.2: Regional geological map of the area surrounding the Shu Shu thermal springs (after Matthews and Charlesworth, 1981).

kinematic metamorphism and are attributable to two discrete events. These events were responsible for the accretion of a composite arc terrane (which developed in response to Mesoproterozoic oceanic-arc tectonics) onto the continental margin of the Kaapvaal Craton (McCourt *et al.*, 2006). Four known deformation events (D_{1-4}), which formed part of the two accretion events, were ultimately responsible for the development of the fold and thrust structures in the region described by Johnston *et al*. (2003) and McCourt *et al*. (2006) (see Figure 2.3). Although it is acknowledged that these structures may act as preferential pathways for the movement of groundwater, associated faults and later faulting are likely responsible for movement of similar volumes (Sami *et al.*, 2002).

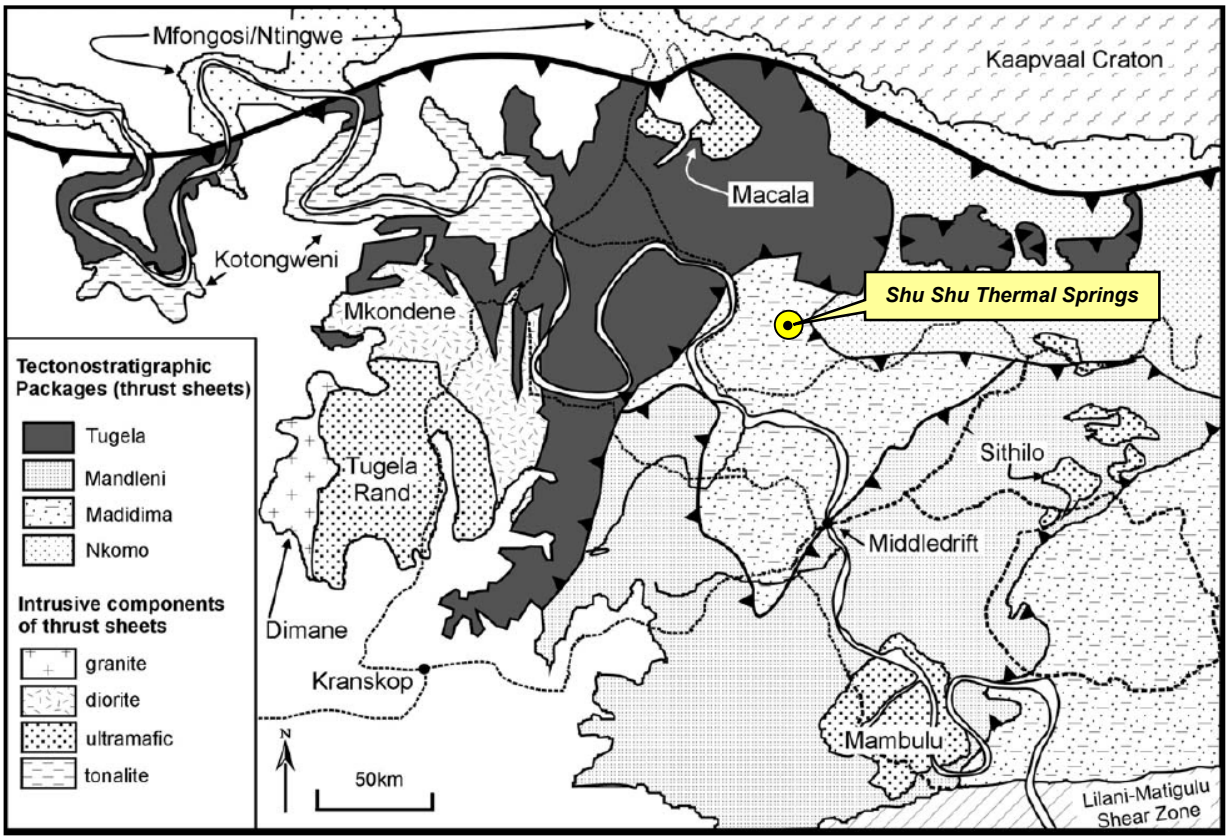

Figure 2.3: Simplified geological map of the Tugela Terrane showing the distribution of the tectonostratigraphic packages and their associated intrusions (McCourt *et al*. (2006) after Matthews and Charlesworth (1981)).

The greater study area, which includes the south-eastern margin of South Africa, coincides with a region of complex faulting which is associated with crustal extension that is related to the Mesozoic breakup of the Gondwana (Watkeys and Sokoutis, 1998). This faulting is best explained through Watkeys' (2002) five stage model describing the breakup of Gondwana,

which accounts for the three principle fault directions that are observed in the greater region as a result of Mesozoic tectonics. These are north – south, east-northeast – west-southwest and north-northeast – south-southwest, and it is their interaction with the northwest – southeast and east-northeast – west-southwest fractures that is of importance when assessing groundwater movement in relation to the Lebombo 'monocline' and the Great South African Escarpment.

The tectonic history and deformation events which resulted in the structures forming in the afore-mentioned orientations are summarized in Table 2.1.

Table 2.1: Summary of the structural events that may have affected the region around the Shu Shu thermal springs (from references in text).

Eon	Age (Ma)	Stratigraphic Unit	Event	Principle Structures	Principle Structure Orientations		
					Extension	Intermediate*	Compression
Phanerozoic			Mid-Cretaceous extraction of the Falkland Plateau from the Natal Valley	Normal faults / strike-slip faults	east-southeast – west-northwest	north-northeast – south-southwest	
	175		Cretaceous break-up separating east and west Gondwana	(Reactivation of pre-existing structures)	north – south & north-northeast – south-southwest	west-southwest – east-northeast	
	300	Karoo Supergroup	Jurassic-Cretaceous fracturing of south-eastern Gondwana associated with Karoo volcanism	Normal faults / strike-slip faults / (reactivation of pre-existing structures)	north – south & north-northeast – south-southwest	west-southwest – east-northeast	
	Unconformity						
	490	Natal Group					
	Unconformity						
Proterozoic	1000	Natal Metamorphic Province (Tugela Terrane)	Uplift tectonics – emplacement of Tugela Terrane onto the margin of the Kaapvaal Craton	D_3 late-stage north verging folds (overthrusting), reactivation / basement control and faults			east-northeast – west-southwest
				D_3 early-stage north-east verging asymmetric folds and faults			north-west – south-east
			Accretion tectonics – crustal thickening and formation of regional deformation fabrics (S_2)	D_2 isoclinal folds (transposition of older contacts)	Unknown		

* Strike-slip movement

Magnetic and electro-magnetic geophysical techniques are often used in South Africa to identify water-bearing structures. Although this type of investigation may be better suited to identifying ore bodies, weathered dolerite contacts and mineralised fracture zones have frequently been delineated through the use of these geophysical techniques. Geomeasure Group (2001), who undertook a geophysical investigation in the vicinity of the Shu Shu thermal springs, identified and confirmed the position of the north-northwest – south-southeast fault passing through the site, which is visible in Figure 2.2. These fractures are considered the principle pathways by which thermal water moves toward the Shu Shu thermal springs, as no recent (<50 Ma) volcanic activity has occurred in southern Africa.

2.2 Hydrogeological Review

The hydrochemical and isotopic signatures of the Shu Shu thermal waters and water sources in the region from published literature are detailed hereafter. Such an exercise typically allows for an initial assessment of the possible source area of the groundwater surfacing at Shu Shu to be made, and by extension, possible maximum depths to which the water descends.

2.2.1 Hydrochemistry

Reporting on the chemical quality (and isotopic signatures) of all groundwater and surface water sources in the vicinity of a thermal spring system is typical, as is undertaken by numerous workers (Mazor and Verhagen, 1983; El-Fiky, 2009; Taran and Peiffer, 2009; Mohammadi *et al*., 2010 as examples). This practice assists in determining if any relationship is in existence between the thermal spring waters, and other ground- or surface waters, which may otherwise alter the hydrochemical and isotopic signatures of a thermal spring. If this is found to be so, calculations based upon this data may need to be assessed further and varied accordingly.

The available hydrochemical and physical data of the Shu Shu thermal springs, and of shallow groundwater in the immediate vicinity, is shown in Table 2.2. However, there are no published water quality data from the Tugela River in the vicinity of the thermal springs.

It must be noted, when assessing the data included in Table 2.2, that the various water samples were analysed 59 years apart. There are hence likely to be laboratory-attributable and methodology-attributable variations, which may account for some of the deviations observed in the data set.

Table 2.2: Hydrochemical and physical data of various Shu Shu water sources.

Determinant	Unit	Shu Shu Thermal Springs[1]	Shu Shu Shallow Groundwater[2]
Temperature	°C	52 – 53	n.d.
pH	pH units	8.2	7.45
E.C.	mS/m	n.d.	n.d.
T.D.S.	mg/l	988.4	n.d.
Na	mg/l	311.9	270
K	mg/l	10.2	n.d.
Ca	mg/l	115.9	80
Mg	mg/l	11.8	30
Fe	mg/l	1.1	1.12
Al	mg/l	10	n.d.
F	mg/l	n.d.	6.6
Cl	mg/l	188	243
SO_3	mg/l	321.5	n.d.
SO_4	mg/l	n.d.	423
CO_2	mg/l	24.6	n.d.
CO_3	mg/l	n.d.	323
HCO_3	mg/l	n.d.	128
P_2O_5	mg/l	2.6	n.d.
SiO_2	mg/l	56.6	n.d.
H_2S	mg/l	0.07	n.d.

[1] Source: Gevers (1942)

[2] Source: Geomeasure Group (2001)

The similarity in the hydrochemical signatures of these two groundwater sources is depicted graphically in Figure 2.4. Due to the availability of data, this Schoeller (1962) diagram plots the concentrations of Ca, Mg, Na (+K) and Cl. As can be seen, although slight variations are in evidence, a similar hydrochemical pattern is observed between the two groundwater sources. Gevers (1942) directly attributes the concentrations of the various dissolved constituents in the Shu Shu thermal waters to the rocks through which they migrate, and hence a similar water type may be expected for shallow groundwater in the region. However, comparable levels of the dissolved constituents is possibly unexpected, given the decreased residence times and circulation depths of shallow groundwater.

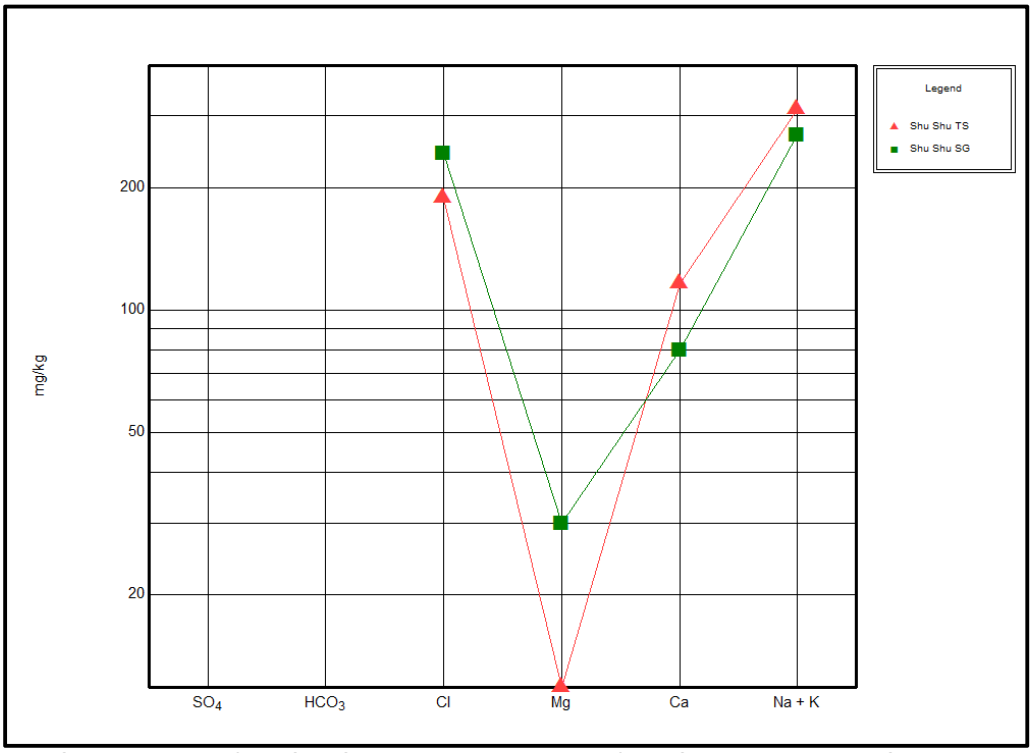

Figure 2.4: Schoeller plot of the Shu Shu water sources (data from Gevers (1942) and Geomeasure Group (2001)).

2.2.2 Isotopic Data and Analysis

In thermal spring investigations, stable isotopes (^{2}H and ^{18}O) are used for climate reconstruction and flow system tracing, whilst radiogenic isotopes (^{3}H and ^{14}C) are used for age-dating (Schwartz and Zhang, 2003). Geographical and climatic processes that may have affected the thermal waters (assuming they are meteoric in origin) can often be identified through the positioning of sample data in relation to Craig's (1961) Global Meteoric Water Line (GMWL), and a Local Meteoric Water Line (LMWL), if available. These are known as the continental (distance from coast) effect, the altitude effect and the latitude effect, whereby an increase in each typically results in a depletion of the heavier oxygen isotope (^{18}O) in water. Such a variation will also transpire when condensation occurs at lower temperatures (Schwartz and Zhang, 2003). The changes in the stable isotope ratio of meteoric water resulting from these effects are depicted graphically in Figure 2.5.

Radiogenic (^{3}H and ^{14}C) isotope data cannot easily be used to calculate the absolute age of water, due to an uncertainty in original atmospheric loading and interference processes

respectively. Consequently, these isotopes are often applied only as a means of determining relative age (Schwartz and Zhang, 2003).

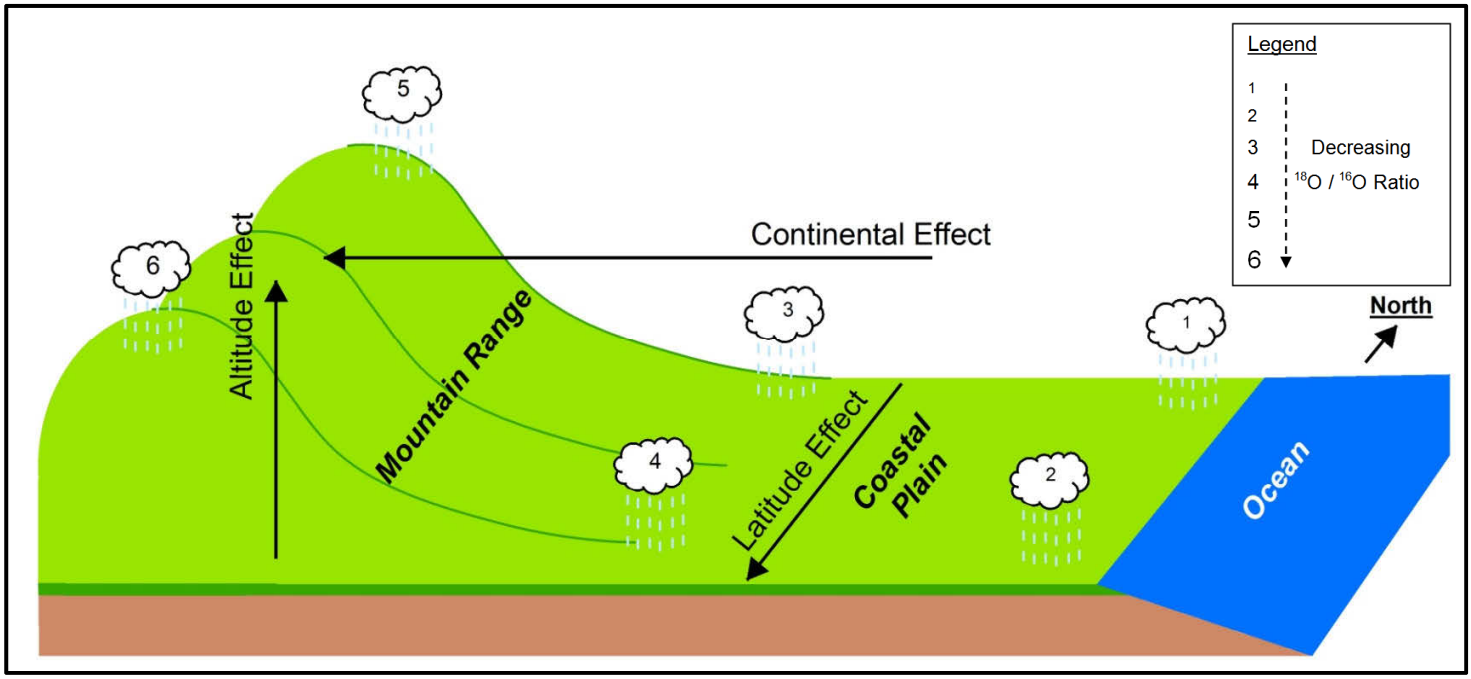

Figure 2.5: Variations in ^{18}O values due to geographic and climatic processes prior to circulation (number size denotes degree of effect).

The preeminent South African thermal springs study undertaken by Mazor and Verhagen (1983) did not include those located at Shu Shu. Only the Natal Spa and Lilani thermal springs were considered in KZN, and deemed to be of meteoric origin. The full data set includes records from five of the sixteen thermal springs located within the north-northwest trending zone, and from a limited number of the remaining central South African thermal springs. The locations and approximate altitudes of these thermal springs are shown on Figure 2.6, whilst Figure 2.7 plots published ^{2}H data vs. corresponding ^{18}O data.

The available data comprise two distinct zones, encircled in solid orange and dot-dash green ellipses respectively, with that of the former encompassing those thermal springs whose water shows increased ^{18}O depletion. These thermal springs are typically located slightly further inland and / or up on the Great South African Escarpment, and so clearly reflect the effects of either the altitude or continental processes, or possibly both. The waters from those thermal springs that plot within the dashed black ellipses, and so near the regional LMWL (as

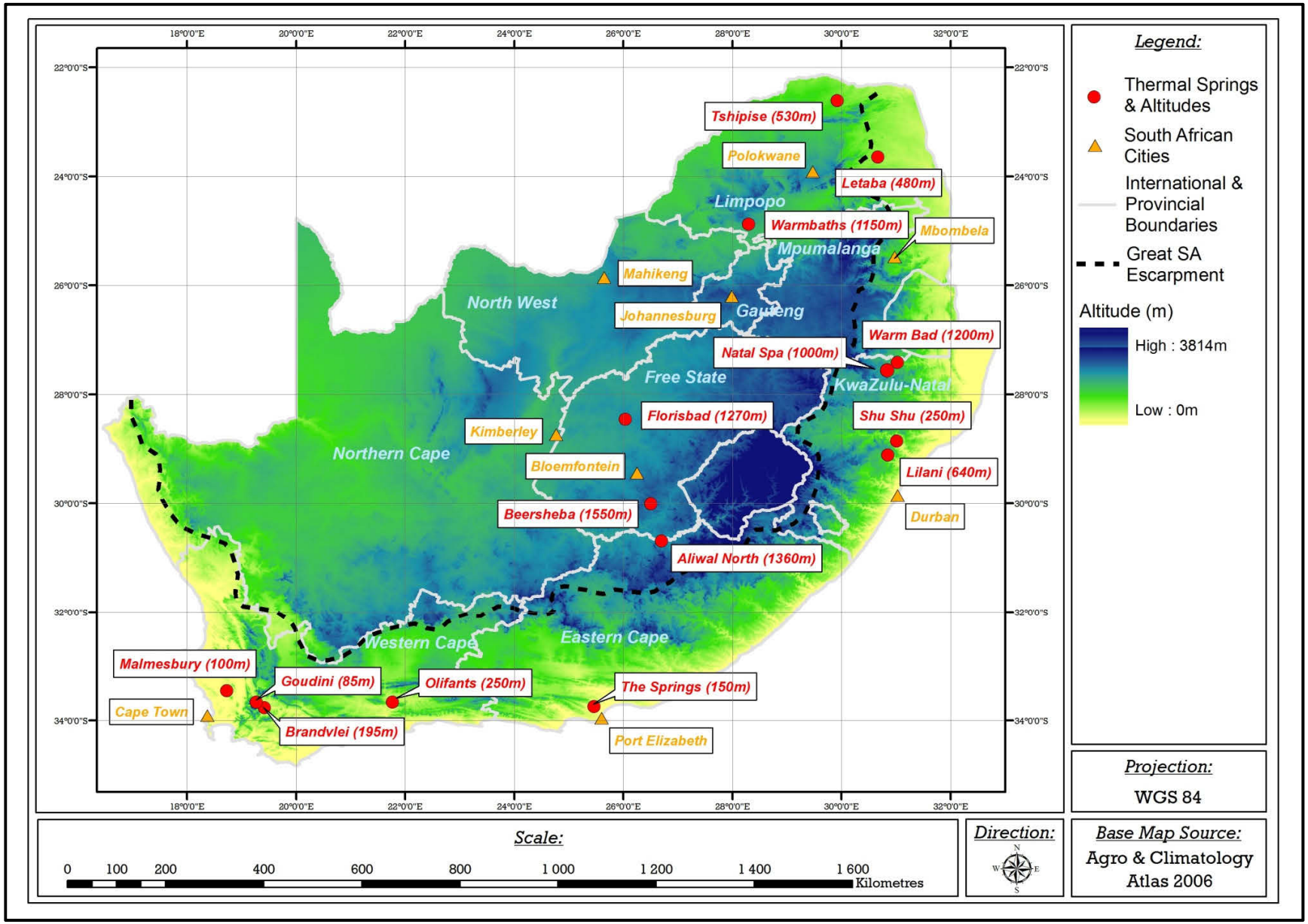

Figure 2.6: South African thermal springs and altitudes correlating to Mazor & Verhagen (1983) isotope data (note that original names have been used to allow for comparison).

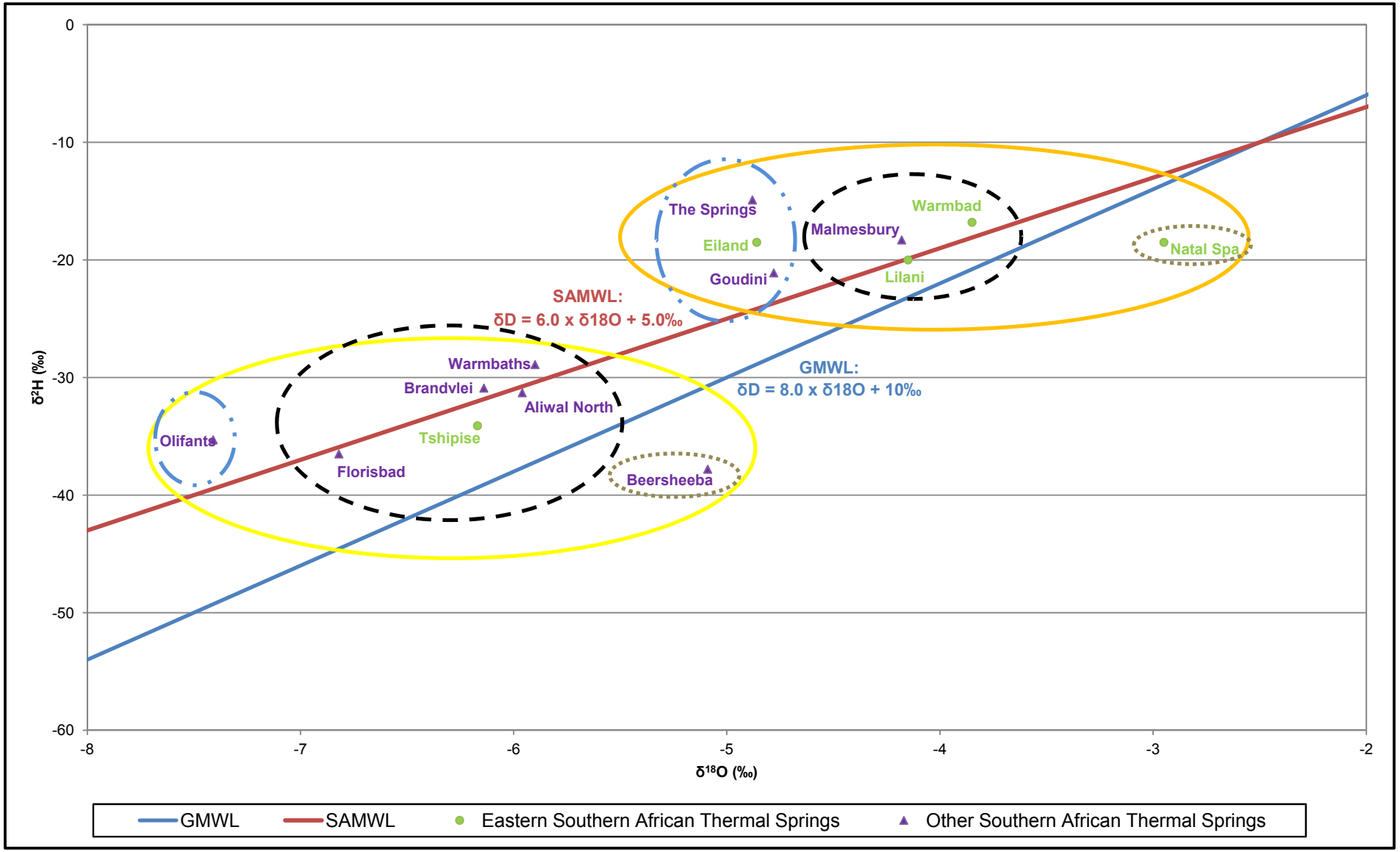

Figure 2.7: South African thermal spring data vs. the Global Meteoric Water Line (GMWL) and the South African Meteoric Water Line (SAMWL) (thermal spring data from Mazor and Verhagen, 1983).

determined from data collected in Pretoria, and hence termed the South African Meteoric Water Line (SAMWL)), typically indicate direct meteoric recharge, with little or no secondary effects. As a direct meteoric recharge comparison is made by Gevers (1963; 1942) between the Lilani and Shu Shu thermal springs, the location of the former on the graph implies the latter is recharged directly by rainfall. This is in contrast to the waters which are encircled in the dot-dot-dash blue and dotted gold ellipses, with their deviation away from the meteoric water lines indicative of active secondary sub-surface processes. The isotopic deviation model as detailed by Schwartz and Zhang (2003) implies that silicate-hydration / hydrogen sulphide interaction has affected the former, and evaporation from an open source / exchange with rock minerals the latter.

2.3 Heat Source

Indirect methods, which often incorporate the analysis of intrinsic thermal water data, offer alternative techniques that may assist in determining the heat source driving thermal spring systems, especially if data pertaining to the magnitude of heat in the upper crust are not in existence.

2.3.1 Geophysical Analysis

The heat flow ability of basement rock in the regions surrounding thermal springs is of critical importance. Jones (1992b) states that terrestrial heat flow can simply be defined as the outward flow of heat, normally through conduction from the Earth's interior, and is determined through the use of the following equation:

$$\mathrm{q} = -\mathrm{K}\frac{d\mathrm{T}}{d\mathrm{Z}} \qquad \text{Eq. (2.1)}$$

Where:

q – heat flow
*d*T/*dz* – vertical temperature gradient near surface (kelvin / 1000 metres)
K – thermal conductivity (watts / metre / kelvin)

As is evident, higher heat flows (q) are directly related to higher geothermal gradients (*d*T/*dz*). Although a distinct correlation is not observed between the locations of five of Kent's (1949) six scalding thermal springs and the areas of elevated heat flow in South Africa, three hot thermal springs are located near the highest known heat flow value of 81mWm^{-2}. This heat flow value was measured in the Namaqua sector of the Namaqua-Natal Metamorphic Province (Jones,

1992b). Furthermore, Jones (1992a) infers that a heat flow value of 80mWm^{-2} is in existence along the southern margin of the Kaapvaal Craton where it abuts against the Natal Sector of the Natal Metamorphic Province, near the Shu Shu thermal springs. The use of a thermal conductivity value of 2.61Wm^{-1}K^{-1} (Kukkonen *et al*., 2001), obtained from a gneiss in a similar geological setting in Sweden, and which is conservative according to the approximate gneiss range (2Wm^{-1}K^{-1} – 7Wm^{-1}K^{-1}) provided by Kappelmeyer and Haenel (1974), in this equation, yields an estimated geothermal gradient of 3.1°C / 100m.

2.3.2 Water Isotope Data and Analysis

An assessment of ^{13}C stable isotope data is often used in an attempt to determine the source of heat driving thermal spring systems. According to Özgür (2003), the amount of ^{13}C in thermal waters is directly related to the source of CO_2, for which four possibilities are given (see Table 2.3).

Table 2.3: CO_2 sources in thermal waters according to ^{13}C values (Özgür (2003)).

CO_2 Source	$\delta^{13}C$ (‰) (PDB)
Production by the reaction of carbonate rocks	± -3.3 to 2.0
Magmatic origin	± -3.7 to -5.5
Mantle-derived	± -5.5 to -8.5
Exchange with organic carbon	± -8.5 to -14.0

$\delta^{13}C$ data that fall outside the ± -3.7 ‰ to -8.5 ‰ range likely infers that the surfacing waters are heated through the natural geothermal gradient, owing to the source of the surfacing CO_2. Of the seven thermal springs for which Mazor and Verhagen (1983) supply relevant information, ^{13}C data for six fall between -16.6 ‰ ± 0.2 ‰ to -24.5 ‰ ± 0.2 ‰, thereby suggesting CO_2 that has originated by exchange with organic carbon (typically decayed vegetation). However, no data are supplied for thermal springs located within the north-northwest trending zone parallel to the Lebombo 'monocline' and Great South African Escarpment.

2.3.3 Hydrochemical / Physical Water Data Analysis

Assessments of hydrochemical and physical water data from thermal springs are undertaken in an effort to determine the maximum reservoir temperature, and the approximate depth of circulation, through indirect methods. These methodologies are based upon the natural geothermal gradient being accepted as the source of heat, as they are typically not accurate if a magmatic or mantle-derived origin is implied.

Mazor (1991) provides an equation, which incorporates the emergence temperature of a thermal spring ($T_{measured}$), the local average annual surface temperature ($T_{surface}$) and the observed geothermal gradient ($\Delta\ T\ /\ 100$), to estimate the depth of circulation. This is based upon the principle that the circulating groundwater will approximate the temperature of the wall rock that it comes into contact with. Gevers (1942) originally utilised this geothermal gradient-based methodology in an attempt to explain the source of the Shu Shu thermal springs. This is supported by the work of Jones (1992b), who identified a heat-flow anomaly below Lesotho which likely accounts for slightly elevated geothermal gradients in the region as compared to those typically observed within the Kaapvaal Craton. The geothermal gradient calculated above (3.1°C / 100m) yields a depth of circulation of ~1093m when utilising an average annual surface temperature of 19°C (Agricultural Research Council, 2010) in Equation 2.2:

$$depth\ (m) = \frac{Tmeasured - Tsurface}{\Delta\ \mathrm{T}/\ 100} \qquad \text{Eq. (2.2)}$$

Mazor (1991) states that such depths are likely approximate and conservative because cooling upon ascent or any other active hydrogeological processes are not considered by Equation 2.2.

Other methodologies utilized to determine the maximum reservoir temperature which may incorporate variations in thermal waters upon ascent and are based upon hydrochemical data, including traditional chemical geothermometers. These have commonly been used for calculating subsurface temperatures of geothermal systems for the purposes of exploitation and exploration (Santoyo and Díaz-González, 2010). Chemical geothermometers incorporate various equations which were developed on the assumption that although the absolute concentrations of different hydrochemical parameters may vary upon ascension to the surface, their ratio will not, as the specific mineral – solute reactions are typically slow to re-equilibrate at cooler temperatures (Karingithi, 2009). Consequently, a number of authors proposed varying equations, developed for specific geological and hydrogeological settings, that are based upon the levels of major cations (Na / K / Mg / Ca), or the concentrations of various silica minerals (quartz / chalcedony / amorphous silica) in the thermal waters. Although numerous geothermometer equations may be utilized, the results are subject to interpretation as over- or under-estimated maximum reservoir temperatures are likely depending upon the geological setting and geochemical processes (Allen *et al*., 2006). This is due to every geothermometer having its limitations (Karingithi, 2009), whilst conductive heat loss and hydrostatic head boiling need to be considered.

The primarily-used traditional geothermometers, which are labelled as Equation 2.3 – Equation 2.19, are given in Table 2.4:

Table 2.4: Various geothermometer equations employed to determine maximum reservoir temperatures (determinant units in mg/l unless specified).

Name and Reference	Chemical Geothermometer (°C)	Equation No.
Quartz Truesdell and Fournier (1976)	$T_{SiO2} = \frac{1315}{5.205 - \log m} - 273.15$	Eq. (2.3)
(1) Quartz Fournier (1977)	$T_{SiO2} = \frac{1522}{5.75 - \log m} - 273.15$	Eq. (2.4)
(2) Quartz Fournier (1977)	$T_{SiO2} = \frac{1309}{5.19 - \log m} - 273.15$	Eq. (2.5)
Chalcedony Arnorsson *et al.* (1983)	$T_{SiO2} = \frac{1112}{4.91 - \log m} - 273.15$	Eq. (2.6)
Amorphous Silica Fournier (1977)	$T_{SiO2} = \frac{731}{4.52 - \log m} - 273.15$	Eq. (2.7)
Chalcedony Fournier (1977)	$T_{SiO2} = \frac{1032}{4.62 - \log m} - 273.15$	Eq. (2.8)
Na-K Truesdell (1976)	$T_{Na/K} = \frac{856}{\log\left(\frac{Na}{K}\right) + 0.857} - 273.15$	Eq. (2.9)
Na-K Fournier (1979)	$T_{Na/K} = \frac{1217}{\log\left(\frac{Na}{K}\right) + 1.483} - 273.15$	Eq. (2.10)
Na-K Arnorsson *et al.* (1983)	$T_{Na/K} = \frac{933}{\log\left(\frac{Na}{K}\right) + 0.993} - 273.15$	Eq. (2.11)
Na-K Giggenbach (1988)	$T_{Na/K} = \frac{1390}{\log\left(\frac{Na}{K}\right) + 1.750} - 273.15$	Eq. (2.12)
Na-K Verma and Santoyo (1997)	$T_{Na/K} = \frac{1289}{\log\left(\frac{Na}{K}\right) + 1.615} - 273.15$	Eq. (2.13)
Na-K Santoyo and Díaz-González (2010)	$T_{Na/K} = \frac{876.3\ (\pm 26.26)}{\log\left(\frac{Na}{K}\right) + 0.8775\ (\pm 0.0508)} - 273.15$	Eq. (2.14)
Na-K-Ca Fournier and Truesdell (1973)	$T_{Na/K/Ca} = \frac{1647}{\log\left(\frac{Na}{K}\right) + \beta[\log\left(\frac{\sqrt{Ca}}{Na}\right) + 2.06] + 2.47} - 273.15$	Eq. (2.15)
K-Mg Giggenbach (1988)	$T_{K/Mg} = \frac{4410}{\log\left(\frac{K}{\sqrt{Mg}}\right) + 14.00} - 273.15$	Eq. (2.16)
Na-Li Kharaka *et al.* (1982)	$T_{Na/Li} = \frac{1590}{\log\left(\frac{Na}{Li}\right) + 0.779} - 273.15$	Eq. (2.17)
Na-Li Verma and Santoyo (1997)[1]	$T_{Na/Li} = \frac{1049}{\log\left(\frac{Na}{Li}\right) + 0.440} - 273.15$	Eq. (2.18)
Mg-Li Kharaka and Mariner (1989)	$T_{Mg/Li} = \frac{2200}{\log\left(\frac{Li}{\sqrt{Mg}}\right) + 5.470} - 273.15$	Eq. (2.19)

Where:

m – SiO_2 in mg/l

β – 4/3 if $T_{Surfacing}$ < 100°C or β = 1/3 if $T_{Surfacing}$ > 100°C

[1] Molal units

The calculation of maximum reservoir temperatures, through the substitution of Shu Shu thermal spring hydrochemical data into these traditional geothermometers, has not been undertaken as part of any published work.

2.4 Source Feature Characterization

The north-northwest trending, 1000km long zone of thermal springs in eastern South Africa is parallel to the Lebombo 'monocline' to the east, and the Great South African Escarpment to the west.

2.4.1 Lebombo 'Monocline'

According to Watkeys (2002), the 700km long and 600m high Lebombo 'monocline' marks a volcanic rifted margin along southeast Africa, which formed approximately 182 Ma. At its southern edge, this feature is constrained by the same metamorphic units of the Natal Metamorphic Province in which the Shu Shu thermal springs are located, whilst the northern regions of the Lebombo coincide with the termination of the Limpopo Belt (Watkeys, 2002), which hosts 'hot' and 'scalding' thermal springs. The Karoo volcanic rocks of the Lebombo 'monocline' comprise of a series of nephelinite-, picritic- and tholeiitic basaltic-lavas which are overlain by siliceous volcanic rocks; the geochemical signatures of which generally allow for their classification as rhyodacites and rhyolites (Duncan and Marsh, 2006). These volcanic rocks form part of the Lebombo Group of the Mesozoic Karoo Igneous Province which are preserved within the central to northeastern areas of southern Africa.

The origin of the formation of the Lebombo 'monocline' is contentious and is highly debated in published literature. That it forms part of a volcanic rifted margin is well established, however a debate exists as to whether it represents a successful or failed system. General characteristics of a typical rifted volcanic margin model are observable within the Lebombo, including a monoclinal flexure induced by coast-parallel faulting, and the mid-ocean ridge basalt-like Rooi Rand dyke swarm, with the former resulting in a seaward dip of the identified volcanic layers (Watkeys, 2002). Du Toit (1929) likened the formation of the Lebombo 'monocline' to the east coast of Greenland. However, Burke and Dewey (1972) first proposed that together within the Save-Mwenezi (Sabi) 'monocline' and the Okavango dyke swarm (see Figure 2.8), the Lebombo and its environs exhibit the classic shape of a triple junction, with the dyke swarm representing the failed arm (Reeves, 1978). It was subsequently proposed that the formation of the region was due to the impact of a plume with the simultaneous development of the three

arms (White and McKenzie, 1989), with the former likely responsible for continental flood basalts.

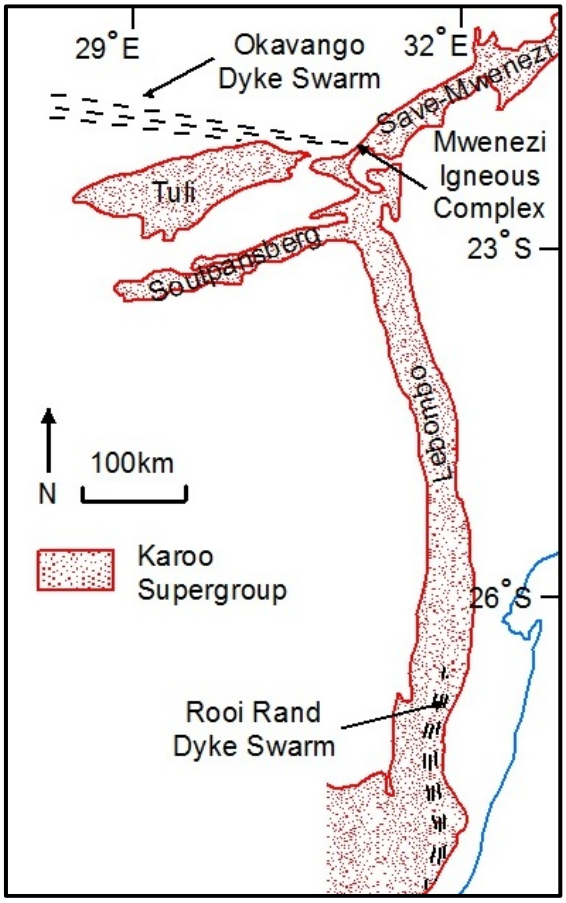

Figure 2.8: Lebombo 'monocline' and surrounding volcanic rifted margin features (redrawn after, and adapted from, Watkeys (2002)).

Further information pertaining to the formation of the Lebombo 'monocline' is included at the end of this study in Appendix B: Theories on the Formation of Thermal Spring Source Features.

2.4.2 Great South African Escarpment

A narrow coastal plain, which is typically separated from an inland plateau by an approximate horse-shoe-shaped escarpment, typically encompasses the generalised description of the physiography of southern Africa (Moore *et al*. 2009). Although along its entire length the Great South African Escarpment incorporates a sharp rise (>1000m) from the coastal parts of the country to the elevated interior plateau, it does not constitute one in the strict sense of the word (King, 1974). According to Flowers and Schoene (2010), it does, however, separate the more

highly denuded passive margins of the country from the less denuded plateau interior, hence giving it the appearance of a true escarpment. Indeed Moore *et al*. (2009) state that the interior of the inland plateau essentially takes the form of a sedimentary basin, with the drainage network of southern Africa being characterized by three, broadly coast-parallel, river divides.

The topography of southern Africa, as observed today, is now known to reflect the long-term interaction of tectonic / magmatic (uplift) and surface (denudation) processes, which account for the evolution of passive continental margins and their adjacent escarpments (Kounov *et al*., 2007). The interior plateau in southern Africa, which is underlain by the Kaapvaal Craton, attained approximately >1000m of elevation gain whilst distal from a convergent plate boundary (Flowers and Schoene, 2010). Furthermore, little upper crustal deformation is observed in southern Africa, which according to De Wit (2007), is unlike most other major continental plateau settings during which horizontal contraction was considerable during plateau elevation gain. Furthermore still, a significant low-seismic-velocity structure within the deep mantle, known as the 'African Superswell', exists beneath the cratonic lithosphere, which together with the Great South African Escarpment and atypical craton elevations, only contributes toward the unusual character of southern Africa (Flowers and Schoene, 2010).

Further information pertaining to the formation of the Great South African Escarpment is included at the end of this study in Appendix B: Theories on the Formation of Thermal Spring Source Features.

2.5 Geothermal Energy Prospects

In hydrothermal systems, there are essentially two possible sources of geothermal energy: dry stream / gas and thermal water. These two sources can typically be converted into electricity through three principle types of geothermal power plants, namely dry steam power plants, flash steam power plants and binary-cycle power plants (U.S. Department of Energy, 2010).

Dry steam power plants are limited to areas where geological activity results in dry steam, with established power plants simply directing the steam through turbines which then results in electricity (U.S. Department of Energy, 2010). According to the U.S. Department of Energy (2010), these types of geothermal power plants typically produce limited amounts of excess steam and other gases, thereby rendering them as eco-friendly. Flash steam power plants use hydrothermal fluids, or thermal waters, to rotate the installed turbines, however they require the

fluids to be at a minimum temperature of 182°C (U.S. Department of Energy, 2010). Hydrothermal fluid is injected into a flask tank that is kept at lower pressure than atmospheric pressure, such that some of the fluid rapidly vapourises, or flashes, with the collected vapour then directed through turbines (U.S. Department of Energy, 2010). Owing to the fact that all the thermal springs in South Africa are unlikely to have maximum reservoir temperatures of >182°C nor be associated with dry steam exhalations, the above two geothermal power plant systems are not appropriate. However, the third principle type, namely a binary cycle geothermal power plant is, and so is discussed further.

Binary cycle power plants are so named because they utilize a secondary (binary) cycle to create the required steam to rotate the turbines, as the temperatures of the thermal waters, even at low pressures, are insufficient to result in water vapour at the Earth's surface. As is shown in Figure 2.9, the hot water (whose minimum required temperature may vary and is dependent upon site-specific conditions) is collected and moved to a chamber which forms part of a heat exchanger with working fluid (U.S. Department of Energy, 2010).

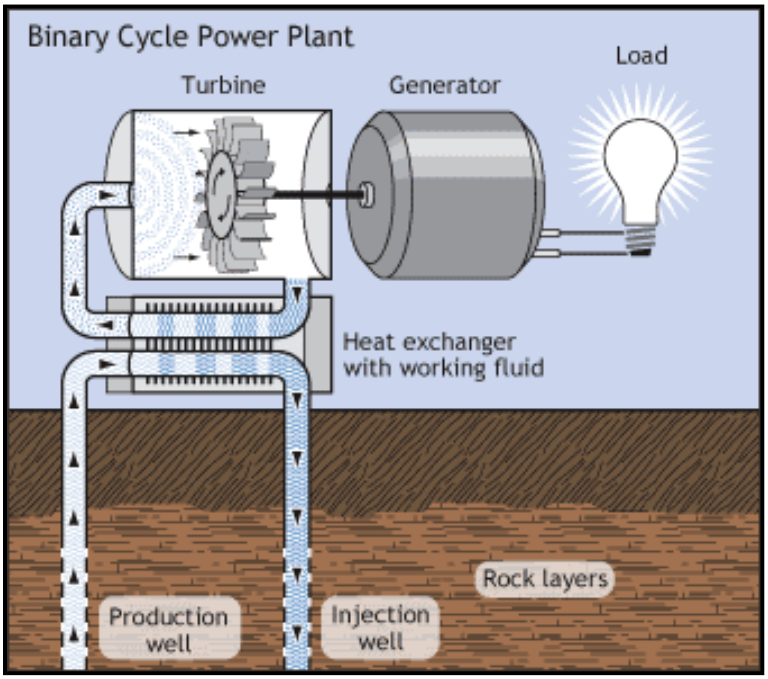

Figure 2.9: Simplified diagram showing a binary cycle power plant (U.S. Department of Energy, 2010).

The U.S. Department of Energy (2010) states that the choice of working fluid is dependent upon the temperature of the thermal water, as the latter must be sufficient to heat the fluid to such a

degree that it itself boils and so produces vapour. Common working fluids are typically hydrocarbons, such as isobutene, isopentane or the R-series fluids, or other liquid compounds whose boiling temperatures are sufficiently low to render them useful (Franco and Villani, 2010). Once steam has been produced, it is sent through turbines and hence results in the production of electricity, whilst the condensed working fluid is sent back to the heat exchanger (U.S. Department of Energy, 2010).

Chapter 3
Results

Published literature has suggested that the Shu Shu thermal springs are meteoric in origin, therefore this model is used hereafter as a framework within which to present the results of this study.

3.1 Geological Evolution

The results of the local geological and tectonic investigation are presented first so that the possible geological controls on the Shu Shu thermal springs can be established.

Two geological cross-sections were drawn from the available geological maps of the Tugela Terrane of the Natal Metamorphic Province through the Shu Shu thermal springs. These cross-sections, which are orientated north – south and northwest – southeast and span a length of 20km either side of the springs, are included in Appendix C: Geological Cross-Sections. The major structures appearing on these cross-sections have been annotated with reference to their orientations, through an assessment of the 1:125 000 regional geological map (Matthews and Charlesworth, 1981). The majority of these principle structures are orientated in a general east-northeast – west-southwest direction, and as such formed during the Proterozoic as a result of the collisional orogeny which resulted in the Natal Metamorphic Province (see Table 2.1).

The locations of the sampled rock types are shown in Appendix D1: Rock Sample Localities, whilst the geological map of the area immediately surrounding the Shu Shu thermal springs is included as Appendix D2: Geological Map.

3.1.1 Local Geology

The gneisses which outcrop in the immediate vicinity of the thermal springs are dominated by SiO_2 and Al_2O_3 (Table 3.1). The amphibolite sample contains lesser amounts of SiO_2 and K_2O, yet more Al_2O_3, FeO*, MgO, CaO and Na_2O, whilst all three rock types contain greater amounts of Mn, Zn, Sr, Zr and Ba as opposed to the other trace elements (Table 3.2). However, the geochemical composition of the gneisses and the amphibolites are typical of a felsic igneous protolith and a mafic igneous protolith respectively.

Table 3.1: Major and minor oxide composition – rock samples.

Basic Field-Identified Rock Type	Sampling Date	Sample Code	Units	SiO_2	Al_2O_3	FeO*	MnO	MgO	CaO	Na_2O	K_2O	TiO_2	P_2O_5	Cr_2O_3	NiO	Total	LOI
Hornblende Gneiss	2010-07-04	KGB01	wt %	71.62	14.26	4.18	0.04	0.61	3.14	3.86	1.65	0.39	0.14	0.02	0	99.90	1.02
Biotite-Hornblende Gneiss	2010-07-04	KGB02	wt %	75.14	13.14	2.64	0.08	0.48	3.60	3.04	1.56	0.24	0.08	0.01	0	100.01	1
Amphibolite	2010-07-04	KGB03	wt %	56.24	17.70	11.25	0.21	1.82	7.24	4.11	0.75	0.48	0.12	0.02	0	99.94	0.48

Table 3.2: Trace element composition – rock samples.

Basic Field-Identified Rock Type	Sampling Date	Sample Code	Units	Sc	V	Cr	Mn	Co	Ni	Cu	Zn	Ga	Rb
Hornblende Gneiss	2010-07-04	KGB01	ppb	12	21	16	319	BDL	4	4	68	13	46.5
Biotite-Hornblende Gneiss	2010-07-04	KGB02	ppb	9	14	14	690	5	8	BDL	38	11	26.2
Amphibolite	2010-07-04	KGB03	ppb	41	261	22	1752	14	6	82	133	18	14.5

Table 3.2 (continued): Trace element composition – rock samples.

Basic Field-Identified Rock Type	Sampling Date	Sample Code	Units	Sr	Y	Zr	Nb	Ba	La	Ce	Nd	Pb
Hornblende Gneiss	2010-07-04	KGB01	ppb	434.8	33.3	107.1	5.8	685.0	6	26	9	11.3
Biotite-Hornblende Gneiss	2010-07-04	KGB02	ppb	360.8	21.4	79.3	5.9	1172.0	6	5	BDL	12.8
Amphibolite	2010-07-04	KGB03	ppb	636.2	15.2	45.3	3.4	462.0	4	14	3	16.7

3.1.2 Tectonic Setting

The available structures which allow the water to ascend to the surface at the Shu Shu thermal springs have been investigated on a local and intermediate scale, in all three dimensions.

The joints and veins of nineteen pavements were mapped within a 1250m radius of the Shu Shu thermal springs. These are included in Appendix D3: Outcrop Locality Maps. The overall results of this mapping are presented in Figure 3.1 in the form of a rose diagram. This illustrates the principle fracture orientations.

Furthermore, fifteen geophysical traverses with a combined length of 2280m were completed in the immediate vicinity of the Shu Shu thermal springs, including the southern bank of the Tugela River and the permanent, vegetated sand bar in which the springs surface. The orientations of the traverses, the detected geophysical anomalies and the inferred structures are shown in Appendix D4: Geophysical Investigation Map, whilst the plotted geophysical data are contained in Appendix E: Geophysical Data Graphs and Information. The anomalies are typical of fracture zones within the underlying bedrock, and generally infer steeper dip values of >60°. Three 'probable' structures were identified in the immediate vicinity of the Shu Shu thermal springs (Table 3.3).

Table 3.3: Geophysically identified 'probable' structures.

Structure Type	Approximate Dip/Strike	Structure Orientation	Dip Direction
Fracture zone [1]	75/122	NW – SE	SW
Fracture zone [2]	68/076	WSW – ENE	SSE
Fracture zone [3]	75/169	NNW – SSE	WSW

The results of the geophysical investigation have been included in Figure 3.1, as separately-delineated features. The relation of the structures identified through pavement mapping, and those detected through geophysical methodologies, can hence be assessed.

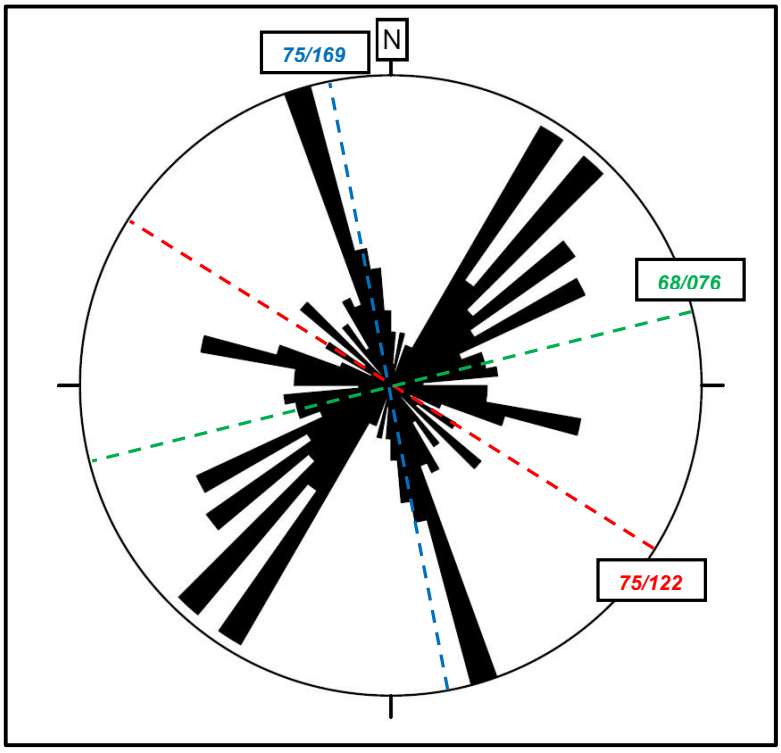

Figure 3.1: Rose diagram – detailed outcrop mapping (n = 350), with geophysically-identified structures shown.

With the exception of Fracture Zone [3], which is consistent with a dominant fracture orientation as identified through pavement mapping, the geophysically-identified fracture zones do not coincide with the orientation of numerous pavement-identified structures.

Finally an area of 58.5km^2 (9.0km x 6.5km) centred around the Shu Shu thermal springs was selected for the photo-geological lineament analysis. The identified possible and inferred lineaments, as well as those structures identified by Von Veh (1994), are shown in Appendix D5: Photo-Geological Lineament Analysis Map. Where the orientations of these structures were consistent with those identified during the local scale mapping exercises, the average, typical dips of the latter were applied to the former, as it is inferred that they are likely similar. Consequently, this allowed for their inclusion in a rose diagram (Figure 3.2) which illustrates the principle fracture directions on an intermediate scale.

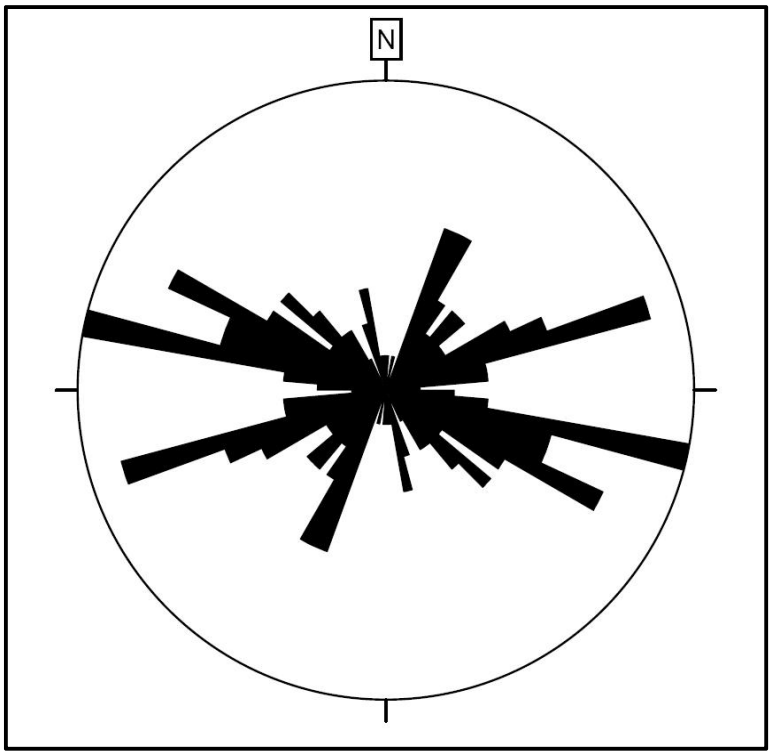

Figure 3.2: Rose diagram – photo-geological lineament analysis (n = 107).

From the local and intermediate scale mapping exercises, the principle structure directions were identified and ranked in order of descending frequency (Table 3.4), and are shown graphically in Figure 3.3. Note that dip directions shown are those most prevalent amongst the gathered data.

Table 3.4: Local and intermediate scale principle structure orientations – descending structure frequency.

Structure Ranking	Local Scale – Structure Orientation (Figure 3.1)	Intermediate Scale – Structure Orientation (Figure 3.2)
Primary	NNW – SSE	WNW – ESE
Secondary	NE – SW	ENE – WSW
Tertiary	WNW – ESE	NNE – SSW

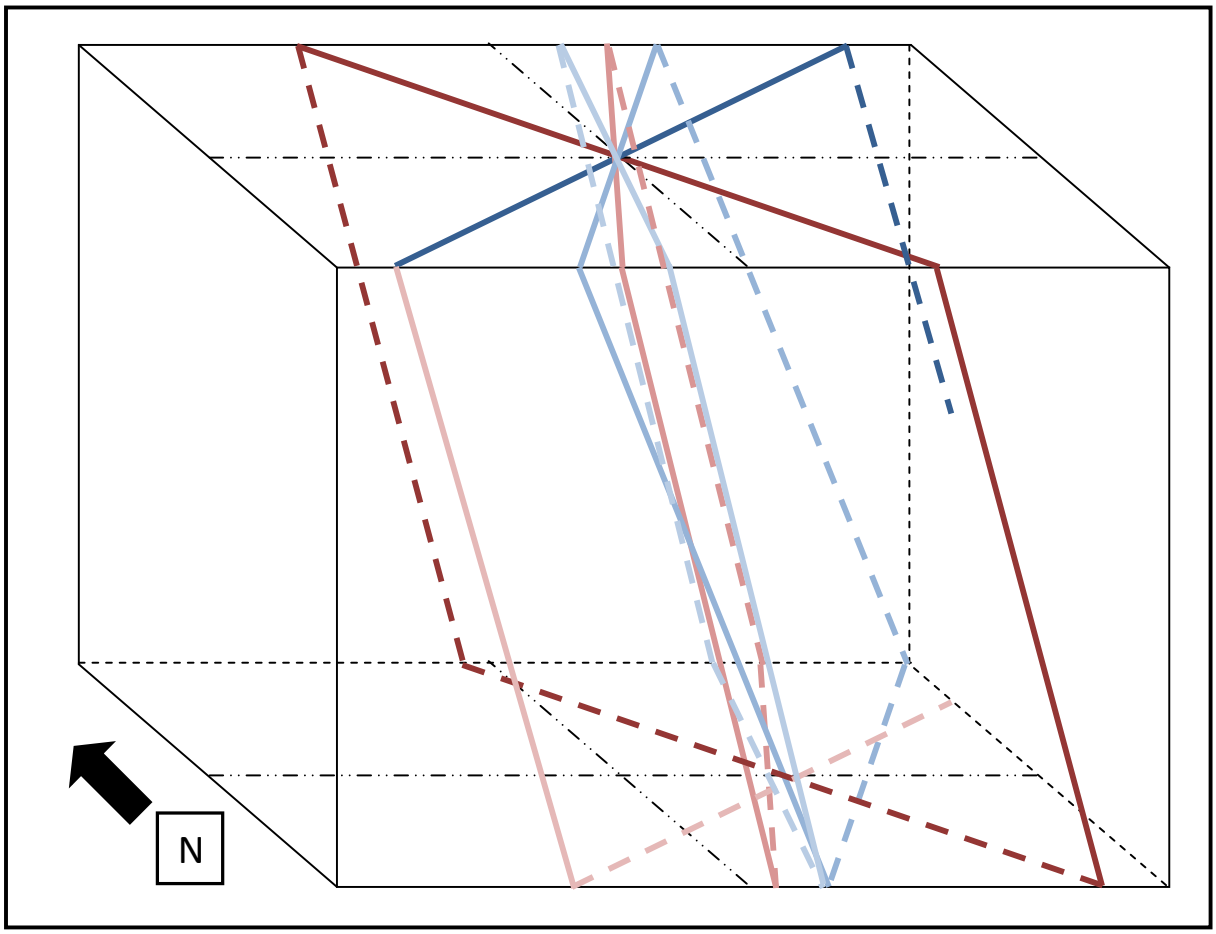

Figure 3.3: Local and intermediate scale principle structure directions.

It is evident that only the west-northwest – east-southeast orientation is observed at both scales. It is possible that the other orientations observed at intermediate (to sub-regional) scale represent master joint sets, however they are not the most frequent at local scale.

3.2 Hydrogeology

The results of the hydrological investigation undertaken as part of this study are detailed hereafter. The locations of the sampled water types, which include rainfall, surface water and shallow groundwater and thermal water, are shown in Appendix D6: Rainfall Sampler Locality and Appendix D7: Water Sample Localities, with important altitudes shown on the former.

3.2.1 Physical Water Parameters and Hydrochemistry

The physical parameters of the groundwater and surface water sources, sampled during different seasons, are presented in Table 3.5 and Table 3.6.

Table 3.5: Physical parameters – groundwater.

Sample Name	Sampling Date	Sample Code	Temp. (°C)	pH	E.C. (mS/m)	T.D.S. (mg/l)
Shu Shu Thermal Springs – Sement Bad	2010-07-05	SB / 2010	50.6	8.23	167	910
Shu Shu Thermal Springs – Wit Bad	2010-07-05	WB / 2010	48.1	8.56	163	890
BH KZN6370227 (Depth: 72 m)	2010-07-05	BH 1 / 2010	23.5	8.22	128	690
BH KZN204078 (Depth: 120 m)	2011-04-28	BH 2 / Late Summer	24.3	8.61	106	650
BH KZNINK35 (Depth: 130 m)	2011-04-28	BH 3 / Late Summer	24.5	8.67	203	1380
Shu Shu Thermal Springs – Sement Bad	2011-06-13	SB / 2011	51.6	8.33	154	840
Shu Shu Thermal Springs – Wit Bad	2011-06-13	WB / 2011	47.5	8.12	153	830
BH KZN6370227	2011-06-13	BH 1 / 2011	27.3	7.89	122	670
BH KZN204078	2011-08-25	BH 2 / Late Winter	21.9	7.54	119	836
BH KZNINK35	2011-08-25	BH 3 / Late Winter	21.5	7.12	237	1775

Table 3.6: Physical parameters – surface water.

Sample Name	Sampling Date	Sample Code	Temp. (°C)	pH	E.C. (mS/m)	T.D.S. (mg/l)
Tugela River	2010-07-05	TR / 2010	17.7	6.9	23	120
Tugela River	2011-06-13	TR / 2011	15.6	8.46	19	100

The temperatures of the samples SB / 2010, WB / 2010, SB / 2011 and WB / 2011 classify the Shu Shu thermal springs as 'hot' according to the Kent (1949) system. Furthermore, the pH balance of the thermal spring samples reveals an alkaline source type (as discussed later), although the value of this parameter, and that of E.C. and T.D.S., display a standard deviation of less than 10% across the two sampling events.

The physical parameters of the groundwater sampled from BH 1 remained constant across the 2010 and 2011 sampling events, with the exception of temperature. A variation of 3.80 °C infers that the 2011-measured temperature categorises this borehole as 'thermal' according to Kent's (1949) classification. This however, may be as a result of atmospheric temperature variations across the two sampling events. The dissimilarity between the pH, E.C. and T.D.S. values of the groundwater sampled from BH 2 and BH 3 is indicative of limited variations often observed

in shallow aquifers, whilst the difference in measured temperatures highlights the general seasonal effects of summer and winter.

With the exception of pH values, which varied by 1.54, similar temperature, E.C. and T.D.S. values were measured across samples TR / 2010 and TR / 2011.

The major and minor and trace element compositions of the various groundwater and surface water sources are presented in Table 3.7 to Table 3.10. Furthermore, the cation-anion balances and the analytical errors / measurements of uncertainty for these results are included in Appendix H: Hydrochemistry of the Shu Shu Thermal Springs and Surrounds.

Table 3.7: Major and minor determinant compositions – groundwater.

Sample Name	Sampling Date	Sample Code	Units	Na^{+}	Ca^{2+}	K^{+}	Mg^{2+}	Si^{4+}	HCO_3^{-}	SO_4^{2-}	Cl^{-}	F^{-}	NO_3^{-}
Shu Shu Thermal Springs – Sement Bad	2010-07-05	SB / 2010	mg/l	223.31	87	7.31	3.04	10.64	34	399	168	7.4	0.38
Shu Shu Thermal Springs – Wit Bad	2010-07-05	WB / 2010	mg/l	206.07	61	6.77	2.82	6.11	40	393	165	7.1	0.34
BH KZN6370227	2010-07-05	BH 1 / 2010	mg/l	222.39	70	7.64	7.20	6.44	61	408	169	6.2	0.36
BH KZN204078	2011-04-28	BH 2 / Late Summer	mg/l	125.47	58	15.54	61.86	11.29	432	23.4	93.57	1.26	0.03
BH KZNINK35	2011-04-28	BH 3 / Late Summer	mg/l	233.49	134	26.38	155.58	11.67	438	169.6	369.93	0.65	37.5
Shu Shu Thermal Springs – Sement Bad	2011-06-13	SB / 2011	mg/l	259.50	58	8.11	3.53	33.85	41	226.93	96.45	6.23	<0.01
Shu Shu Thermal Springs – Wit Bad	2011-06-13	WB / 2011	mg/l	257.66	61	8.12	3.11	33.53	34	227.75	97.15	6.13	0.44
BH KZN6370227	2011-06-13	BH 1 / 2011	mg/l	224.70	58	7.86	16.60	18.10	199	267.10	109.94	6.16	<0.01
BH KZN204078	2011-08-25	BH 2 / Late Winter	mg/l	118.30	58	14.85	61.30	1.67	444	26.38	90.91	1.31	0.01
BH KZNINK35	2011-08-25	BH 3 / Late Winter	mg/l	215.91	127	25.01	152.01	2.36	484	171.32	366.47	0.64	0.01

Table 3.8: Trace element compositions – groundwater.

Sample Name	Sampling Date	Sample Code	Units	Sr	Fe	Li	Al	Ba	Cs	Mn	Zn	Se
Shu Shu Thermal Springs – Sement Bad	2010-07-05	SB / 2010	µg/l	3370	265	137	35	25	18	13	0	2
Shu Shu Thermal Springs – Wit Bad	2010-07-05	WB / 2010	µg/l	3107	219	126	45	21	16	10	10	5
BH KZN6370227	2010-07-05	BH 1 / 2010	µg/l	3302	1529	129	77	22	14	28	950	4
BH KZN204078	2011-04-28	BH 2 / Late Summer	µg/l	688	212	9	1	4	0	240	6162	4
BH KZNINK35	2011-04-28	BH 3 / Late Summer	µg/l	11602	509	15	6	74	2	29	2972	11
Shu Shu Thermal Springs – Sement Bad	2011-06-13	SB / 2011	µg/l	3728	340	138	148	27	17	21	4	5
Shu Shu Thermal Springs – Wit Bad	2011-06-13	WB / 2011	µg/l	3793	290	136	48	27	17	16	5	5
BH KZN6370227	2011-06-13	BH 1 / 2011	µg/l	2909	3577	83	28	42	20	82	613	3
BH KZN204078	2011-08-25	BH 2 / Late Winter	µg/l	748	600	10	8	177	0	170	2992	1
BH KZNINK35	2011-08-25	BH 3 / Late Winter	µg/l	12787	550	16	9	74	2	35	5922	12

Table 3.8 (continued): Trace element compositions – groundwater.

Sample Name	Sampling Date	Sample Code	Units	Cr	Ni	Cu	Mo	As	Hg	Ag	Cd	Co	Pb
Shu Shu Thermal Springs – Sement Bad	2010-07-05	SB / 2010	µg/l	1	3	4	2	1	3	0	0	0	0
Shu Shu Thermal Springs – Wit Bad	2010-07-05	WB / 2010	µg/l	4	3	2	0	1	1	0	0	0	0
BH KZN6370227	2010-07-05	BH 1 / 2010	µg/l	4	3	9	1	2	4	0	0	0	0
BH KZN204078	2011-04-28	BH 2 / Late Summer	µg/l	17	19	2	1	1	0	0	0	2	0
BH KZNINK35	2011-04-28	BH 3 / Late Summer	µg/l	26	7	9	6	2	0	0	0	1	0
Shu Shu Thermal Springs – Sement Bad	2011-06-13	SB / 2011	µg/l	2	3	4	2	1	2	0	0	1	0
Shu Shu Thermal Springs – Wit Bad	2011-06-13	WB / 2011	µg/l	2	3	4	2	1	1	0	0	1	0
BH KZN6370227	2011-06-13	BH 1 / 2011	µg/l	1	3	7	2	1	1	0	0	1	0
BH KZN204078	2011-08-25	BH 2 / Late Winter	µg/l	19	10	2	0	1	2	0	0	1	0
BH KZNINK35	2011-08-25	BH 3 / Late Winter	µg/l	24	8	6	6	2	1	0	0	1	1

Table 3.9: Major and minor determinant compositions – surface water.

Sample Name	Sampling Date	Sample Code	Units	Na^+	Ca^{2+}	K^+	Mg^{2+}	Si^{4+}	HCO_3^-	SO_4^{2-}	Cl^-	F^-	NO_3^-
Tugela River	2010-07-05	TR / 2010	mg/l	23.09	17	2.06	11.44	2.99	101	14	12	0.22	0.39
Tugela River	2011-06-13	TR / 2011	mg/l	19.23	15	1.71	10.63	7.33	93	11.84	7.9	0.27	0.21

Table 3.10: Trace element compositions – surface water.

Sample Name	Sampling Date	Sample Code	Units	Sr	Fe	Li	Al	Ba	Cs	Mn	Zn	Se
Tugela River	2010-07-05	TR / 2010	µg/l	127	250	2	169	68	0	28	10	1
Tugela River	2011-06-13	TR / 2011	µg/l	130	306	2	563	92	0	3	6	1

Table 3.10 (continued): Trace element compositions – surface water.

Sample Name	Sampling Date	Sample Code	Units	Cr	Ni	Cu	Mo	As	Hg	Ag	Cd	Co	Pb
Tugela River	2010-07-05	TR / 2010	µg/l	7	2	3	0	0	2	0	0	0	0
Tugela River	2011-06-13	TR / 2011	µg/l	3	3	4	0	1	3	0	0	2	2

Discernible variations are observed in the levels of certain hydrochemical parameters in the groundwater samples across 2010 and 2011 / late summer and late winter. Si concentrations appear highly variable in all samples, although the dissimilarities thereof are inconsistent across the different sampling events. Other hydrochemical parameter variations are confined primarily to the Shu Shu thermal springs and thermal borehole samples. Concentrations of Na in the former increased in 2011 as compared to those detected in 2010, whilst the levels of SO_4 and Cl decreased considerably in 2011 across all thermal waters. Aside from limited variations in the concentrations of Fe and Al, thermal spring trace element levels remained consistent across the 2010 and 2011 sampling events. However marked variations in the concentrations of Sr, Fe, Li, Al, Ba, Mn and Zn were detected in groundwater sampled from BH 1. Cold groundwater trace element levels also remained constant, save for the concentrations of Fe and Zn. Given the range of hydrochemical parameter values and inconsistent variations across different seasons, inconsistent recharge areas or groundwater mixing is speculated. Intermixing is a common process at shallow depths in thermal systems (Gianelli *et al*., 1997; Pirlo, 2004; Bahati *et al*., 2005; Guangcai *et al*., 2005).

Aside from a noticeable increase in the level of Si being observed, the water quality in the Tugela River remained steady across 2010 and 2011. The generally lower values of the majority of the hydrochemical parameters measured in 2011 are attributed to dilution as a result of heavy rains prior to the final sampling event.

As a result of the similarity observed between the physical water and hydrochemical similarities of the Shu Shu thermal spring samples and the shallow groundwater sampled from BH 1, this borehole was profiled vertically through the measurement of certain physical water parameters. The results of this investigation are shown graphically in Figure 3.4 from a static water level (SWL) of 5.63m to the borehole completion depth of 72.00m.

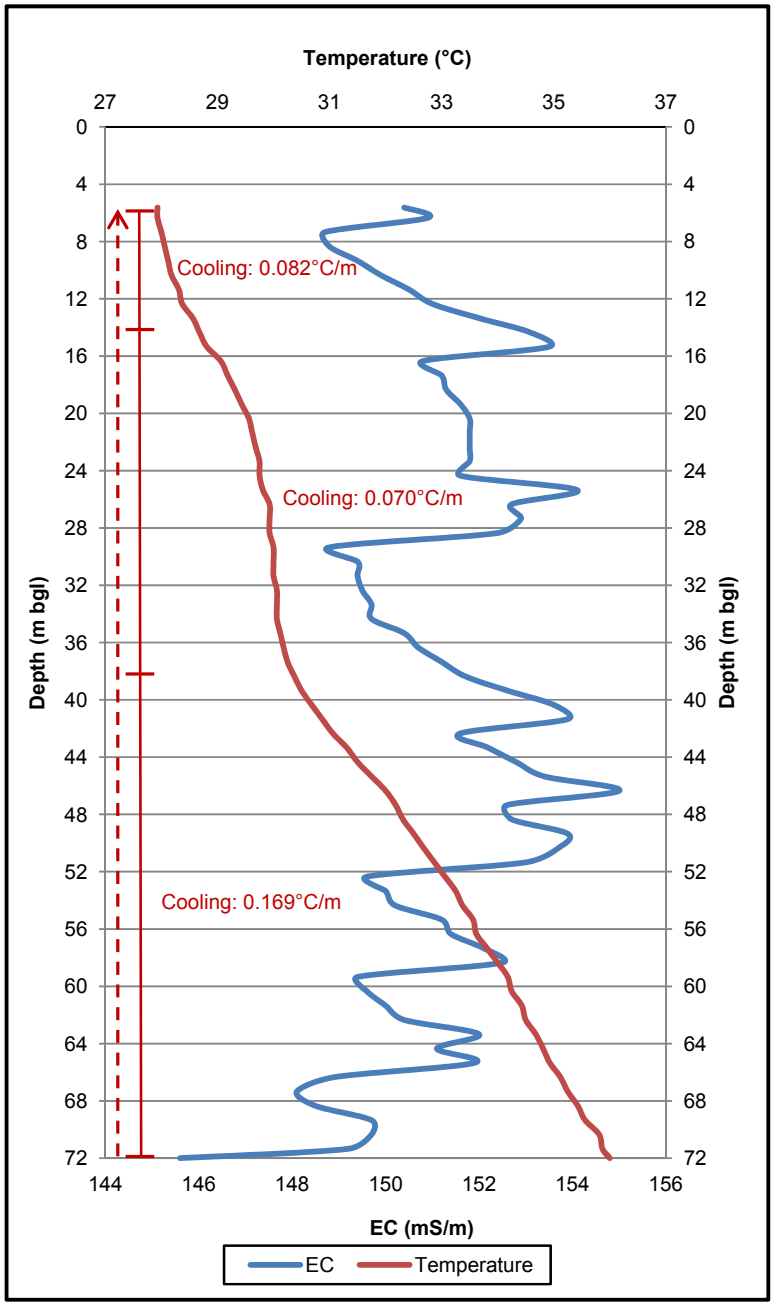

Figure 3.4: BH 1 EC and temperature borehole profile.

The three principle thermal gradients that were measured which are shown on the profile above, indicate that temperatures decrease at the greatest rate at a depth of more than 38m bgl in this shallow borehole. The general increase in EC values at depths of ~6m bgl to ~25m bgl and ~29m bgl to ~46m bgl may be attributable to an increase in dissolved solid concentration associated with the weathered and fractured horizon profiled at these depths. However, an overall decreasing EC trend is exhibited, which may either be attributable to temporal variations,

or it possibly infers the addition of cold groundwater at depths of more than 38 m bgl, and so is consistent with the greatest rates of cooling measured.

3.2.2 Isotopic Data and Analysis

Stable and radiogenic isotope results of the various water sources sampled during different seasons are presented in Table 3.11 to Table 3.13 and graphically as a δD vs. $\delta^{18}O$ plot in Figure 3.5. The GMWL, and a LMWL based upon KwaZulu-Natal data (E. van Wyk, pers. comm.), are shown.

Table 3.11: Stable and radiogenic isotope analysis results – rainfall.

Sample Name	Sampling Date	Sample Code	δD (‰) SMOW	$\delta^{18}O$ (‰) SMOW	^{3}H (T.U.)
Summer Storm-Event Rainfall	2010-12-16	SER / Summer	-18.5	-4.15	1.6 ± 0.3
Summer Cumulative Rainfall	2010-12-16 to 2011-03-03	CR / Summer	-12.3	-3.57	2.1 ± 0.3
Autumn Storm-Event Rainfall	2011-03-26	SER / Autumn	-9.1	-2.86	1.4 ± 0.3
Autumn Cumulative Rainfall	2011-03-03 to 2011-04-28	CR / Autumn	-16.3	-4.25	2.1 ± 0.3

Table 3.12: Stable and radiogenic isotope analysis results – groundwater.

Sample Name	Sampling Date	Sample Code	δD (‰) SMOW	$\delta^{18}O$ (‰) SMOW	^{3}H (T.U.)
Shu Shu Thermal Springs – Sement Bad	2010-07-05	SB / 2010	-16.5	-3.75	0.0 ± 0.2
Shu Shu Thermal Springs – Wit Bad	2010-07-05	WB / 2010	-16.1	-3.68	0.0 ± 0.2
BH KZN6370227	2010-07-05	BH 1 / 2010	-15.3	-3.75	0.0 ± 0.2
BH KZN204078	2011-04-28	BH 2 / Late Summer	-16.5	-3.69	0.0 ± 0.2
BH KZNINK35	2011-04-28	BH 3 / Late Summer	-20.8	-3.54	0.0 ± 0.2
Shu Shu Thermal Springs – Sement Bad	2011-06-13	SB / 2011	-16.8	-4.23	0.9 ± 0.2
Shu Shu Thermal Springs – Wit Bad	2011-06-13	WB / 2011	-15.9	-3.96	0.0 ± 0.2
BH KZN6370227	2011-06-13	BH 1 / 2011	-15.3	-3.80	0.5 ± 0.2
BH KZN204078	2011-08-25	BH 2 / Late Winter	-18.5	-3.60	0.8 ± 0.2
BH KZNINK35	2011-08-25	BH 3 / Late Winter	-19.6	-3.82	1.0 ± 0.3

Table 3.13: Stable and radiogenic isotope analysis results – surface water.

Sample Name	Sampling Date	Sample Code	δD (‰) SMOW	$\delta^{18}O$ (‰) SMOW	^{3}H (T.U.)
Tugela River	2010-07-05	TR / 2010	-1.1	-3.10	2.9 ± 0.3
Tugela River	2011-06-13	TR / 2011	-9.6	-2.50	2.1 ± 0.3

Cumulative and storm-event rainfall samples contain slightly different ^{2}H and $\delta^{18}O$ values, with only the storm event sample collected during summer plotting away from the LMWL. Furthermore, seasonal variations were observed in the radiogenic isotope data with increased amounts of ^{3}H in the cumulative rainfall samples possibly reflecting the effects of attenuation. The Shu Shu thermal spring waters and BH 1 groundwater, although appearing meteoric, typically plot below and to the right of the LMWL, hence possibly reflecting the effects of climatic and geographic processes (continental, altitude and latitude effects). Cold groundwater intercepted by BH 2 and BH 3 appears to be recharged away from the study area with the latter more so. The Tugela River samples are enriched in the heavier oxygen isotope in relation to rainfall and so clearly have been affected by evaporation. Finally, a variation in recharge source area, or possibly mixing, is inferred through inconsistent ^{3}H data observed across the different sampling events. However, the variation in Shu Shu thermal springs ^{3}H data in 2011 may be indicative of contamination, although such a source is difficult to quantify.

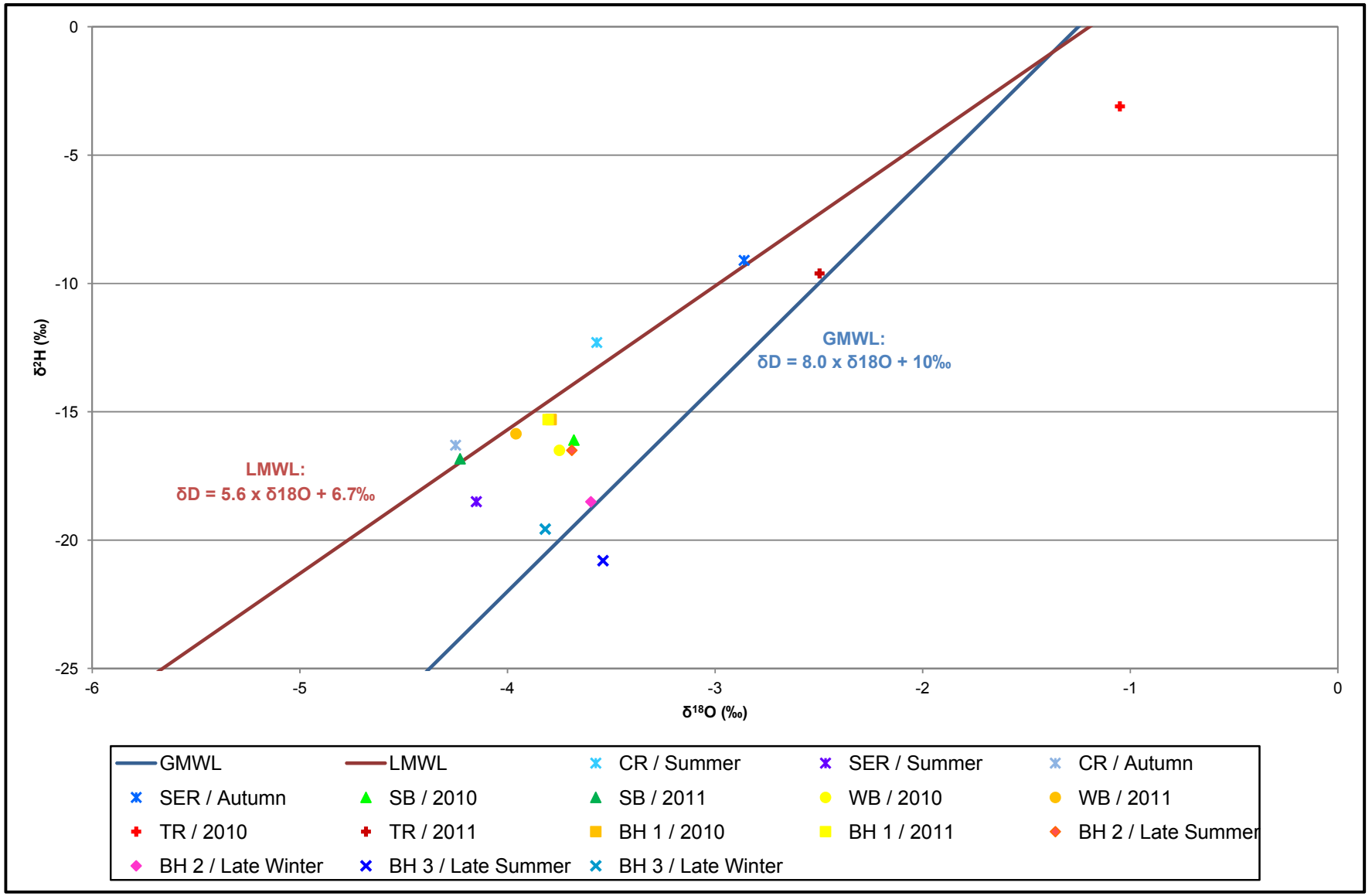

Figure 3.5: Local rainfall data, Shu Shu thermal spring data, local groundwater data and surface water data vs. Global Meteoric Water Line (GMWL) and a Local Meteoric Water Line (LMWL).

3.3 Geothermal Investigations

The subsurface heat flow in the region surrounding the Shu Shu thermal springs could not be measured due to the lack of existing boreholes of sufficient depths in the study area. However, the heat source and maximum reservoir temperatures is / are inferred below through the use of indirect methods. These are based upon the ^{13}C isotope, physical and hydrochemical data of the Shu Shu thermal spring and thermal borehole waters.

3.3.1 Heat Source: ^{13}C Data

The results of the ^{13}C analysis, undertaken on selected thermal water samples, are presented in Table 3.14 below.

Table 3.14: ^{13}C analysis results – selected thermal waters.

Sample Name	Sampling Date	Sample Code	Units	^{13}C
Shu Shu Thermal Springs – Sement Bad	2011-06-13	SB / 2011	$\delta^{13}C$ (‰) PDB	BDL
BH KZN6370227	2011-06-13	BH 1 / 2011	$\delta^{13}C$ (‰) PDB	-5.32

The amount of ^{13}C within the SB / 2011 sample was below the detection limit of the laboratory as there was an insufficient amount of HCO_3 present, even though pH values of >8.00 infer the presence thereof. Consequently though, a value could not be determined. The $\delta^{13}C$ value within the BH 1 / 2011 sample (-5.32‰) is possibly inaccurate and hence cannot be used for its intended purpose. However, it theoretically infers a magmatic / partially mantle-derived origin for the CO_2 surfacing in the thermal borehole (thermal springs). Note that further information is included in Section 4.3.1.

3.3.2 Maximum Reservoir Temperatures

The maximum reservoir temperatures can possibly be determined from the available Shu Shu thermal springs hydrochemistry data through the use of selected, applicable geothermometer equations (Table 3.15).

Table 3.15: Geothermometer-derived maximum reservoir temperatures (note that calculated outlier temperatures have been excluded).

Name and Reference	Units	Shu Shu Thermal Springs – Sement Bad		Shu Shu Thermal Springs – Wit Bad	
		2010-07-05	2011-06-13	2010-07-05	2011-06-13
Quartz Truesdell and Fournier (1976)	°C	42	85	27	84
(1) Quartz Fournier (1977)	°C	49	87	36	87
(2) Quartz Fournier (1977)	°C	41	84	27	84
Na-K Truesdell (1976)	°C	92	89	93	90
Na-K Fournier (1979)	°C	137	134	137	135
Na-K Arnorsson *et al.* (1983)	°C	103	100	104	101
Na-K Giggenbach (1988)	°C	157	154	157	154
Na-K Verma and Santoyo (1997)	°C	143	140	143	140
Na-K Santoyo and Díaz-González (2010)	°C	98	94	98	95
Na-K-Ca Fournier and Truesdell (1973)	°C	58[1]	79[2]	25[1]	81[2]
Na-Li Kharaka *et al.* (1982)	°C	125	119	125	119

[1] Mg correction applied as $T_{Na\text{-}K\text{-}Ca}$ (original) > 70°C and 5 < R < 50 (see reference for details)

[2] Mg correction not applied as Δt_{Mg} < 0°C

The shaded values are those which fall below the measured thermal spring temperature and cannot be considered for analysis. The utilized geothermometer equations infer two possible ranges of maximum reservoir temperatures (Table 3.16).

Table 3.16: Geothermometer-derived maximum reservoir temperature ranges (note that the calculated, shaded outlier temperatures have been excluded).

Name and Reference	Units	Shu Shu Thermal Springs – Sement Bad		Shu Shu Thermal Springs – Wit Bad	
		2010-07-05	2011-06-13	2010-07-05	2011-06-13
Lower Range	°C	80.5 ± 22.5	89.5 ± 10.5	98.5 ± 5.5	91 ± 10
Higher Range	°C	141 ± 16	136.5 ± 17.5	141 ± 16	136.5 ± 17.5

3.3.3 Depths of Circulation

The derived geothermal gradient of 3.1°C / 100m is employed in a basic manner to determine the depths of circulation. This is based upon the assumption then that the geothermal gradient (heat flow) through the subsurface geology in the region is the source of the heat of the thermal waters.

The maximum measured issuing temperatures of the Shu Shu thermal springs can be used in Equation 2.2, along with the derived geothermal gradient, to determine the minimum depths of circulation. These average 997m ± 67m, however the nature of this exercise excludes the effects of secondary factors acting upon the surfacing thermal groundwaters (Mazor, 1991). Mazor (1991) denotes that one of the secondary factors acting upon the surfacing thermal groundwaters, namely cooling upon ascent, is only applicable to thermal water outflow rates of less than an approximate amount of 8.33l/sec (which is equivalent to 30 000l/hr). An attempt was made to measure the outflow rate of the principle eye at the Shu Shu thermal springs, with this water flowing into the Sement Bad. As can be seen in Table 3.17 below, the measured outflow rate averaged 0.63l/sec (which is equivalent to 2 264l/hr).

Table 3.17: Measured discharge rates for the principle Shu Shu thermal spring eye.

Discharge Rate Test Number	Units	Measured Outflow
DRT #1	l/sec	0.61
DRT #2	l/sec	0.62
DRT #3	l/sec	0.64
DRT #4	l/sec	0.63
DRT #5	l/sec	0.65
Average	l/sec	*0.63*

Owing to the morphology of the river bed, the elevation of surfacing groundwaters through other eyes, and the construction of other baths, it was not possible to measure the total outflow of thermal water. However, local knowledge and historical information gathered at the Shu Shu thermal springs suggests a total outflow rate of approximately double that measured which equates to 1.26l/sec, or 4536.00l/hr. Such a rate falls within the 'moderate' class (> 0.5l/sec – 3.0l/sec) of borehole / spring yields as classified according to those categories proposed by Groundwater Consulting Services (1993) for the former Department of Water Affairs and Forestry for South Africa. Consequently, based solely upon outflow rates, cooling upon ascension to the surface likely does indeed occur at the Shu Shu thermal springs.

The utilization of the derived geothermal gradient, in conjunction with the geothermometer-derived maximum reservoir temperatures and Equation 2.2, allows for the calculation of the maximum depths of circulation (Table 3.18). Excluded depths include those calculated from geothermometer-derived maximum reservoir temperatures which are less than the corresponding surfacing issuing temperatures.

Table 3.18: Applicable, geothermometer-derived maximum depths of circulation.

Name and Reference	Units	Shu Shu Thermal Springs – Sement Bad		Shu Shu Thermal Springs – Wit Bad	
		2010-07-05	2011-06-13	2010-07-05	2011-06-13
Quartz Truesdell and Fournier (1976)	m	n.a.	2141	n.a.	2128
(1) Quartz Fournier (1977)	m	n.a.	2234	n.a.	2223
(2) Quartz Fournier (1977)	m	n.a.	2136	n.a.	2122
Na-K Truesdell (1976)	m	2393	2292	2401	2310
Na-K Fournier (1979)	m	3846	3756	3854	3772
Na-K Arnorsson *et al.* (1983)	m	2752	2654	2760	2671
Na-K Giggenbach (1988)	m	4487	4400	4494	4416
Na-K Verma and Santoyo (1997)	m	4035	3947	4041	3963
Na-K Santoyo and Díaz-González (2010)	m	2570	2468	2578	2486
Na-K-Ca Fournier and Truesdell (1973)	m	1262	1962	n.a.	2022
Na-Li Kharaka *et al.* (1982)	m	3466	3267	3461	3256

n.a. as geothermometer temperature less than surface issuing temperature

The utilized geothermometer equations infer two possible ranges of maximum depths of circulation (Table 3.19).

Table 3.19: Geothermometer-derived maximum depths of circulation ranges.

Name and Reference	Units	Shu Shu Thermal Springs – Sement Bad		Shu Shu Thermal Springs – Wit Bad	
		2010-07-05	2011-06-13	2010-07-05	2011-06-13
Lower Range	m	2007 ± 745	2308 ± 346	2581 ± 180	2347 ± 1325
Higher Range	m	3778 ± 510	3834 ± 567	3978 ± 517	3836 ± 580

Chapter 4
Discussion

4.1 Geological Setting

A knowledge of local geology (including rock types and compositions, as well as tectonic evolution) aids in defining the source of the dissolved constituents in the groundwater at Shu Shu and the pathways by which it migrates and surfaces.

4.1.1 Local Geology

An assessment of the major and minor oxide compositions and trace element concentrations of the rock types surrounding the Shu Shu thermal springs aids in the correct classification of the rock types. It also establishes the likely source for leachable minerals.

The theoretical mineral assemblages of the collected rock samples, according to the MesoNorm and CataNorm in accordance with the mesozone and catazone respectively, are included in Appendix F: Additional Local Geology Information. The gneiss samples are expectedly dominated by quartz, plagioclase feldspar (including albite and anorthite), alkali feldspar, hematite and the hydrous minerals (biotite and amphibole). As biotite resulted from the replacement of hornblende (Gevers, 1942), a greater wt % thereof is not observed. Elevated amounts of pyroxene (diopside), hornblende and the Ti-bearing minerals (ilmenite, titanite and rutile) are typical of amphibolites.

The description of the thin-sections of the three rock samples collected is included in Appendix F: Additional Local Geology Information. Hornblende gneiss outcropping in the area is comprised predominantly of plagioclase (observed as a solid-solution of albite-anorthite) and microcline, lesser amounts of quartz and hornblende, as well as various accessory minerals. Similarly, quartz, feldspar (microcline, orthoclase and plagioclase), biotite, hornblende, epidote and titanite dominate the biotite-hornblende gneiss. Finally, amphibolite contains, in decreasing order of modal abundance, hornblende, epidote-clinozoisite, quartz, plagioclase feldspar, biotite and titanite. Given the stability series of these minerals, elevated amounts of Ca, Na, Al, K, Mg, F and possibly Si in groundwaters are likely through dissolution processes.

4.1.2 Tectonic Evolution

The available structures which allow the water to ascend to the surface at the Shu Shu thermal springs are discussed with reference to the tectonic evolution of the area on a local, intermediate and (sub-) regional scale. However, as it is only the principle structures that have been detailed thus far, the importance of joints with respect to their possible modes of formation and water-transporting characteristics are described.

Joints form in rock in response to stress and strain in both brittle and ductile deformation environments. Joints that originate in brittle environments depend upon the magnitude and orientation of the three principle orthogonal stress axes (σ_1 (maximum compression stress), σ_2 (intermediate compression stress) and σ_3 (minimum compression stress)) in relation to σ_t, the tensile strength of the rock (Pollard and Aydin, 1988). Either single extension joints, which are parallel to the orientation of the σ_1-σ_2 plane, or two shear joints, which are orientated at an inclined angle to σ_1, will form in response to brittle forces. Fold-related joints typically form in similar orientations to those which form in brittle environments. However another joint set will form perpendicular to σ_1 under ductile deformation settings. The formation of joints is further detailed in Appendix G: Additional Tectonic Evolution Information.

If the tectonic evolution of a region is known, the expected joint orientations may be predicted. Table 4.1 includes the various joint orientations likely to theoretically have formed in the Shu Shu area.

Table 4.1: Fault-related and fold-related joint orientations formed in response to Proterozoic and Phanerozoic tectonics.

Eon	Principle Structure Orientations			Possible Fault-Related Joint Orientations	Possible Fold-Related Joint Orientations
	Extension	Intermediate*	Compression		
Phanerozoic	(9) east-southeast – west-northwest	(10) north-northeast – south-southwest		(9.1) east-southeast – west-northwest (9.2) east – west (9.3) northwest – southeast (10.1) north-northeast – south-southwest (10.2) north – south (10.3) northeast – southwest	
	(7) north – south (6) north-northeast – south-southwest	(8) west-southwest – east-northeast		(6.1; 7.2) north-northeast – south-southwest (6.2; 7.1) north – south (6.3; 8.3) northeast – southwest (7.2) north-northeast – south-southwest (7.3) north-northwest – south-southeast (8.1) west-southwest – east-northeast (8.2) east – west	
	(4) north – south (3) north-northeast – south-southwest	(5) west-southwest – east-northeast		(3.1; 4.2) north-northeast – south-southwest (3.2; 4.1) north – south (3.3; 5.3) northeast – southwest (4.2) north-northeast – south-southwest (4.3) north-northwest – south-southeast (5.1) west-southwest – east-northeast (5.2) east – west	
Proterozoic			(2) east-northeast – west-southwest		(2.1) north-northwest – south-southeast (2.2) east-northeast – west-southwest (2.3) north-west – south-east (2.4) north – south
			(1) north-west – south-east		(1.1) north-east – south-west (1.2) north-west – south-east (1.3) north-northeast – south-southwest (1.4) east-northeast – west-southwest

* Strike-slip movement

The orientations of these stochastically-deduced principle structures, and of the related joints, are shown graphically in Figure 4.1. Note that numerous principle structure / related joint orientations may be defined by one line, whilst related joint orientations are not shown should they coincide with principle structure orientations. The theoretically-formed structures may then be compared to the observed structures.

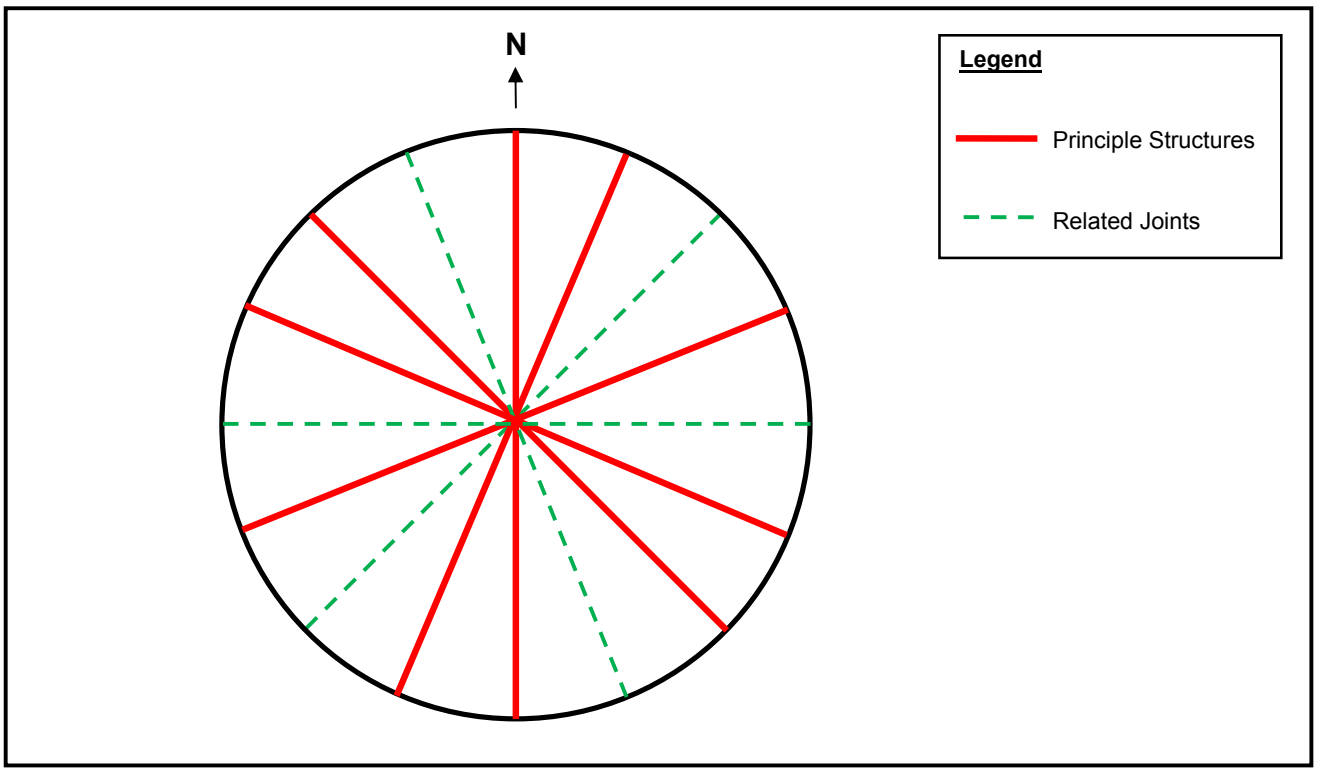

Figure 4.1: Stereographic illustration of principle structure orientations and theoretical joint orientations in the region surrounding the Shu Shu thermal springs (see Table 4.1 for details).

As is detailed by Sami *et al*. (2002), not all structures have the ability to transmit groundwater. This characteristic is typically dependent upon the mode of formation of the structure, the variation in the stress regime of the region since its formation and its current orientation with respects to the orientation of present σ_1, σ_2 and σ_3. Consequently broad analyses of the various formation events are required to detail the structural geological history of the region surrounding the Shu Shu thermal springs. Such an analysis is detailed in Appendix G: Additional Tectonic Evolution Information. However, a summary of the different tectonic (volcanic) events that may have resulted in these variably-orientated structures, in relation to the primary, secondary and tertiary inferred air-photograph lineaments and the structure orientations as determined through

the detailed outcrop mapping exercise and the geophysical investigation, is presented in Table 4.2.

Table 4.2: Likely Shu Shu thermal springs principle structure formation events.

Discovered Structure Source	(Oldest) Structure Formation Event (Youngest)				
	Mid-Cretaceous Extraction of the Falkland Plateau from the Natal Valley	**Cretaceous Break-up Separating East and West Gondwana**	**Jurassic-Cretaceous Fracturing of South-Eastern Gondwana Associated with Karoo Volcanism**	**Uplift Tectonics – Emplacement of Tugela Terrane onto the Margin of the Kaapvaal Craton**	**Accretion Tectonics – Crustal Thickening and Formation of Regional Deformation Fabrics (S_2)**
Detailed Outcrop Mapping (Local Scale)		Primary: NNW – SSE	Primary: NNW – SSE	Primary: NNW – SSE	
	Secondary: NE – SW	Secondary: NE – SW	Secondary: NE – SW		Secondary: NE – SW
	Tertiary: WNW – ESE				
Geophysical Investigation (Intermediate Scale)	FZ [1]: NW – SE			FZ [1]: NW – SE	FZ [1]: NW – SE
		FZ [2]: WSW – ENE	FZ [2]: WSW – ENE	FZ [2]: WSW – ENE	FZ [2]: WSW – ENE
		FZ [3]: NNW – SSE	FZ [3]: NNW – SSE	FZ [3]: NNW – SSE	
Photo-Geological Lineament Analysis (Sub-regional Scale)	Primary: WNW – ESE				
		Secondary: ENE – WSW	Secondary: ENE – WSW	Secondary: ENE – WSW	
	Tertiary: NNE – SSW		Tertiary: NNE – SSW	Tertiary: NNE – SSW	Tertiary: NNE – SSW

Although the formation of the principle structures in the region surrounding the Shu Shu thermal springs can be explained through various deformation events, the inconsistencies in primary, secondary and tertiary orientations at differing scales requires further analysis.

The primary detailed outcrop mapping structure orientation of north-northwest – south-southeast is observed at an intermediate scale, but not at a regional scale. This infers that these structures formed in relation to a small number of principle fractures orientated in a similar direction which pass near the springs. Indeed a sub-regional fault passes through the detailed outcrop mapping study area, and is observable on the regional geological map (Figure 2.2).

West-northwesterly – east-southeasterly orientated structures are seen at all three scales, and possibly owe their origin to normal faulting associated with a similarly-orientated mid-ocean ridge which formed during Cretaceous Gondwana break-up offshore of KwaZulu-Natal (Watkeys, 2002). Furthermore, structures orientated in a general north-east – south-west to north-northeast – south-southwest direction were mapped at a local and sub-regional scale

which confirms their significance in the tectonic evolution of the region. Although some of these structures may have formed in association with Natal Metamorphic Province accretion tectonics, it is likely the majority formed (and some were reactivated) during Gondwana break-up.

According to Sami *et al*. (2002), a thorough structural and geodynamic analyses of a region allows for the identification of the orientation of the three principle stress axes, but in particular, the orientation of σ_3. Broad analyses of the various deformation events, as detailed above, permits the completion of this task, and so consequently serves to highlight the orientation of those fractures perpendicular to σ_3, and hence the structures that theoretically exhibit greater transmissivity values. Anderson's (1951) theory of faulting, although possibly simplistic, is used to identify the orientation of σ_1, σ_2 and σ_3, in relation to the formation of the structures evident in the region surrounding the Shu Shu thermal springs (Table 4.3). Those structures orientated perpendicular to σ_3, or parallel to σ_2, are deemed to have possibly been open during their formation, and hence were able to transmit greater amounts of groundwater.

Table 4.3: Principle structure stress axis and theoretical open fracture orientations at time of formation.

Eon	Normal Fault / Thrust Fault Orientations	Principle Stress Axes Orientations			Orientation of Open Fractures
		σ_1	σ_2	σ_3	
Phanerozoic	(10) north-northeast – south-southwest	Vertical	NNE – SSW	WNW – ESE	NNE – SSW
	(9) east-southeast – west-north-west	Vertical	ESE – WNW	NNE – WSW	ESE – WNW
	(8) west-southwest – east-northeast	Vertical	WSW – ENE	NNW – SSE	WSW – ENE
	(7) north – south	Vertical	N – S	E – W	N – S
	(6) north-northeast – south-southwest	Vertical	NNE – SSW	WNW – ESE	NNE – SSW
	(5) west-southwest – east-northeast	Vertical	WSW – ENE	NNW – SSE	WSW – ENE
	(4) north – south	Vertical	N – S	E – W	N – S
	(3) north-northeast – south-southwest	Vertical	NNE – SSW	WNW – ESE	NNE – SSW
Proterozoic	(2) west-southwest – east-northeast	NNW – SSE	WSW – ENE	Vertical	WSW – ENE
	(1) north-west – south-east	NE – SW	NW – SE	Vertical	NW – SE

These principle orientations in which fractures were open at the time of their formation are included in Table 4.4, which denotes the variation in transmissivity state through the various deformation events, and hence those fractures actually able to transmit groundwater during the present time.

Table 4.4: Transmissivity state variation of principle fractures through deformation events.

	Deformation Event	Transmissivity State Variation	Legend
Proterozoic	Mid-Cretaceous Extraction of the Falkland Plateau from the Natal Valley	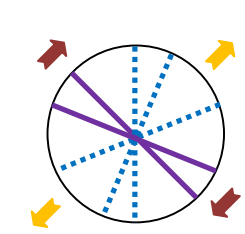	Closed fractures Open fractures Compression direction Extension direction Intermediate direction*
	Cretaceous Break-up Separating East and West Gondwana	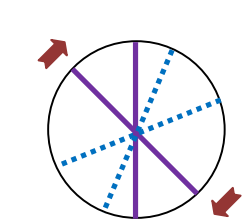	Closed fractures Open fractures Compression direction Extension direction Intermediate direction*
	Jurassic-Cretaceous Fracturing of South-Eastern Gondwana Associated with Karoo Volcanism	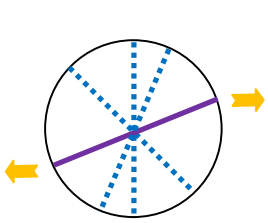	Closed fractures Open fractures Compression direction Extension direction Intermediate direction*
Phanerozoic	Uplift Tectonics – Emplacement of Tugela Terrane onto the Margin of the Kaapvaal Craton	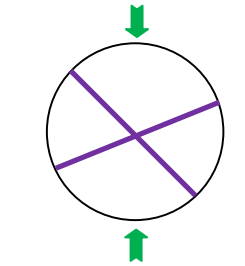	Closed fractures Open fractures Compression direction Extension direction Intermediate direction*
	Accretion Tectonics – Crustal Thickening and Formation of Regional Deformation Fabrics (S_2)	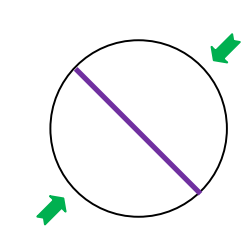	Closed fractures Open fractures Compression direction Extension direction Intermediate direction*

* Strike-slip movement

As can be seen, after the mid-Cretaceous extraction of the Falkland Plateau from the Natal Valley, all of these principle structures, save the northwest – southeast and west-northwest – east-southeast sets, would have been open and hence able to transmit elevated amounts of

groundwater. However, it is observable that north – south and north-northeast – south-southwest orientated structures do not occur in significant quantities in the region around the Shu Shu thermal springs, and hence likely do not account for movement of groundwater there-towards. Consequently, it is those structures orientated west-southwesterly – east-northeasterly that play a significant role in movement of thermal waters both toward the Shu Shu thermal springs, and the surfacing therein. This orientation is perpendicular to the contact of the Archaean Kaapvaal Craton with the Natal Metamorphic Province.

An assessment of Figure 4.2 highlights the dominance of this trend with respect to sub-regional to regional fault orientations. This then typically denotes the importance of (sub-) vertical structures. However a horizontal component is generally recognized as being of equal importance (Healy and Hochstein, 1973). Furthermore, surfacing thermal waters typically require sufficient residence time at depth to allow for the movement of heat through conduction from the wall rocks and into the groundwater (Durance and Heath, 1985). The cross-sections included in Appendix C illustrate the apparent decreasing dip of certain thrust structures in the region surrounding the Shu Shu thermal springs at depths of ~1200 m below mean sea level and onwards. It has been shown that when reactivated and subjected to extension, these structures have the ability to transmit elevated amounts of groundwater (cf. Sami *et al*., 2002). Consequently it can be said that not only do these structures allow sufficient residence time at depth for circulating groundwaters, they also promote surfacing. When considering only the Shu Shu thermal springs, it becomes apparent that once thermal waters have risen near surface along the west-southwesterly – east-northeasterly fault, they abut against the north-northwesterly – south-southeasterly fault, through which cold groundwater likely migrates, which results in their surfacing. This is confirmed by the fact that partially thermal waters were detected in BH 1, which was drilled to intersect this structure.

4.2 Local Hydrogeology

The local hydrology of the area, as determined through hydrochemical and isotopic investigations, is detailed hereafter. This ultimately allows for the source and evolution of the thermal waters to be assessed.

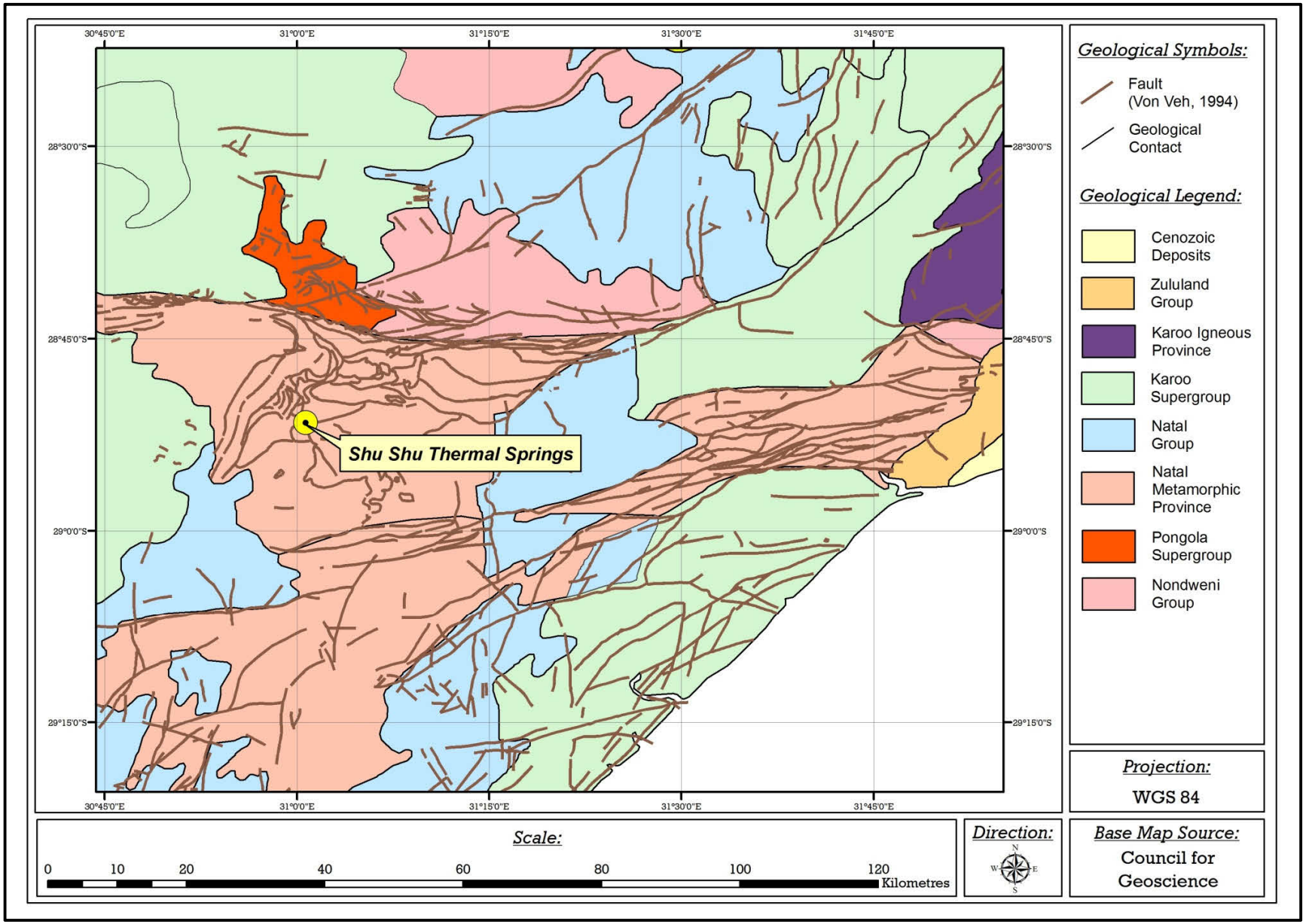

Figure 4.2: Basic geological fault map showing the distribution of faults in the region surrounding the Shu Shu thermal springs.

4.2.1 Surface Water and Groundwater Hydrochemistry

This study concurs with Gevers (1942) and Kent (1949) in that the hydrochemistry of the Shu Shu thermal spring waters is attributable to the geological units in which the groundwater circulates (as detailed in Appendix H: Hydrochemistry of the Shu Shu Thermal Springs and Surrounds). Whilst the majority of the dissolved constituents owe their origins to dissolution of the metamorphic rocks in the region, SO_4 concentrations are attributable to the oxidation of pyrite at depth. The hydrochemical signatures of shallow groundwater in the region share a similar origin, although anthropogenic influences on the concentrations of certain major and minor determinants (Mg and NO_3) and trace elements (Zn) are detectable. This is also typically applicable to the waters flowing in the adjacent Tugela River. The varying hydrochemical water types / facies of the different groundwater and surface water sources, sampled during various seasons, are included in Table 4.5.

Table 4.5: Groundwater and surface water hydrochemical water types / facies.

Sample Name	Sampling Date	Sample Code	Hydrochemical Signature
Groundwater Sources			
Shu Shu Thermal Springs – Sement Bad	2010-07-05	SB / 2010	Na-SO_4
	2011-06-13	SB / 2011	Na-SO_4
Shu Shu Thermal Springs – Wit Bad	2010-07-05	WB / 2010	Na-SO_4
	2011-06-13	WB / 2011	Na-SO_4
BH KZN6370227	2010-07-05	BH 1 / 2010	Na-SO_4
	2011-06-13	BH 1 / 2011	Na-SO_4
BH KZN204078	2011-04-28	BH 2 / Late Summer	Na-HCO_3
	2011-08-25	BH 2 / Late Winter	Na-HCO_3
BH KZNINK35	2011-04-28	BH 3 / Late Summer	Mg-Cl
	2011-08-25	BH 3 / Late Winter	Mg-Cl
Surface Water Sources			
Tugela River	2010-07-05	TR / 2010	Na-HCO_3
	2011-06-13	TR / 2011	Mg-HCO_3

These hydrochemical signatures, which have been determined from Figure 4.3, identify different water types and are indicative of the water sources' flow path evolution.

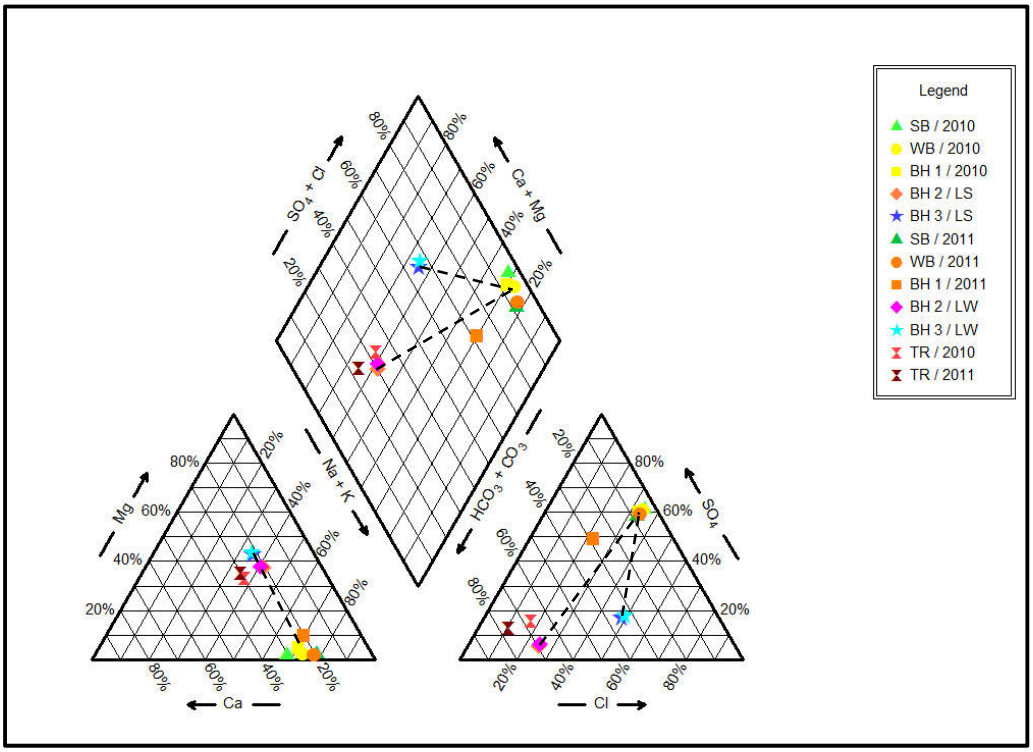

Figure 4.3: Groundwater and surface water Piper (1944) plot showing water types (indicative of flow path evolutions), and selected, possible intermixing lines.

The consistency in hydrochemical signatures observed across the Shu Shu thermal springs samples, and the BH 1 samples, once again confirm a common origin. The lack of a Mg and a HCO_3 component and the presence of a SO_4 component in the thermal water samples, as compared to those collected from BH 2 and BH 3, typically represent the dominant variation in water types across the samples having prolonged interaction times with lithologies in the study area. The absence of the former is likely attributable either to the precipitation of chlorite or actinolite, or to adsorption onto clay minerals, both of which typically account for very low Mg concentrations characteristic of thermal waters (Karangithi, 2009). The variation in the presence of a SO_4 component likely confirms the findings of Gevers (1942), with the dissemination of pyrite and associated solubility of SO_4 typically enhanced at higher temperatures. A Cl component is typical of groundwater sources, as is observed in the BH 3 samples, as it is a hydrochemical evolution product. This concept may account for decreased Cl concentrations in the Tugela River as this watercourse forms part of a flushed system in which hydrochemical evolution may only be fully complete toward ultimate base level.

The Piper (1944) plot of all these water sources yields interesting results as the time-dependant variation in the Shu Shu thermal springs samples and the BH 1 samples merely suggest partial dilution in 2011. This is suggested as a result of the typical proximity of their plot positions across the two sampling periods, which is common should two different samples display a constant ratio in concentration between two different determinants. Indeed, as is evident from the hydrochemical water types, the shallow groundwater samples too display similarity with only the plot positions of the Tugela River samples varying from 2010 to 2011. This is thought highly possible due to the potential variability in seasonal anthropogenic and climatic effects.

The position of the surface water and groundwater samples within the central diamond confirm that all but one type of water is typically represented by this hydrogeological system. The Shu Shu thermal springs samples and the BH 1 samples from 2010 and 2011 are all dominated by old water as they are relatively enriched in Na (and possibly Cl) which suggests they are nearing their end point in the water evolution sequence as these are hydrochemical evolution products. However, their plot positions along the upper right boundary infer a slight stagnant water component due to the supposed presence of $CaSO_4$- / $MgSO_4$- and $CaCl_2$- / $MgCl_2$-rich groundwater. The samples collected from BH 3 during late summer and late winter too show a stagnant water component, which is prevailing although not dominant. The proximity of the BH 2 late summer and late winter samples and those collected from the Tugela River in 2010 and 2011, is observed, with these samples possibly representing recent water; water that has been recently recharged and hence contains elevated amounts of $CaHCO_3$ / $MgHCO_3$. This is somewhat surprising as ^3H measurements do not infer recent recharge for the BH 2 / late summer sample, although a dynamic water component in the samples may explain such a trend.

Further classification diagrams, in the form of Giggenbach (1991) and modified Giggenbach (1991) triangles are included in Figure 4.4 and Figure 4.5. The plotting positions of the various groundwater samples in Figure 4.4 are expected with the Shu Shu thermal spring samples closer to an equilibrium state than the borehole samples. In accordance with the classification and equilibrium lines given by Gianelli *et al*. (1997), it can be seen that none of the samples have reached full equilibrium, with only the Shu Shu thermal spring samples and the BH 1 samples possibly just falling within the partial equilibrium field. This is possibly unexpected given that the Piper (1944) plot infers that these samples have likely reached the end point of their evolution sequence. In Figure 4.5, the Shu Shu thermal spring samples and the BH 1

samples fall within the steam-heated waters field, as delineated by Gianelli *et al*. (1997). This is likely due to the increased concentrations of SO_4 as the dominant anion, as a result of the dissemination of pyrite at depth.

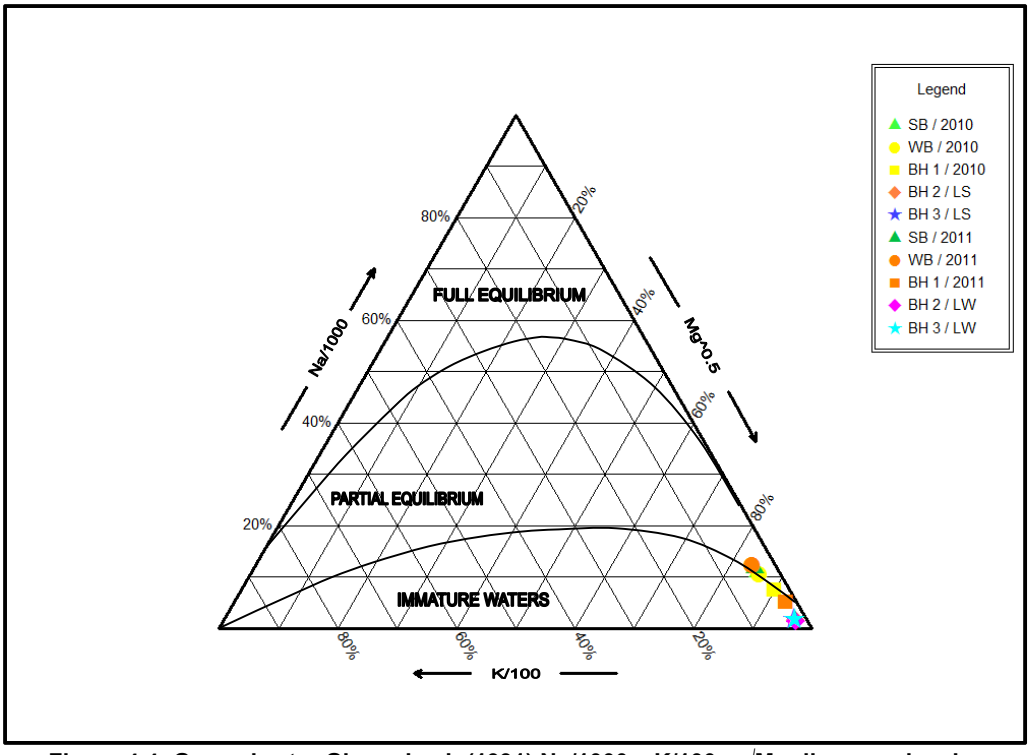

Figure 4.4: Groundwater Giggenbach (1991) Na/1000 – K/100 – √Mg diagram showing equilibrium states (note that only applicable samples have been included).

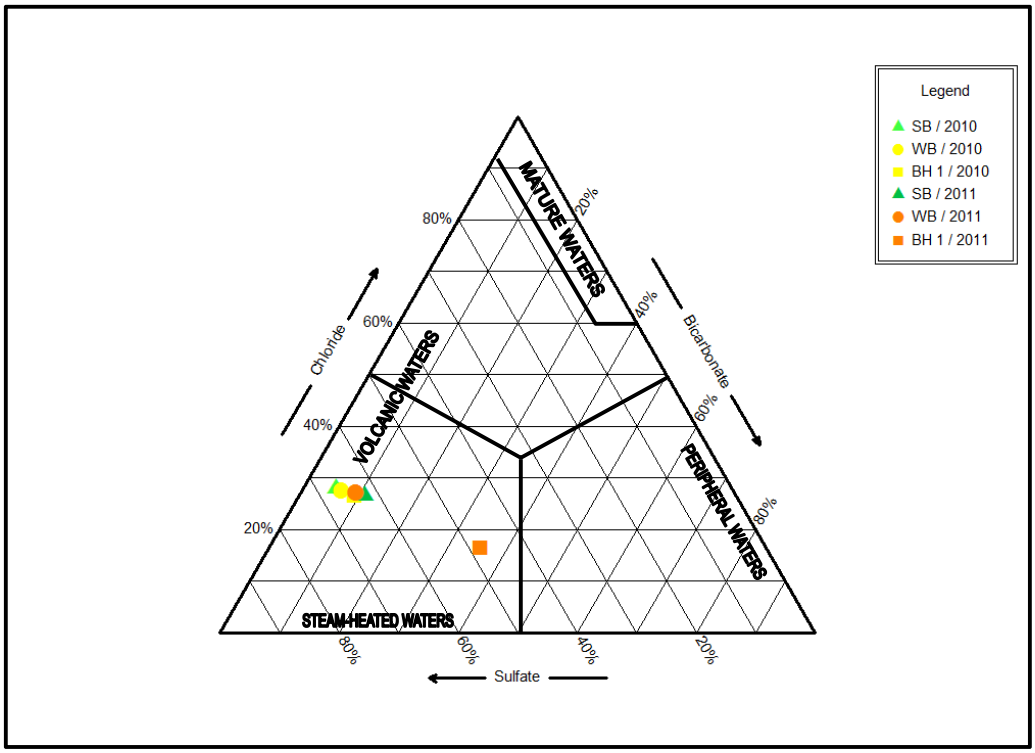

Figure 4.5: Thermal groundwater modified Giggenbach (1991) Cl – HCO_3 – SO_4 diagram showing water types (note that only applicable samples have been included).

Included as Figure 4.6 is a Ca – Mg – Cl ternary plot, which further assists in classifying the various groundwater types. Increased concentrations of Mg in some of the cold groundwater samples prove a general lack of thermal component, although decreased concentrations thereof in the BH 1 samples suggest intermixing. The subsequent quantification of prevailing intermixing processes is troublesome at best, particularly in a study area devoid of shallow and deep exploration boreholes. It is addressed in further detail hereafter through an assessment of the measured physio-chemical and major, minor and trace element compositions of the sampled water sources. A relatively increased Ca component across the 2011 Sement Bad, Wit Bad and BH 1 samples confirm increased dissolution from country rock, whilst the dominance of Cl across all of these samples, but especially 2011 Sement Bad, Wit Bad and BH 1 samples, substantiate a meteoric origin.

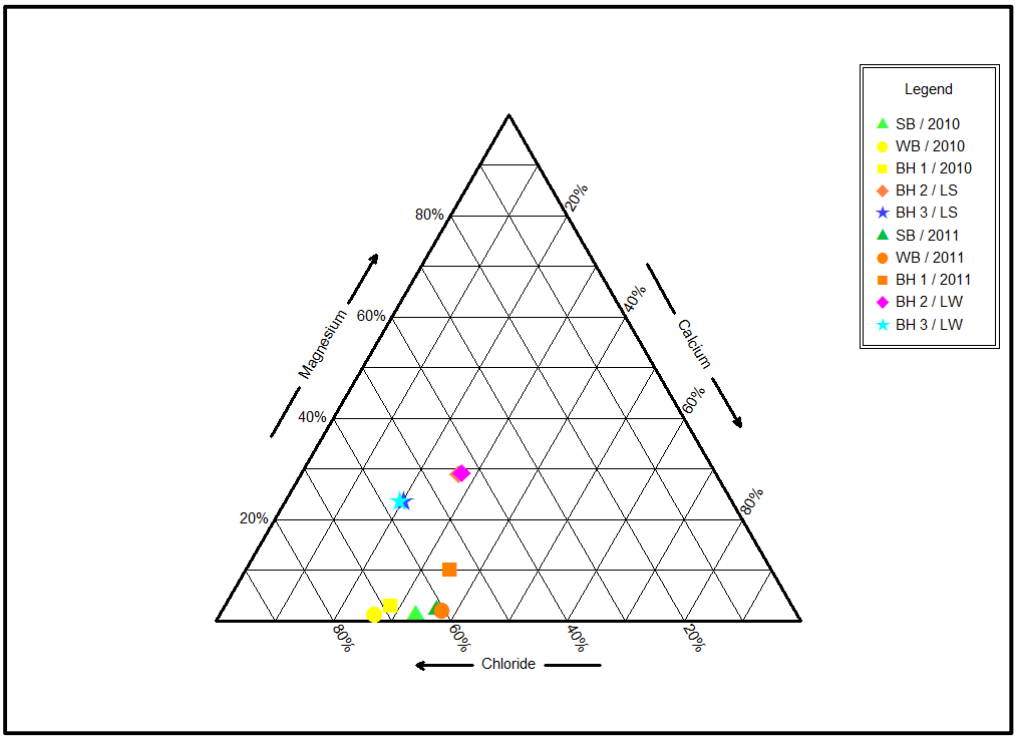

Figure 4.6: Groundwater ternary Cl-Ca-Mg classification diagram showing water types (note that only applicable samples have been included).

Trace element concentration assessments are typical of geothermal investigations, given that some are elevated relative to others when present in hydrothermal systems. Such assessments often allow for the identification of thermal water source zones, adsorption and dissolution processes, geothermometer accuracy analyses and groundwater hydrochemical evolution studies (Cortecci *et al*., 2005). These elements / metals are incorporated into ratios, whereby greater values denote the significance of thermal (groundwater) sources.

Li:Na, Na:K, Li:Mg, Cs:Na, Sr:Mg and Al:Na ratios have been calculated from the available hydrogeochemical data, and are included in Appendix H: Hydrochemistry of the Shu Shu Thermal Springs and Surrounds. Note that these trace elements were selected given their elevated concentrations in the thermal water sources. It is evident that the thermal waters sampled from the Sement Bad represent a slightly more dominant geothermal component, however variations are in evidence when Sr, Mg and Al concentrations are incorporated into ratios. When assessed in accordance with the rock geochemistry, and given observed consistencies and ratio patterns, it is inferred that Li likely represents the most suitable geothermal indicator metal.

4.2.2 Isotopic Analysis: Origins of the Thermal Waters

With the exception of the storm-event rainfall sample collected in summer, the stable isotope rainfall data plot along the KZN LMWL (as provided by E. van Wyk (pers. comm.)). Schwartz and Zhang (2003) refer to the fact that the location of the samples along the LMWL is typically determined by the continental effect, the altitude effect and the latitude effect. However the ratio of ^{2}H to ^{18}O appears to remain constant across the limited set of data available. The storm-event rainfall sample collected during summer is depleted in the heavier oxygen isotope (^{18}O) and deuterium. According to Abbott *et al*. (1999), this may be attributable to minimal fractionation by rainout resulting from a localised cloudburst. This may be due to the amount effect (Dansgaard, 1964; Rozanski *et al*, 1993; Scholl *et al*, 2009), although neither the frequency nor spatial variation of sampling was adequate to correctly quantify such effects.

The Shu Shu thermal springs samples and the thermal borehole samples plot above the GMWL and just below the LMWL and so these thermal waters are definitely meteoric in origin. The Tugela River samples, which plot away to the upper right of the rainfall and groundwater samples, are enriched in ^{18}O and ^{2}H and so clearly reflect the effects of selective fractionation associated with evaporation from an open source. Consequently a stable isotopic relationship does not exist between the Shu Shu thermal springs waters and the waters in the Tugela River. These findings are consistent with those at numerous other thermal springs and their nearest rivers throughout South Africa (Mazor and Verhagen, 1983). Evaporative effects acting on the water in the Tugela River preclude a comparison to the LMWL, and hence the regional recharge area cannot be identified. However, although it is possible that limited local recharge may have occurred, the geomorphology of KwaZulu-Natal suggests a source area away to the west at higher altitudes.

Although meteoric in origin, the Shu Shu thermal springs samples, and half of the various borehole samples, plot (just) below the LMWL. Diamond and Harris (2000) describe the effects of isotope exchange between rock and water as a possible explanation for this observed variation. It is often observed that isotopic signatures of groundwater are altered due to the exchange of ^{18}O between the water and the rocks through which they pass, with this commonly being observed in volcanic areas (Diamond and Harris, 2000). Should this have occurred, then according to Diamond and Harris (2000), only ^{18}O values would be affected, due to the fact that rocks generally comprise up to 50% O_2, whilst typically containing very little H. However, it is mainly a variation in ^{2}H values that are observed between the LWML and the Shu Shu thermal

spring and borehole samples. Furthermore, if indeed ^{18}O exchange had occurred, these groundwater samples would have plotted further to left, as compared to the rainfall sample locations. Consequently, as such exchange reactions typically occur at temperatures elevated well above those measured at the springs (Diamond and Harris, 2000), and as ^{18}O exchange has likely not occurred, it can be stated that the maximum reservoir temperatures likely do not exceed 100ºC.

As groundwater – rock isotope exchange interaction does not account for the variation seen between these groundwater samples and the LMWL, Diamond and Harris (2000) reported four climatic processes to account for this shift. They include (a) recharge during an earlier period of colder climate; (b) the amount effect; (c) the continental effect and (d) recharge at higher altitude. Mazor and Verhagen (1983) discounted recharge during a colder climate as they observed very little correlation between O_2 and H isotope ratios and ^{14}C data (which was used as a measure for time). Furthermore, the similarity observed between the plotting positions of late summer shallow groundwater (BH 2) and 2010 Shu Shu thermal spring water discounts the possibility of selective recharge of deep waters during periods of intense rainfall (amount effect). This is attributable to the lack of consistency in isotopic signatures observed between the partially-thermal groundwater (BH 1) and the Shu Shu thermal spring water, as the former is more likely to have tapped a deeper aquifer than the shallow groundwater. Consequently recharge at higher altitudes and further inland has resulted in the variation observed between the groundwater samples and the LMWL. The exact area would be difficult to identify without historical rainfall isotope data but the recharge area must be to the west given the geomorphology of KZN.

The variation observed between the Shu Shu thermal spring samples / half of the borehole samples and the plotting positions of late winter shallow groundwater (BH 2 and BH 3) / late summer shallow groundwater (BH 3) is noted, as the latter plot well below and to the right of the former. That these shallow groundwaters are meteoric in origin is beyond contestation given their proximity to the GMWL. However they do appear to have been affected by one or more subsurface / climatic processes. ^{18}O exchange with country rock is unlikely given their low temperatures as is the possibility that these shallow groundwaters were recharged during an earlier period of a colder climate due to limited residence times. Selective recharge from a deep aquifer during periods of intense rainfall may have occurred, although the impact there-from is likely minimal when considering the effects of attenuation (reduction of the effect of such waters,

due to infrequent recharge) and the local geomorphology of the area. Consequently a variation in recharge area must account for the difference in the observed isotopic signature. Note that whilst this variation is greater for ^{2}H as opposed to ^{18}O, given the relative masses of the two, levels of the former have decreased, whilst those of the latter have increased. This is unexpected as Diamond and Harris (2000) clearly state that a relationship exists between these two isotopes and any changes in the levels of one should be similarly reflected in the other. The much lower ^{2}H values in the shallow groundwater, as opposed to the thermal waters, may be attributable to a lower 'deuterium excess' (*d*) in the former, where $d = \delta D - 8\delta^{18}O$ (Dansgaard, 1964), with levels thereof elevated in areas of greater humidity. Local recharge (although decreased humidity levels are unlikely) or seasonal recharge (during the winter months) may therefore account for the isotopic signature of the shallow groundwater. Yet, once again, neither the frequency nor spatial variation of sampling was adequate to correctly quantify such effects.

As is described by numerous authors (Fontes, 1980; Mazor, 1991; Abbott *et al*., 1999; Schwartz and Zhang, 2003), the uncertainty and complexity of atmospheric loading typically provides difficulty in interpreting ^{3}H data. Even when values of ^{3}H in water are known, the tritium half-life decay equation cannot simply be used to determine absolute age. Atmospheric thermonuclear testing in the early 1950s to late 1970s resulted in ^{3}H loading which is today only just detectable in South Africa. Consequently any samples that contain ^{3}H must contain a component of water that was recharged in the last 61 years, or post-1952 (the year in which nuclear testing commenced) (Fontes, 1980). Note that water sources that do not contain detectable amounts of ^{3}H were not necessarily recharged pre-1952, as radioactive decay may have accounted for the lack of ^{3}H that may have once been detectable, should the water have been recharged recently. In the study area though, given ^{3}H values in rainfall, this does not seem applicable.

The presence of ^{3}H in the rainfall samples is expected, with the slightly comparatively increased levels thereof in the cumulative samples possibly reflecting the effects of attenuation. These effects are likely observable in the samples collected from the Tugela River which, although is likely recharged by rainfall, contains comparatively greater levels of ^{3}H. Such an interpretation is given as radioactive decay and anthropogenic influences are discounted here as possible sources of ^{3}H level alteration. The variation in ^{3}H levels in the groundwaters sampled during 2010 / late summer and 2011 / late winter is clearly observable, with the latter seemingly recharged well after (more recently than) the former. Considerably different recharge areas or a

significant variation in residence time, which may otherwise account for such a variation, are disregarded here for the thermal waters considering the regional flow patterns which maintain the springs. However, shallow groundwater does not appear to have a consistent residence time, and may be recharged intermittently by rainfall, although not immediately. Consequently then, intermixing between deep thermal waters and shallow groundwater must account for the sudden variation in the levels of ^{3}H in the former, thereby highlighting the existence of a relationship between the two.

4.3 Heat Source, Maximum Reservoir Temperatures and Active Hydrogeological Processes

The heat source, and maximum reservoir temperatures, is / are inferred below through the use of indirect methods, which are based upon the stable isotope, physical and hydrochemical data of the surfacing thermal waters.

4.3.1 ^{13}C Stable Isotope Datum Analysis

The analysis of the limited available $\delta^{13}C$ values, which include only BH 1 / 2011 results, cannot be used to suggest a magmatic / partially mantle-derived origin for the CO_2 surfacing in the thermal springs. This is due to the fact that the ^{13}C in the sampled water sources is typically comprised predominantly of HCO_3, as opposed to CO_2 (cf. Geyh, 2001), whilst any CO_2 that may have been present in the sample may have been lost during sampling exercises and laboratory submission via atmospheric interaction. Furthermore, the $\delta^{13}C$ results from only one sample cannot be accepted as being scientifically representative of prevailing conditions, whilst low HCO_3 / CO_2 concentrations in the sampled water sources also reduces analysis accuracy (cf. Geyh, 2001). Consequently, whilst the available $\delta^{13}C$ results do not preclude the possibility of a magmatic / partially mantle-derived origin for the CO_2 surfacing in the thermal springs, they cannot be utilized to infer the existence of such a theory. However, the determined $\delta^{13}C$ value in the sample collected from BH 1 in 2011 does fall within the range of naturally-occurring HCO_3 in groundwater (Geyh, 2001). This is uncommon in groundwater sourced from fractured amphibolite and gneiss which clearly exhibits a thermal signature, and suggests a component of shallow, cold groundwater.

4.3.2 Active Hydrogeological Processes: Intermixing at Shallow Depths?

The notion of intermixing of deep, thermal groundwater with shallow, cold groundwater has already been mentioned, with the variable hydrochemistry of the Shu Shu thermal spring and

BH 1 samples likely attributable to this process. Intermixing of different, sampled water types is explored in more detail hereafter.

In accordance with Guangcai *et al*. (2005), geochemical speciation modelling was undertaken such that an understanding of hot water – rock interaction equilibrium could be attained. Selected mineral saturation indices, according to those detailed by Guangcai *et al*. (2005), for the Shu Shu thermal spring and BH 1 samples, which are included in Table 4.6, were determined through the use of hydrochemical parameter concentrations and measured emergence / sampling temperatures.

Table 4.6: Empirically-derived saturation indices for selected minerals.

Mineral and Formula	Shu Shu Thermal Springs – Sement Bad		Shu Shu Thermal Springs – Wit Bad		BH KZN6370227	
	2010-07-05	2011-06-13	2010-07-05	2011-06-13	2010-07-05	2011-06-13
Anhydrite ($CaSO_4$)	-1.15	-1.47	-1.31	-1.49	-1.39	-1.61
Aragonite ($CaCO_3$)	0.2	0.25	0.39	-0.01	0.02	0.23
Calcite ($CaCO_3$)	0.32	0.38	0.51	0.11	0.17	0.37
Chalcedony (SiO_2)	-0.5	-0.01	-0.74	-0.94	-0.41	0
Dolomite ($CaMg(CO_3)_2$)	-0.36	-0.81	0.14	-0.6	-0.34	0.56
Gypsum ($CaSO_4:H_2O$)	-1.08	-1.41	-1.23	-1.4	-1.16	-1.4
Quartz (SiO_2)	-0.18	0.34	-0.41	-0.58	0	0.42

Note that for the sake of simplicity, 0 has been employed as the break-point, which hence implies that when saturation indices are positive, then precipitation will occur, whilst if they be negative, then dissolution is likely.

As Guangcai *et al*. (2005) state, information pertaining to hot water – rock equilibrium can be used to deduce the recharge characteristics of groundwater. The variation in saturation indices, which primarily arises due to variable hydrochemical parameter concentrations across different sampling events, is particularly evident amongst aragonite, calcite, chalcedony, dolomite and quartz. Undersaturation of dolomite typically suggests groundwater recharge in up-gradient areas of regional flow systems. However in contrast, equilibrium or oversaturation of carbonate minerals, such as aragonite in this study, may occur when groundwater has had extended contact with certain Ca-bearing minerals (Guangcai *et al*., 2005). This apparent inconsistency in flow system characteristics is indicative of dynamic subsurface conditions associated with

intermixing. Indeed Guangcai *et al*. (2005) state that a decrease in saturation and certainly undersaturation may occur with respect to calcite due to shallow, cold groundwater intermixing with rising thermal waters. The former is observed across the Shu Shu thermal spring and groundwater samples collected in 2011. Furthermore, as was observed in the field, Gevers (1942) identified silica in the immediate vicinity of the Shu Shu thermal springs, which he attributed to precipitation from thermal water. It is likely that the thermal spring waters were originally oversaturated with respects to silica minerals, however upon precipitation, due to a decrease in temperature associated with intermixing, the saturation indices dropped to that which is shown in Table 4.6 (as the thermal water sources were sampled post-precipitation).

Further evidence of hydrogeological intermixing processes is observed. Natural groundwater circulating at depth in the lithological units in the region likely exhibits an acidic pH. As a result, original pyrite is disseminated at depth, as detailed by Gevers (1942). Although this may account for small quantities of SO_4 in the thermal waters, the reducing conditions under which this occurs typically results in the formation of H_2S, which is seen bubbling up in the thermal springs. However, subsurface intermixing with shallow, cold groundwater results in the oxidation of H_2S, such that concentrations rapidly decrease to those measured by Gevers (1942), whilst SO_4 concentrations increase upon surfacing. Furthermore, although calcite might precipitate out of the thermal waters upon rising, as a result of a drop in pressure (which decreases the solubility of Ca), the increased concentrations of HCO_3 from shallow, cold groundwater likely once again result in calcite oversaturation. This then raises the pH above neutral toward those basic values measured in the Shu Shu thermal spring waters in 2010 and 2011, whilst the positive calcite saturation indices in Table 4.6 are then accounted for (as is the presence of calcite along principle fractures).

The possibility of intermixing is further explored and possibly partly quantified through the use of bivariate scatter plots. In Figure 4.7 a – p the concentrations of the thermal water sources have been plotted against the Mg concentrations of the samples collected from BH 2 and BH 3 in 2010 and 2011. The conservative value of Mg is used in this study as an end-member due to the observed variation of this determinant in thermal and non-thermal waters. Note that meq/l is used as the unit of choice to allow for comparison on a molar basis, and furthermore to ascertain the relevant importance of Mg and hence the possible degree of intermixing.

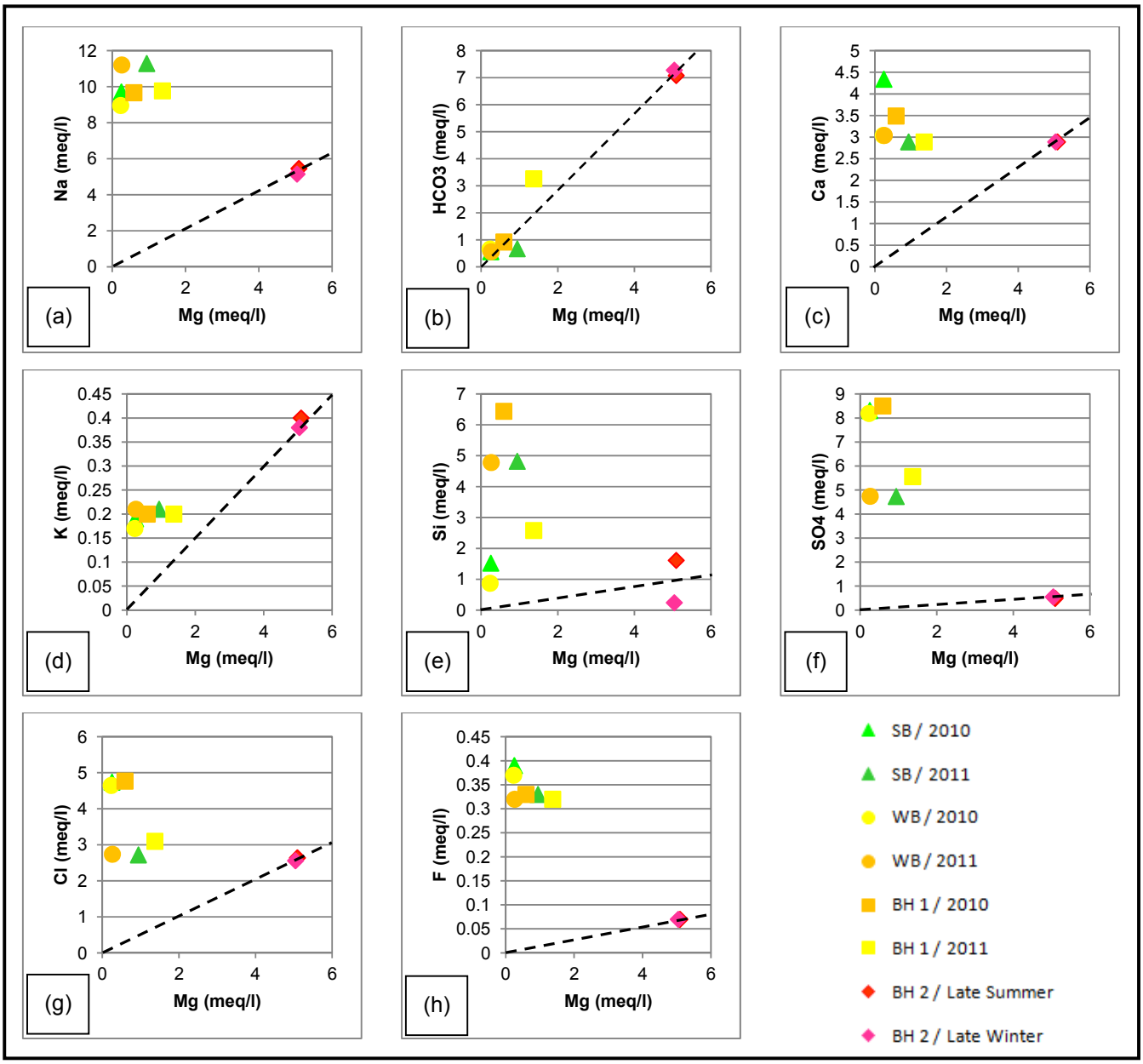

Figure 4.7 (a – h): Relationship between various ions in Shu Shu thermal waters versus BH 2 Mg concentrations with intermixing lines shown.

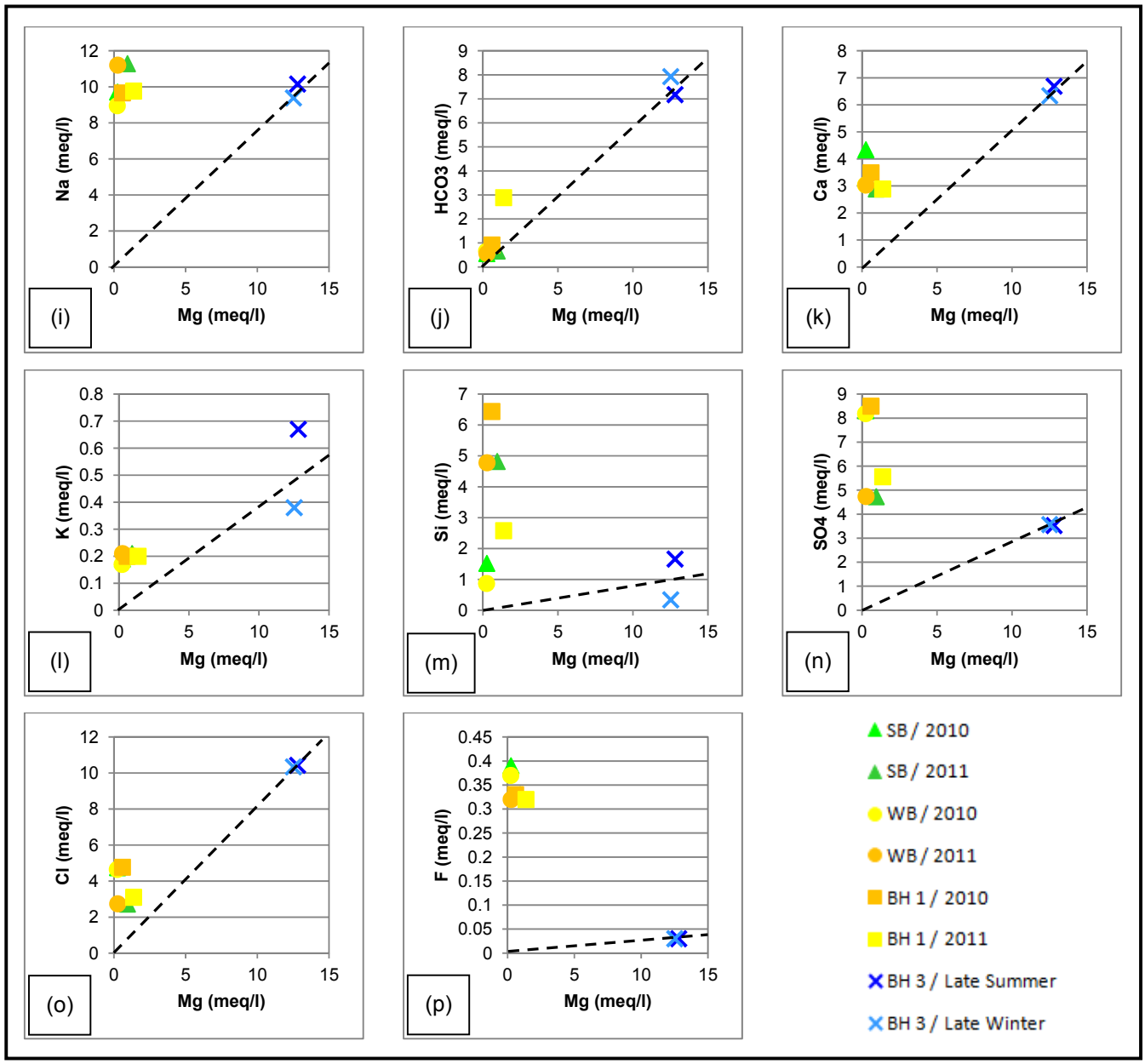

Figure 4.7 (i – p): Relationship between various ions in Shu Shu thermal waters versus BH 3 Mg concentrations with intermixing lines shown.

The X-Y graphs of BH 2 and BH 3 generally display similar trends across all determinants and intermixing lines; the only exception with respects to the latter being those of SO_4 and Cl (as discussed hereafter). El-Fiky (2009) states that when the thermal waters plot along the intermixing line as drawn from the origin through the determinant concentrations of the selected end-member, a good correlation exists that is attributable to intermixing. In light of this, and

after an assessment of Figure 4.7 a – p, it can be seen that although intermixing likely does occur, the hydrochemistry of the thermal waters is not strongly influenced.

This is clear in the Mg-HCO_3 graphs, as a correlation should not exist between these two given that Mg concentrations are low in thermal waters, whilst HCO_3 are typically elevated in shallow groundwaters. Generally however, as samples plot above the intermixing line, it can be seen that the thermal waters are enriched in the particular determinant as opposed to the shallow groundwater samples. Note though, that the position of the thermal water sources above the intermixing line possibly implies the contribution of such determinants from other (variable) sources. Given that the thermal waters appear to have reached (at least) partial equilibrium, these contributory determinants may be (partly) indicative of shallow groundwater intermixing. This is perhaps best illustrated in the SO_4 and Cl bivariate plots, across BH 2 and BH 3, where two distinct year-based groupings are in existence. These two determinants are characteristic of thermal waters (at Shu Shu), yet it would appear that in 2011, greater intermixing occurred. This highlights the variability associated with intermixing, as does the appreciable variation in the positions of the various samples in the Si-Mg plots.

The gradient of the intermixing line typically defines the degree of intermixing, with steeper lines suggesting a greater shallow groundwater influence in this study. It can be seen that the thermal waters appear to show a greater degree of intermixing with BH 3 groundwaters, due to the determined correlation values. This is in accordance with the findings of the Piper (1944) plot (Figure 4.3), where greater similarity in the plotting positions of the BH 3 samples to the thermal water samples in the (thermally-dominant) anion triangle is observed. It hence seems plausible to suggest that the thermal waters may diffuse into the BH 3 aquifer, which hence accounts for that which is observed, however this merely a tentative notion.

This is furthered upon through an assessment of the BH 2 and BH 3 trace element ratios, in accordance with that performed by Cortecci *et al*. (2005). Given the variability in Sr, Mg and Al concentrations, the use of Li as a geothermal indicator metal yields interesting results. Actual Li concentrations are greater in the BH 3 samples, however as Na concentrations are too, Li:Na ratios are higher when the BH 2 sample data are evaluated. Of course Na concentrations in the former (as opposed to the latter) certainly show a greater similarity to those measured in the thermal sources, which may otherwise lend further credence to this notion. Unfortunately,

additional assessments of other trace element ratios remain difficult, given that Sr, Mg and Al concentrations do not appear uniformly representative of actual conditions.

Further evidence for intermixing is from the results of the temperature profiling of BH 1 (Figure 3.4). It is inferred that the rate of cooling observed below 38m (~169°C/km) is most representative of conditions at depth, with the slowest measured cooling rate (~70°C/km) attributable to other cooling processes (further information is included in Section 4.4.2). This value is in contrast to the highest cooling rate (~31°C/km) that might otherwise be in evidence, should sufficient time exist during the surfacing of the thermal waters to allow temperature re-equilibration with the country rock. Consequently, as observed, cooling rates are approximately five times those otherwise expected, and hence it can be stated that intermixing between the thermal waters and shallow, cold groundwater must occur beneath the springs at depths of more than 38m.

4.3.3 Chemical Geothermometer Analysis

Although the use of various geothermometer equations yield numerous possible maximum reservoir temperatures, it is important to remember that '*the choice and interpretation of geothermometer data are the art of the exploration geochemist*' (Karangithi, 2009). This is due to the fact that every geothermometer has its limitations which need to be considered in its use whilst numerous conditions exist on ascent of the thermal water to the surface which might act to change the prevailing hydrogeological conditions (as detailed by Allen *et al*., 2006). This may prove problematic in the use of geothermometers as it is typically assumed that no changes in water composition have occurred on ascension to the surface. According to Karangithi (2009), experience has shown that good conformity between geothermometer-determined maximum reservoir temperatures is indicative of equilibrium and as such, results are taken as accurate. However, although a variation in results typically denotes disequilibrium, this can be used to quantify various processes which are part of the geothermal system; this has been undertaken hereafter in accordance with the analysis completed by Allen *et al*. (2006). Disequilibrium appears a very strong possibility with respects to the Shu Shu thermal springs as geothermometer-derived maximum reservoir temperatures, which are greater than the surfacing temperatures, vary from ~58°C to ~157°C (Table 3.15). This is furthermore inferred given that which is learnt from the saturation indices presented in Table 4.6.

An initial assessment of the geothermometer results suggests that cooling on ascent to the surface is certainly possible. According to Truesdell *et al*. (1977), the temperature of thermal waters flowing from a 1km deep reservoir at 0.40l/sec in a vertical pipe flow model will reduce by half. Furthermore, when assessing remote thermal springs which exhibit flow rates of <1.00l/sec, conductive cooling is expected to be of significant importance. As the geographically isolated Shu Shu thermal springs typically flow at approximately 1.26l/sec, surfacing temperatures of ~50°C seem to be a minimum.

As various silica geothermometer (quartz, chalcedony or amorphous silica) equations were developed on the basis of experimentally-derived variations in the solubility of varying silica species (as a function of pressure and temperature), numerous thermal spring types under various conditions can be assessed (Karangithi, 2009). An initial assessment of the prevailing hydrogeological data is required however before geothermometer-derived maximum reservoir temperatures can be accepted. As the surfacing pH values of water in the Shu Shu thermal springs exceed 7.6, Fournier (1981) suggests increased solubility and hence an increased concentration of Si. This may initially act to overestimate reservoir temperatures, however the likelihood that the measured Si concentrations are those of post-precipitation must be noted and taken cognisance of, or at least considered.

Without exception, the lower Si concentrations observed from 2010 water quality have resulted in geothermometer-derived maximum reservoir temperatures which are lower than the surfacing temperature at the Shu Shu thermal springs. Therefore, only the reservoir temperatures from the 2011 water quality data have been assessed hereafter with respects to the silica geothermometers. Quartz geothermometer equations are best applied to deep fluids at temperatures in excess of 180°C as at this temperature, they are in equilibrium with quartz. Geothermometer (1) Quartz Fournier (1977) was initially developed for maximum steam loss conditions and is applicable to thermal springs with high discharge rates and silica sinter deposits evident. Due to the likely loss of Si on ascent, the maximum reservoir temperature of ~87°C may only be partly applicable. Geothermometer (2) Quartz Fournier (1977) is best applied to thermal springs whereby steam loss has not occurred but rather conductive cooling has; this defines a constant solute content from depth to surface. As higher Si concentrations were possibly originally in evidence, the determined temperature of ~84°C is possibly too low. The low levels of Si observed in the Shu Shu thermal springs samples from 2010 and 2011 are below the minimum for the amorphous silica curve developed by Truesdell and Fournier (1976),

even at excessively low temperatures. Consequently it is suggested that the groundwater circulating in the rocks of the Tugela Terrane is naturally devoid of elevated amounts of silica, and as such, the quartz-derived reservoir temperature of 69.44°C, as per the quartz curve suggested by Truesdell and Fournier (1976), may indeed only be partially representative of thermal conditions at depth.

The Na-K geothermometer is typically recognized as the most-used equation in geothermal exploration and subsurface assessments; its development has relied upon the experience gained in various geothermal fields (Santoyo and Díaz-González, 2010). This is likely due to the fact that geochemical processes, including intermixing with shallow groundwater and degassing, do not considerably affect the calculated maximum reservoir temperatures (Santoyo and Díaz-González, 2010). This is likely due to the response of the Na-K geothermometer being based upon a temperature cation exchange reaction between K-feldspar and albite (Karangithi, 2009). The numerous Na-K geothermometers that are in existence today have not necessarily been developed to suit specific springs types, as with silica geothermometers, but rather are based upon ever-increasing amounts of geochemical data from specific thermal spring areas.

Karangithi (2009) states that the Na-K geothermometer is typically suitable up to temperatures of 350°C, although water from high temperature reservoirs (180°C) generally yields more accurate results. It is preferred to the silica geothermometer by some exploration geochemists as its re-equilibration is slower, and as such may be indicative of the deeper part of a given geothermal system. However re-equilibration is possible at cooler temperatures and shallow depths in very slow rising fluids (Karangithi, 2009). Furthermore, on more rapid ascent to the surface, in waters at lower temperatures, the Na-K ratio is governed by leaching rather than equilibrium, thereby possibly delineating inaccurate reservoir temperatures. Such a variation without knowledge of prevailing geochemical and hydrogeological processes may result in difficulty being experience when assessing the performance of the Na-K geothermometer.

The Na-K geothermometer is limited in its application in two fundamental ways: (1) below 100°C, poor results are typically observed and (2) it is unsuitable when high calcium concentrations are present. An assessment of the Na-K geothermometer-derived maximum reservoir temperatures for the Shu Shu thermal springs reveals a range of ~68°C, from ~89°C to ~157°C; the former being just below the 100°C ‘threshold’. However, Karangithi (2009)

explicitly states that Na-K geothermometer should only be used when the equation below yields a negative value

$$x = \log\left(\frac{\sqrt{Ca}}{Na}\right) + 2.06 \qquad \text{Eq. 4.1}$$

Applying Shu Su thermal springs water quality data to this equation yields a positive value and as such calcium concentrations are too high to yield accurate results. Furthermore, the Na-K geothermometer is best applied to Cl waters that are near neutral; average thermal springs pH values of 8.31 therefore negate its use. Indeed these conditions may account for the higher range of reservoir temperatures as defined in Table 3.16, which are primarily attributable to Na-K chemical geothermometers.

Although the Na-K geothermometer does not yield appreciably high reservoir temperatures, which is a characteristic of thermal waters containing elevated Ca concentrations, the Na-K-Ca geothermometer is likely best applied. The use of this empirical equation is advantageous as compared to the standard Na-K geothermometer and silica geothermometer as it does not yield high or grossly misleading temperatures even for slightly thermal to cold, non-equilibrated waters. As Shu Shu thermal springs waters are neither acidic upon surfacing (although they likely are at increased depths), nor do they circulate in rocks with unusually high or low alkali concentrations, Karangithi (2009) states that this geothermometer is initially suitable for use. However a variation in the concentration of Ca in the thermal waters, which may result from cooling and dilution, will slightly affect the validity of the inferred maximum reservoir temperatures. According to Karangithi (2009), the principle effect of such an occurrence is the precipitation of calcite, a notion already established as occurring at the Shu Shu thermal springs. The consequent loss of dissolved Ca results in Na-K-Ca-derived maximum reservoir temperatures that are too high – the amount of error is typically proportional to the amount of CO_2 observed in the thermal waters. In accordance with Gevers (1942), who stated that only limited amounts of CO_2 could be captured to allow for a field titration, it is suggested that the Geothermometer Na-K-Ca Fournier and Truesdell (1973) maximum reservoir temperatures of ~79°C to ~81°C for 2011 Shu Shu thermal springs water quality data may only be slightly too high.

Note that when the Mg correction was applied to this equation, when utilizing 2010 water quality data, decreased reservoir temperatures of ~25°C to ~58°C resulted. This is despite the fact that such a correction is best applied to cooler temperature systems, although high

discharge rates, as detailed by Karangithi (2009), are not in evidence. It is interesting to note however, that the determined Mg concentrations in the waters of the Shu Shu thermal springs are highly in excess of the 'typical' maximum value of 0.20 mg/l described by Karangithi (2009) as defining the upper limit in waters hotter than 180°C; this indeed suggests lower reservoir temperatures below the Shu Shu thermal springs, even when possible intermixing is considered.

The remaining cation geothermometers have not found as much favour with exploration geochemists as they appear fairly condition-specific. Karangithi (2009) states that the K-Mg geothermometer is typically applied to thermal waters where dissolved Ca and Na have not equilibrated between the fluid and rock. This appears applicable to the Shu Shu thermal springs due to the precipitated calcite around the individual eyes. However this geothermometer re-equilibrates quickly at cooler temperatures and as such may infer incorrect maximum reservoir temperatures. The Na-Li geothermometer was developed on the assumption that the ratio of Na to Li is constant on ascent of the thermal waters to the surface. However, as stated by Karangithi (2009), Li is likely 'lost' to precipitation during cooling, and as such, incorrect reservoir temperatures may result. The possibility of such an occurrence is dependent upon whether cation exchange with clays along the fractures has taken place. Although Geothermometer Na-Li Kharaka *et al*. (1982) yields realistic temperatures of ~119°C to ~125°C, is does indeed seem likely that Li is 'lost' to precipitation upon surfacing, as these temperatures are likely too high.

An attempt to statistically analyse the results of the geothermometer assessment, using the techniques of Pirlo (2004) proved unsuccessful. This is due to the fact that an initial correlation and regression test performed on the individual silica, Na-K and cation geothermometer temperatures (when compared only to data within each of these same sets), yielded negative correlation values. This is consistent with the findings of the qualitative analysis undertaken above, and as Karangithi (2009) suggests disequilibrium in the thermal waters due to various geochemical processes being in evidence.

4.4 Conceptual Source Model: Shu Shu Thermal Springs

A conceptual hydrogeological model for the source of the Shu Shu thermal springs and possibly other thermal springs in the eastern interior of southern Africa is presented here.

4.4.1 Ultimate Maximum Reservoir Temperatures and Depths of Circulation

Although it has been shown that hydrogeological processes are variable below the Shu Shu thermal springs, an attempt is made to quantify the maximum reservoir temperatures and depths of circulation. Utilising the available geothermometer, stable isotope and physio-chemical data, it is suggested that the thermal waters emitted at the Shu Shu thermal springs reach a maximum temperature of between 75°C and 85°C at depth before surfacing. Such a value infers cooling not only through intermixing of deep thermal waters with shallow cold waters, but also a loss of heat upon ascension through conduction into the surrounding country rocks, and via the effects of the atmosphere. If the standard geothermal gradient for the region of 3.1°C / 100m is applied, then it is stated that these thermal waters descend to a depth of between ~1827m and ~2153m. It must be noted however, that assuming a linear relationship is a simplistic approach, as according to Allen *et al*. (2005), depth integrated geothermal gradients may vary up to 20%.

4.4.2 Source Models: Lebombo 'Monocline' and the Great South African Escarpment

In light of the work undertaken as part of this study, and that which has been determined and detailed above, these two possible source models are evaluated with respects to the Shu Shu thermal springs.

The Lebombo 'monocline' and the numerous thermal springs within eastern southern Africa within the north-northwest trending zone may share a common heat source. This particular notion, as first suggested by M. Watkeys (pers. comm.), is best detailed through the use of the extensional tectonic model proposed by Wernicke (1985). Wernicke (1985) propositioned a model based upon asymmetrical simple shear stretching of the lithosphere, which he applied to the Basin and Range Province which extends eastwards beneath the western margin of the Colorado Plateau and Rocky Mountain region. Of course the application of such a model to the Lebombo 'monocline' highlights another possible origin for its formation, as the possibility of off-shore tectonic structures may account for the consequent basin structure of the region. Such a possibility may highlight a relationship between the Lebombo 'monocline' and the numerous thermal springs within eastern southern Africa.

In Wernicke's (1985) model, the basin is stretched asymmetrically by a large-scale detachment fault which extends from the upper crust to the lower lithosphere, and possibly even the upper asthenosphere (Figure 4.8). This results in the formation of extensional allochthons, which in a South African model may coincide with the Lebombo 'monocline'. These would

however be located well away from the zone of thermal upwelling and so consequently, only limited amounts of thermal subsidence is accommodated. Indeed rather, the footwall of the shear zone likely experiences minor amounts of uplift due to latent heat from the asthenosphere, which will eventually sink back down to a 'typical height' after cooling (Buck *et al.*, 1988). This 'residual, thermal fingerprint' might coincide with the position of the north-northwest trending thermal spring zone in eastern South Africa, thereby so long as the required structures are in place, allows for the formation of so many thermal springs (M. Watkeys, pers. comm.). To complete the possible model, and as is shown, the Rooi Rand dyke swarm might be positioned in the area of thinnest crust, hence allowing for its formation.

Increased heat flow along the north-northwest trending zone, possibly in existence as a result of the formation of the Lebombo 'monocline' according to Wernicke's (1985) model can neither be proven nor disproven, through the resultant ^{13}C values measured in the Shu Shu thermal waters. Furthermore, should such a model be correct, it is questioned whether a 'remnant, thermal fingerprint' resulting from thermal uplift would be recognisable, and indeed present, within less than 2000m of the surface, thereby resulting in only a slightly increased geothermal gradient (as observed in comparison to the rest of South Africa) and hence the presence of numerous thermal springs. Although this source model remains a possibility in explaining the heat source, and hence possibly the spatial pattern, of the thermal springs, it fails to account for the recharge areas, whilst it is clear that the associated north – south orientated structures do not account for thermal water movement. Consequently, the possibility of a relationship existing between the Great South African Escarpment, and the southernmost six thermal springs in the north-northwest trending zone, is explored in more detail.

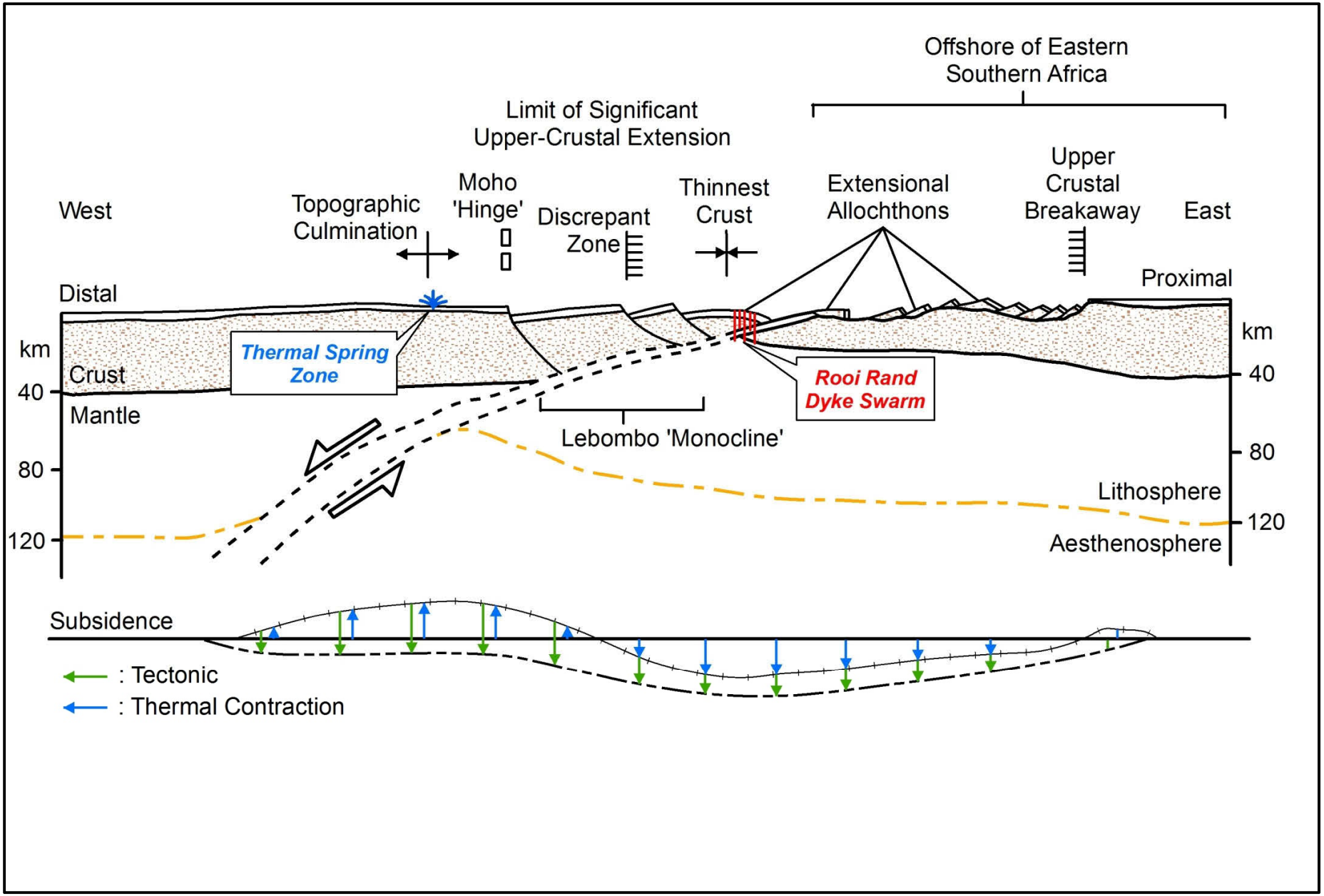

Figure 4.8: Asymmetrical simple shear stretching of the lithosphere (redrawn after Wernicke (1985) and annotated from M. Watkeys (pers. comm.)).

The preparation of a conceptual source model detailing a possible relationship between the Shu Shu thermal springs and the Great South African Escarpment is difficult. Such a model has not, as far as is known, been proposed before in published literature. It is considered best to further explore the topography of the region to the west of the thermal springs as is shown in Figure 4.9 through the use of a digital terrane model before embarking on the formulation of such a model as has been described. The topography of this region is shown through the use of ASTER (2011) imagery which is based upon 50m contour intervals.

Figure 4.9 has been employed to construct a topographical profile along line A – B as is shown. Although showing a vertical exaggeration of 15x, this profile has been used in the creation of a cross-section along line A – B (Figure 4.10) to aid in describing the possible relationship in existence between the thermal springs and the Great South African Escarpment. Such a relationship is best described by commencing with the recharge area of the Shu Shu thermal springs. This is ultimately inferred to be a small inland plateau east of the Drakensberg. However as is alluded to by the stable isotopic data, it is likely that rainfall to the east at lower altitudes also forms part of the hydrogeological system that surfaces at Shu Shu. It is suggested that prevailing infiltration and percolation characteristics allow the water to descend to depth, where it enters intermediate to deep flow systems, although the orientation of any dominant structures which allow for this are unknown. These meteoric waters descend to an average depth of ~1990m bgl at which point they would be at the temperature of the wall rock which at this depth and at the determined geothermal gradient would be approximately 80°C. This appears as a crucial depth however, as a characteristic of the rock at this depth must promote the movement of groundwater in an easterly direction toward the north-northwest trending zone of thermal springs.

It is firstly inferred that, due to an increasing confining pressure which acts equally in all directions (Van Der Pluijm and Marshak, 2004) and can be ascribed to the escarpment itself, the vertical structures that promoted percolation of the originally meteoric water to these depths no longer remain open. However, as Flemming *et al*. (1999) document, average plateau denudation rates of approximately 6.0m / Ma suggest that the actual depths at which the structures close will increase with time in relation to current values. The movement of these waters from west to east toward the thermal springs is attributed to the sudden drop in altitude that is experienced off the plateau resulting in a considerable variation in the mass of land in

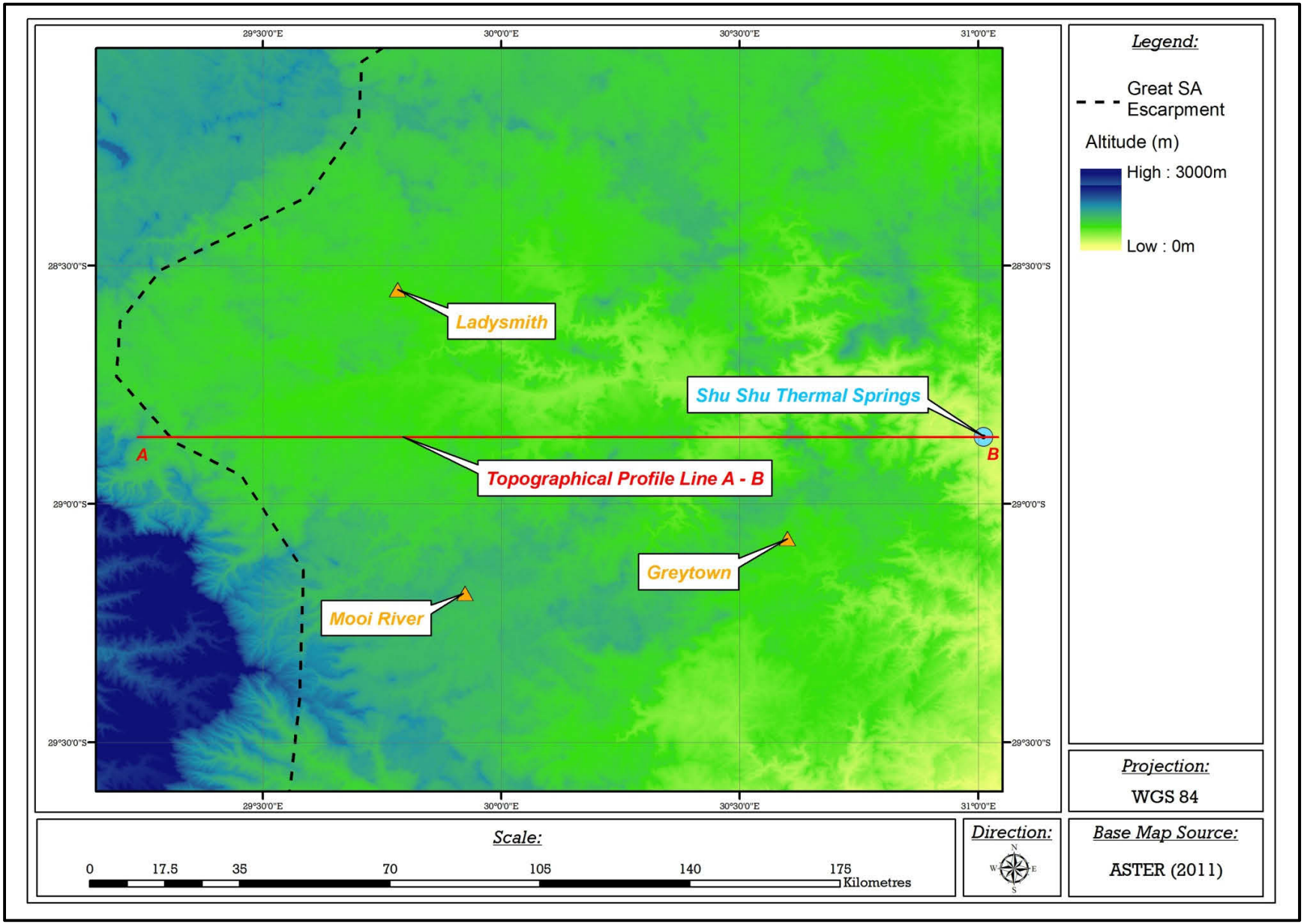

Figure 4.9: ASTER (2011) generated digital terrane model westwards from the Shu Shu thermal springs, with topographical profile line A – B shown.

existence above these key depths. Flemming *et al*. (1999) state that denudation rates of the Great South African Escarpment in KZN and thus its movement inland have occurred at 50m / Ma to 95m / Ma since the mid- to late-Cretaceous. Over millions of years this may lead to the migration of the north-northwest trending zone toward the west, whilst the recharge region of the thermal springs would remain at an approximately constant distance.

In relation to mean sea level, the maximum depths that the waters descend to, would correlate to an altitude of -740m (amsl), if the altitude of the recharge region is accepted as being at ~1250m amsl. Consequently, as the Shu Shu thermal springs are located at an altitude of 250m amsl, it is suggested that once below the 'coastal' plain, the thermal waters only rise approximately 990m. As has been calculated from Geomeasure Group (2001) recovery pump-test data, once in the basement rocks in the Tugela Valley, the groundwater migrates toward the Shu Shu thermal springs at an average rate of 0.20 m / day. Indeed if this value is accepted as an approximation of that which is in existence along much of the flow path, residence times can be estimated at ~2400 years. An increasing, confining pressure then likely promotes vertical, upward movement through the structures, as it is in this preferential direction that they remain open. The movement of the thermal waters to the surface is likely aided by a variation in both pressure (in relation to the elevated temperatures), and hydraulic / piezometric head; the latter due to a sizeable altitude difference as alluded to by Gevers (1942). It is from this depth that the waters start to rise and hence are affected by numerous, active hydrogeological processes, however this conceptual model may account not only for the Shu Shu thermal springs, but possibly the six southern-most thermal springs in the north-northwest trending zone that is in existence in the eastern interior of southern Africa.

It is important to make an attempt to quantify the degree of effect that the various cooling sources have on the Shu Shu thermal waters at depth. When utilising the relationship inferred by Truesdell *et al*. (1977) between the depth from which the thermal waters ascended, and the measured outflow rate, and assuming a possibly simplistic linear relationship between these two factors, calculations can be undertaken to determine the approximate decrease in temperature due to conductive cooling upon ascent. Assuming an average, maximum depth of circulation of ~1990m (although the thermal waters would only have risen approximately 990m, as detailed),

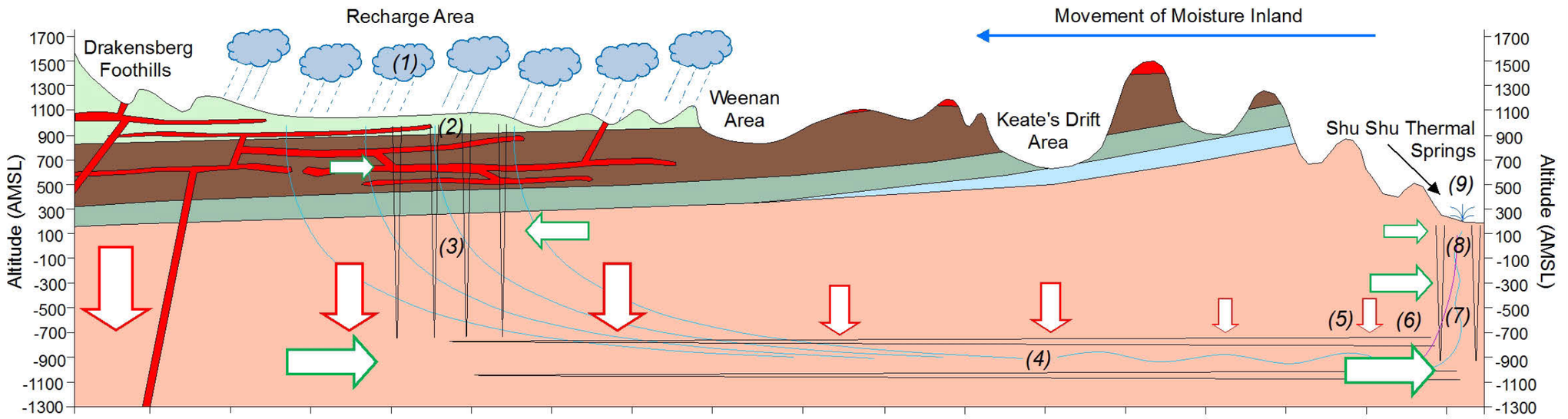

Geological Symbols:

- Geological Contact
- Vertical Joint - Opening
- Horizontal Joint - Opening
- Groundwater Movement Pathway
- Thrust Zone

Pressure Symbols:

- Confining Pressure
- Vertical Pressure

Geological Legend:

Drakensburg Group		Dolerites
Beaufort Group	Karoo Supergroup	Sandstones
Ecca Group	Karoo Supergroup	Shales & Sandstones
Dwyka Group	Karoo Supergroup	Tillites
Natal Group		Sandstones
Natal Metamorphic Province (Basement)		Granulite, Amphibolite & Greenschist Metamorphics

Conceptual Source Model:

(1) Recharge along Great South African Escarpment

(2) Vertical downward percolation / infiltration

(3) Vertical movement of groundwater through closing joints to a maximum depth of 1990m bgl

(4) Horizontal groundwater movement eastwards along opening joints at an approximate temperature of 80 C

(5) Horizontal groundwater movement at 0.2 m/day in basement rocks in Tugela Valley

(6) Sub-vertical movement upward along NMP thrust zones

(7) Vertical movement of groundwater through opening joints and consequent cooling upon ascent

(8) Intermixing of deep, thermal groundwater with shallow, cold groundwater, and atmospheric cooling, at shallow depths

(9) Emergence of the thermal water in the Shu Shu thermal springs at an approximate temperature of 50 C

Scale:

0 20 40 60 80 100 120 Kilometres

Vertical Exaggeration: 15x

Topographical Profile Source: ASTER (2011)

Figure 4.10: Conceptual model depicting the origin of the Shu Shu thermal springs.

and hence an average, maximum reservoir temperature of 80°C, it is inferred that the Shu Shu thermal spring waters cool by ~13°C as they rise, due to conductive cooling only. However, according to Allen *et al*. (2006)., the effect of atmospheric temperature cooling is clearly discernible near-surface, with ICAX (2007) stating that such impacts extend to a maximum depth of 50m bgl, whereby temperatures recorded at such depths are typically similar to the local average annual surface temperature; this is approximately 19°C (Agricultural Research Council, 2010). When assessing the temperature profile of BH 1 (Figure 3.4), it is evident that an appreciably different cooling rate is observed at depths of less than 38 m, which is likely due to the impact of atmospheric temperature. An approximate drop in temperature of 10% was measured here, which implies that the thermal waters would otherwise surface at a temperature of approximately 55°C were it not for this cooling. The 12°C difference between the conductive cooling temperature, and the atmospheric cooling temperature, is attributable to intermixing with shallow, cold groundwater (at a depth of more than 38m). If the temperature thereof is accepted as being approximately 23°C, further calculations confirm that the water surfacing at the Shu Shu thermal springs per second is composed of ~0.92l deep, thermal water and ~0.34l shallow, cold groundwater; this corresponds to a relationship of 2.71:1.00.

When assessing the hydrochemistry of the thermal and cold groundwater near Shu Shu, in comparison to this model, it can be seen that most major and minor determinant concentrations are likely higher in deep thermal waters, prior to intermixing occurring. Ca, Si and Cl concentrations in the samples collected from BH 3 result in difficulty when attempting to fully explain this model, however K concentrations are likely slightly lower in the deep thermal waters, given that the highest concentrations were measured in the cold groundwater. Mg and HCO_3 concentrations are much lower in the thermal groundwater samples, however it is possible to explain why they do not simply increase in accordance with the proposed mixing model. The solubility of Mg increases with an increase in pH, however the pH of the thermal waters only increase at shallow depths immediately prior to surfacing, and as such, disequilibrium does not allow for an increase in Mg concentrations. The solubility of HCO_3 is heavily dependent upon the temperature, with lower temperatures typically increasing the concentration of HCO_3. As temperatures remain elevated even after intermixing has occurred, HCO_3 concentrations remain low.

4.5 Shu Shu Thermal Springs and Geothermal Energy?

Given that which has been determined as part of this investigation, the possibility of geothermal energy is best explored through an assessment of a similar geothermal system which is already being employed for such a purpose. Erkan *et al*. (2008) state that the meteoric-in-origin Chena thermal springs system, which is located in central Alaska, likely owes its heat source to depth-descent, as an absence of recent volcanic rocks precludes the possibility of a magmatic source. According to Erkan *et al*. (2008) the maximum surfacing temperature of the thermal waters is 74°C, with the geochemistry of the waters indicating a reservoir temperature of 100°C – 130°C; a conservative depth of circulation of approximately 3500m is therefore proposed based upon a geothermal gradient of 3.5°C / 100m.

The Chena hot springs are used to run a 400kW binary cycle power plant and are the lowest-temperature springs known to produce geothermal energy (Chena Hot Springs Resort, 2010). Despite the predicted maximum temperatures of 100°C to 130°C at depth, the system utilizes 74°C water from shallow injection wells; this reduces the capital and running costs as piping hotter water from further down is not required for the system (Chena Hot Springs Resort, 2010). According to Chena Hot Springs Resort (2010), the thermal waters are collected and passed through an evaporator upon which they are returned to the geothermal reservoir via the injecting system. At this stage, the working fluid (R134-a – a common refrigerant found in many air conditioning units) is passed into the heat transfer unit / evaporator shell, such that the temperatures cause it to evaporate (Chena Hot Springs Resort, 2010). Once the evaporation of the refrigerant is sufficient, it is expanded supersonically through the turbine nozzle, resulting in the turbine blades spinning at 13500 rpm and the generator spinning at 3600 rpm (Chena Hot Springs Resort, 2010).

If a similar design to that which is in existence at Chena is envisaged for Shu Shu, and in accordance with that information detailed by Saleh *et al*. (2007), then thermal waters at a temperature of approximately 75°C (assuming negligible cooling when pumped to the surface) would be required for the system. Back-calculating, and taking cognisance of all cooling, such thermal waters with these temperature are likely to be found at a depth of approximately ~827m below the floor of the Tugela Valley. The evidence as to why R134a is best utilised at Shu Shu is detailed by Saleh *et al*. (2007), however this was based upon a power output of 1000kW, as opposed to the 400kW produced at Chena; consequently, a linear relationship has been used to determine applicable quantities, where required.

Of the available working fluids that can be utilised in an Organic Rankine Cycle, which might be employed at a hypothetical Shu Shu geothermal power plant, R134a represents one of the only types that can be used in conjunction with thermal water temperatures of 70°C – 75°C. When evaporated at supercritical pressures of ~38 bar, R134a has a thermal efficiency (η_{th}) (which allows for steam generation) of 9.21% when an internal heat exchanger (IHE) is employed in a s2 cycle – this thermal efficiency is one of the highest for such low-temperature thermal waters (Saleh *et al*., 2007). Furthermore, according to Saleh *et al*. (2007), at these 'settings', the volume flow rate (V_3) at the inlet of the turbine is at one of the lowest allowable values ($0.11m^3/s$). Together, these two characteristics of R134a confirm the most efficient way to produce electricity at Shu Shu. However, of critical importance too is the heat transfer from the thermal water to the working fluid, and it is here that the relatively diminished flow rate of the Shu Shu thermal springs may be problematic.

Theoretically, for the production of 400kW of electricity, the system would require a mass flow rate (m_c) of 16.96kg/s or ~16.96l/s (Saleh *et al*., 2007), which is approximately 13.48 times more water than that surfacing at Shu Shu. However, it is unlikely that the hypothetical power plant would be operating at 100% capacity over a 24-hour period (due to required borehole water level recovery and diminished night-time use). Although it is unknown the amount of thermal water that could be safely extracted from depth, pump-test data from BH 1 confirms that a maximum rate of only 0.14l/s could be safely abstracted from the shallow aquifer. Such an issue is of critical importance however, as it is imperative that any geothermal power plant operations do not reduce the current flow rate at the Shu Shu thermal springs. Such values require further investigation, through exploratory drilling, in an effort to determine the production capacity of a possible geothermal power plant.

Should a geothermal power plant at Shu Shu be scientifically feasible, as seems a possibility, it remains to be detailed the costs of such an enterprise, including those of continuing operations. As a similarity has already been drawn between a hypothetical power plant at Shu Shu and that which is already in existence at Chena, it appears suitable to continue in this trend. Holdmann (2007) states that the cost of producing electricity, even in remote areas like Chena (96km northeast of Fairbanks), can be reduced to 5¢ / kW/hr, or ~40c / kW/hr, as opposed to the price the electricity is currently sold at in South Africa, which is ~61c / kW/hr. Whilst it is accepted that these costs are variable depending on importing duties, temperature of water used, volume of water used and construction required, it illustrates that if the correct geological conditions exist, geothermal energy remains a financially feasible possibility at Shu Shu. If a small plant of

400kW is envisaged, then based upon the fact that typical, small electricity installation projects suggest that 50 informal settlement homes utilize 32kW, approximately 625 rural homes can be serviced by a hypothetical geothermal power station at Shu Shu. Furthermore, the socio-economic benefits of such a venture, including its pioneering ability, cannot be overlooked.

Chapter 5
Conclusions

As part of this study, the local geological, structural, hydrological, isotopic and geothermal characteristics of the Shu Shu thermal springs have been investigated. In was endeavoured to use such determined data and information to not only derive the intrinsic features, and a consequent conceptual model, of this system, but also to assess whether or not geothermal energy is a scientific and financial possibility here in the future. Furthermore, a north-northwestern trending thermal springs zone, located within the eastern interior of South Africa, was investigated in relation to the Lebombo 'monocline' and the Great South African Escarpment. The latter of these two possible source features was ultimately favoured as forming part of the system's origin, and is hence characterized as part of the conceptual model, through a description of the intrinsic features of the Shu Shu thermal springs.

Stable isotope data sourced from collected rainfall, cold, shallow groundwater and deep, thermal groundwater samples confirm that the water surfacing in the Shu Shu thermal springs is meteoric in origin, with the recharge area located at higher altitudes and further inland toward the west. Radiogenic isotope levels in these samples vary between undetectable and slightly above the natural detectable limit, across different sampling events undertaken during various seasons. These data not only infers variable Shu Shu thermal waters ages of < 61 years or > 61 years (at present), but suggests intermixing between shallow, cold groundwater in the region, and surfacing deep, thermal water. Although it remains unknown through which rock units the thermal groundwater moves as it traverses away from its recharge area, they likely have a similar geochemical signature to those in which the Shu Shu thermal springs surface, with these gneisses and amphibolites, which are predominant, containing elevated amounts of quartz, feldspar, hornblende, biotite and epidote-clinozoisite. Consequently, the surfacing thermal water, and the shallow groundwater in the region, contain elevated concentrations of Na, K, Ca, Mg, Fe, Al, Si, F and Sr, which are attributable to leaching from country rock, whilst the presence of SO_4 is explained through the dissemination of pyrite. Although the sampled thermal waters are typically old by Piper (1944) classification, they have not attained a state of full equilibrium, which is considered unusual. This further points to active intermixing processes as has been detailed thus far.

^{13}C analysis undertaken on selected thermal waters returned inconclusive results which, although cannot be used to determine its origin, do fall within the range of values for natural

groundwater. Consequently, a mathematically derived, slightly elevated geothermal gradient of 3.1°C / 100m is accepted as the heat source for the Shu Shu geothermal springs. Intermixing was however, further investigated before maximum reservoir temperatures and depths of circulation could be studied through the use of this information. Geochemical speciation modelling, bivariate intermixing graph evaluation and thermal borehole profiling furthermore strongly suggest intermixing between rising, deep thermal waters and cold, shallow groundwater, with the latter investigation technique inferring that such active geohydrological processes are in existence predominantly at depths of greater than 34.00m bgl. Consequently, although geothermometer-derived maximum reservoir temperatures are variable, an evaluation of their applications to relevant Shu Shu thermal springs characteristics advocate maximum thermal water temperatures of approximately 75°C – 85°C. Hence, the utilisation of the determined geothermal gradient, and these temperatures, suggest circulation depths of approximately 1827m – 2153m below the altitude of the recharge area.

Photographic lineament interpretation, detailed outcrop mapping, geophysical investigations and cross-sectional construction and analyses highlighted six principle structure orientations in the region surrounding the Shu Shu thermal springs. These structures are attributable to pre-existing basement trends, folding and faulting associated with the development of the Tugela Terrane of the Natal Metamorphic Province, faulting associated with the Karoo Igneous Province and faulting associated with the break-up of Gondwana. A tectonic analysis undertaken on these structures, in relation to the orientation of σ_1, σ_2 and σ_3, shows that those structures trending west-southwest – east-northeast, west-northwest – east – southeast and north-northwest – south-southeast likely transmit elevate amounts of groundwater. However, it is apparent that once thermal waters have risen near surface along the west-southwesterly – east-northeasterly faults, they abut against the north-northwesterly – south-southeasterly faults which results in their surfacing.

The above information and data pertaining to the Shu Shu thermal springs does not preclude the Lebombo ‘monocline’ possibly representing a conceptual source feature to, and hence being an origin of, the thermal springs within the north-northwest trending zone within the eastern interior of South Africa. This may be due to the formation of the Lebombo through asymmetrical stretching of the lithosphere, thereby resulting in a ‘remnant thermal fingerprint’ underlying the eastern interior of southern Africa, that can be ascribed to thermal uplift and hence accounts for a slightly elevated geothermal gradient which acts as the principle heat source for many of the springs. Whilst this conceptual model is a possibility, it is considered likely rather, that the Great

South African Escarpment provides the necessary intrinsic geomorphological characteristics and features to allow for the formation of six of the thermal springs. After recharge has occurred in this region, the altitude of the Escarpment likely provides the required amount of heat, through a slightly elevated geothermal gradient, to sufficiently raise the temperature of the thermal waters. Furthermore, weathering and denudation processes reduce the altitude of the coastal plain, thereby reducing the natural cooling effects common to rising, isolated thermal waters, thereby allowing for hotter surfacing temperatures. These temperatures are further diminished somewhat, by active geohydrological intermixing processes and atmospheric cooling, at least below the Shu Shu thermal springs, which reduce the temperature of the rising water by approximately 17°C.

The determined maximum reservoir temperatures of the Shu Shu thermal waters, which are set at 75°C – 85°C, are sufficient to maintain an operational geothermal power plant. However, such thermal waters at the temperatures required will likely be encountered at a depth of approximately 827m below the floor of the Tugela Valley, with a reduction in drilling depths decreasing establishment costs. If an Organic Rankine Cycle is employed at a hypothetical Shu Shu power plant, R134a likely represents the only suitable working fluid that can be used, although it will be ideally suited to this task. This is due to the fact that at supercritical pressures of ~38 bar, thermal efficiency and volume flow rate values are favourable, indeed to such a degree that operational costs are reduced. It is possible however, that heat transfer values may be problematic, as the measured mass flow rate of the springs may be too low to allow for continuous energy production. Such values require further investigation, through exploratory drilling, in an effort to determine the production capacity of a possible geothermal power plant. If however, such investigations return favourable results, it appears possible that a 400kW plant can be constructed, whilst electricity could be produced at half the price it is sold at currently. The capacity of a hypothetical 400kW power plant is likely sufficient to service 625 rural homes in the area, although the socio-economic benefits of such a venture, including its pioneering ability, cannot be overlooked.

Acknowledgements

First and foremost, my heartfelt thanks are extended to my supervisor, Prof. M. K. Watkeys and my boss, Mr. R. Sebire, without whose selfless help, guidance and time, this project would not have been possible. You have shown me the subtle rewards of continued hard work in the field of geological sciences; an example that will always be appreciated and respected. Sincere thanks are extended to my co-supervisor, Dr. M.B. Demlie, for the continued assistance given not only in reviewing the geohydrological component of this investigation, but for urging me to always give more. Furthermore, I wish to thank Prof. S. McCourt, Dr. J. Reinhardt, Mr. P. Suthan, Mr. R. Seyambu, Mr. M. Seyambu and Ms. J. Naicker, from whom the given assistance was always greatly appreciated. To Mr. C. Mandew and Mr. F. McKenna of Geomeasure Group, sincere thanks are given for the geophysical investigation analysis assistance. A special debt of gratitude is extended to Mrs. T. Swales and Dr. W. Hastie, whose motivation and inspiration will always be appreciated. Mrs. V. Talbot and Ms. A. Nathanael from Talbot Laboratories are acknowledged for assistance with sample analysis, whilst Mr. R. Botes is thanked for his knowledge and support given in relation to GIS techniques, from whom the ASTER (2011) data was sourced. Mr. M. Butler of iThemba Labs is thanked for environmental isotope analysis and data interpretation, whilst the borehole profiling assistance provided by Mr. S. Govender from Aquatec Pumps is gratefully acknowledged. Furthermore, to Mrs. C. Nel and the staff at St. Cathryn's, and big thank-you for all the aid and support given with regards to field work accommodation; without which, the mapping undertaken for this report may not have been completed. Hannes and John from the Shu Shu Campers Association are thanked not only for their assistance in the field, but also for their support. Mr. K. Gordon is especially thanked for his unwavering assistance and dedication in the field, for without which the long, hot days would have been that much more difficult. A special word of thanks is given to Ms. S. Brijraj for assistance with the petrological analysis, and more importantly, for the continued support and motivation through the length of this study. The National Research Foundation is belatedly thanked for a previous bursary which assisted with costs, whilst the financial assistance of Geomeasure Group is gratefully appreciated. To my late father, Mr. L. Gravelét-Blondin, thank-you for all the time and knowledge selflessly given with regards to water chemistry analysis. This is for you. To my family and all my friends, for all the support and motivation I have received that made this report possible, a big thank-you. My final word of thanks is extended to my mother, without whose selfless support through over three years would have made this project especially difficult to complete. That which I have achieved is due to you.

References

ABEM Geophysics. (1991). ABEM Instruction Manual – ABEM WADI VLF Instrument. *ABEM*, Sweden, 36 pp.

Abbott, M.D., Lini, A. and Bierman, P.R. (1999). $\delta^{18}O$, δD and ^{3}H measurements constrain groundwater recharge patterns in an upland fractured bedrock aquifer, Vermont, U.S.A. *Journal of Hydrology*, **228**, 101–112.

Advanced Spacebourne Thermal Emission and Reflection. (2011). ASTER Global Digital Elevation Model. *North American Space Association*. Japan.

Agricultural Research Council. (2010). Hazyview (Kranskop) – Long Term Report: Averages and Totals. *ARC-ISCW*, Cedara, South Africa. 2pp.

Allen D.M, Grasby, S.E. and Voormeij, D.A. (2006). Determining the circulation depth of thermal springs in the southern Rocky Mountain Trench, south-eastern British Columbia, Canada using geothermometry and borehole temperature logs. *Hydrogeology Journal*, **14**, 159 – 172.

Anderson, E.M. (1951). Dynamics of faulting and dyke formation. *Oliver and Boyd*, Edinburgh, Scotland.

Arima, M., Tani, K., Kawate, S. and Johnston, S.T. (2001). Geochemical characteristics and tectonic setting of metamorphosed rocks in the Tugela terrane, Natal belt, South Africa. *Memoirs of the National Institute of Polar Research*, **55**, 1-39.

Arnorsson, S., Gunnlaugsson, E. and Svavarsson, H. (1983). The chemistry of geothermal waters in Iceland. Chemical geothermometry in geothermal investigations. *Geochimica et Cosmochimica Acta*, **47**, 567-577.

Bahati, G., Pang, Z., A´rmannsson, H., Isabirye, E.M. and Kato, V. (2005). Hydrology and reservoir characteristics of three geothermal systems in western Uganda. *Geothermics*, **34**, 568-591.

Bau, M., Alexander, B., Chesley, J.T, Dulski, P. and Brantley, S.L. (2004). Mineral dissolution in the Cape Cod aquifer, Massachusetts, USA: I. Reaction stoichiometry and impact of accessory feldspar and glauconite on strontium isotopes, solute concentrations, and REY distribution. *Geochimica et Cosmochimica Acta*, **68**, 1199–1216.

Bisnath, A., McCourt, S., Frimmel, H.E. and Buthelezi, S.B.N. (2008). The metamorphic evolution of mafic rocks in the Tugela Terrane, Natal Belt, South Africa. *South African Journal of Geology*, **111**, 369-386.

Bond, G.W. (1946). A Geochemical Survey of the Underground Water Supplies of the Union of South Africa. *Memoirs of the Geological Survey of South Africa* (**41**), South Africa. 208 pp.

Breiner, S. (1973). Applications Manual for Portable Magnetometers. *Geometrics*, U.S.A. 57 pp.

Brown, R.W., Rust, D.J., Summerfield, M.A., Gleadow, A.J.W. and de Wit, M.J. (1990). An accelerated phase of denudation in the south-western margin of Africa: evidence from apatite fission track analysis and the offshore sedimentary record. Nuclear Energy Tracks and Radiation Measurements, **17**, 339-350.

Buck, W.R., Martinez, F., Steckler, M.S. and Cochran, J.R. (1988). Thermal consequences of lithospheric extension: pure and simple. *Tectonics*, **7**, 213-234.

Burke, K. and Dewey, J.F. (1972). Plume-generated triple junctions: Key indicators in applying plate tectonics to old rocks. *Journal of Geology,* **81**, 406-433.

Burke, K., and Gunnell, Y. (2008). The African Erosion Surface: A continental-scale synthesis of geomorphology, tectonics, and environmental change over the past 180 million years. *Geological Society of America Memoir*, **201**, 66 pp.

Butler, M.J., Malinga, O.H.T. and Mabitsela, M. (2010) Environmental isotope analysis on four (4) water samples. *iThema Labs – Environmental Isotope Laboratory*, South Africa, 4 pp.

Chae, G, T., Yun, S.T., Kwon, M.J., Kim, Y.S. and Mayer, B. (2006). Batch dissolution of granite and biotite in water: Implication for fluorine geochemistry in groundwater. *Geochemical Journal*, **40**, 95-102.

Chena Hot Springs Resort. (2010). Renewables – Geothermal Power *[on-line]*. Chena Hot Springs Resort, U.S.A., http://www.chenahotsprings.com/geothermal-power/. Accessed on 25 September 2010.

Cornell, D.H., Thomas, R.J, Moen, H.F.G., Reid, D.L. Moore, J.M and Gibson, R.L. (2006). The Namaqua-Natal Province. *In*: Johnson, M.R., Anhaeusser, C.R. and Thomas, R.J. (Eds). *The Geology of South Africa*. Geological Society of South Africa, Johannesburg, 325 – 380.

Cortecci, G., Boschetti, T., Mussi, M., Herrera Lameli, C., Mucchino, C. and Barbieri, M. (2005). New chemical and original isotopic data on waters from El Tatio geothermal field, northern Chile. *Geochemical Journal*. **39**, 547 – 571.

Cox, K.G. (1992). The Karoo igneous activity, and the early stages of the break-up of Gondwanaland. *In:* Storey, B.C, Alabaster, T. and Pankhurst, R.J. (Eds). Magmatism and the Causes of Continental Break-Up. Geological Society, London, England. Special Publications, 68, 137–148.

Craig, H. (1961). Isotopic variations in meteoric waters. *Science*, **133**, 1702–1703.

Dansgaard, W. (1964). Stable isotopes in precipitation. *Tellus*, **16**, 436–468.

Davis, G.L. (1977). The ages and uranium contents of zircons from kimberlites and associated rocks. *Yearbook of the Carnegie Institute in Washington*, **76**, 631–635.

De Wit, M.J. (2007). The Kalahari epeirogeny and climate change: Differentiating cause and effect from core to space. *South African Journal of Geology*, **110**, 367–392.

Department of Water Affairs. (2011). Groundwater Resource Information Project. *Database Manager: Geomeasure Group*, South Africa.

Diamond, R.E. and Harris, C. (2000). Oxygen and hydrogen isotope geochemistry of thermal springs of the Western Cape, South Africa: recharge at higher elevations? *Journal of African Earth Sciences*, **31**, 467-481.

Du Toit, A.L. (1929). The volcanic belt of the Lebombo: A region of tension. *Transactions of the Royal Society of South Africa*, **18**, 189-218.

Du Toit, A.L. (1931). The Geology of the Country Surrounding Nkandhla – Explanation of Sheet 109. *Union Geological Survey Publication*, South Africa, 15 pp.

Du Toit, A.L. (1933). Crustal movements as a factor in the geographical evolution of South Africa. *South African Geography Journal*, **16**, 1-33.

Duncan, A.R. and Marsh, J.S. (2006). The Karoo Igneous Province. *In*: Johnson, M.R., Anhaeusser, C.R. and Thomas, R.J. (Eds). *The Geology of South Africa*. Geological Society of South Africa, Johannesburg, 501 – 520.

Durrence, E.M and Heath, M.J. (1985). Thermal groundwater movement and radionuclide movement in SW England. *Mineralogical Magazine*, **49**, 289-299.

Eglington, B.M., Harmer, R.E. and Kerr, A. (1989). Isotope and geochemical constraints on Proterozoic crustal evolution in South-eastern Africa. *Precambrian Research*, **45**, 159-174.

El-Fiky, A.A. (2009). Hydrogeochemistry and Geothermometry of Thermal Groundwater from the Gulf of Suez Region, Egypt. *Journal of King Abdulaziz University: Earth Sciences*, **20**, 71-96.

Erkan, K., Holdmann, G., Benoit. W. and Blackwell, D. (2008). Understanding the Chena Hot Springs, Alaska, geothermal system using temperature and pressure data from exploration boreholes. *Geothermics*, **37**, 565-585.

Fahrig, W.F. (1987). The tectonic settings of continental mafic dyke swarms. *In*: Halls, H.C. and Fahrig, W.F. (Eds.). Mafic dykes swarms. *Geological Association of Canada Special Paper*, **34**, 331-348.

Fleming, A., Summerfield, M.A., Stone, J.O.H., Fifield, L.K. and Cresswell, R.G. (1999). Denudation rates for the southern Drakensberg escarpment, SE Africa, derived from in-situ-produced cosmogenic ^{36}Cl: initial results. *Journal of the Geological Society*, **156**, 209-212.

Flowers, R.M and Schoene, B. (2010). (U-Th)/He thermochronometry constraints on unroofing of the eastern Kaapvaal Craton and significance for uplift of the southern African Plateau. *Geology*, **38**, 827-830.

Fontes, J.C. (1980). Environmental isotopes in groundwater hydrology. *In*: Fritz, P. and Fontes, J.C. (Eds.). Handbook of Environmental Isotope Geochemistry. Elsevier Science and Technology, U.S.A. 75-140 pp.

Fournier, R.O. (1977). Chemical geothermometers and mixing models for geothermal systems. *Geothermics*, **5**, 41–50.

Fournier, R.O. (1979). A revised equation for the Na-K geothermometer. *Geothermal Resources Council Transactions*, **3**, 221–224.

Fournier, R.O. (1981). Application of water geochemistry to geothermal exploration and reservoir engineering. *Geothermics*, 10, 55–70.

Fournier, R.O. and Truesdell, A.H. (1973). An empirical Na-K-Ca geothermometer for natural waters. *Geochimica et Cosmochimica Acta*, **37**, 1255–1275.

Franco, A. and Villani, M. (2010). Optimal design of binary cycle power plants for water dominated, medium-temperature geothermal fields. *University of Pisa*, Italy, 40pp.

Freeze, R.A. and Cherry, J.A. (1979). Groundwater. *Prentice Hall*, U.S.A. 604 pp.

Geomeasure Group. (2001). Report on the Drilling and Pumptesting of Boreholes at KwaShuShu – Mapumulo. *Geomeasure Group*, South Africa. 23 pp.

Gevers, T.W. (1942). The hot springs in the Tugela River near Kranskop, Natal. *Transactions of the Geological Society of South Africa*, **45**, 65-74.

Gevers, T.W. (1963). Thermal Springs at Lilani, Natal, and Their Geologic Setting. *Transactions of the Geological Society of South Africa*, **65**, 129-155.

Geyh, M., Amore, F.D., Darling, G., Paces, T., Pang, Z., and Silar, J. (2001). Groundwater – Saturated and Unsaturated Zone. *In*: Mook, W.G. (Eds.). Environmental Isotopes in the Hydrological Cycle – Principles and Applications. *International Atomic Energy Agency*, Austria. 117 pp.

Gianelli, G., Piovesana, F. and Huu Quy, H. (1997). A Reconnaissance Geochemical Study of Thermal Waters of South and Central Vietnam. *Geothermics*, **26**, 519-533.

Giggenbach, W.F. (1988). Geothermal solute equilibria. Derivation of Na-K-Mg-Ca geoindicators. *Geochimica et Cosmochimica Acta*, **52**, 2749-2765.

Giggenbach, W. F. (1991) Collection and analysis of geothermal and volcanic waters and gas discharges. *In:* D'Amore, F. (Eds). Application of Geochemistry in Geothermal Reservoir Development*. UNITAR*, Rome, 119-144.

Gilchrist, A.R. and Summerfield, M.A. (1991). Denudation, isostacy and landscape evolution. Earth Surface Processes and Landforms,**16**, 555-562.

Groundwater Consulting Services. (1993). Characterization and Mapping of the Groundwater Resources – KwaZulu-Natal Province: Reconnaissance Phase. *Department of Water Affairs and Forestry*, South Africa. 108 pp.

Guangcai, W., Zuochen, Z., Min, W., Cravotta, C.A. and Chenglong, L. (2005). Implications of Ground Water Chemistry and Flow Patterns for Earthquake Studies. *Ground Water*, **43**, 478-484.

Hartnady, C.J.H. (1985). Uplift, faulting, seismicity, thermal spring and possible incipient volcanic activity in the Lesotho-Natal region, SE Africa: The Quathlamba hotspot hypothesis. *Tectonics*, **5**, 371-377.

Healy, J. and Hochstein, M.P. (1973). Horizontal Flow in Hydrothermal Systems. *Journal of Hydrology (NZ)*, **12**, 71-82.

Hoffmann, J.R.H. (1979). Die Chemiese Samestelling van Warmwaterbronne in Suid- en Suidwes-Afrika. *Centre for Scientific and Industrial Research*, South Africa, 21 pp.

Holdmann, G. (2007). The Chena Hot Springs 400kW Geothermal Power Plant: Experience Gained During the First Year of Operation. *Chena Power*, Alaska. 9pp.

Huang, W.H. and Kiang, W.C. (1972). Laboratory Dissolution of Plagioclase Feldspars in Water and Organic Acids at Room Temperature. *American Mineralogist*, **57**, 1849-1859.

Hutchison, C.S. (1974). Laboratory Handbook of Petrographic Techniques. *John Wiley and Sons*. London, England. 527 pp.

Johnston, S.T., McCourt, S., Bisnath, A. and Mitchell, A.A. (2003). The Tugela Terrane, Natal Belt: Kibaran magmatism and tectonism along the southeast margin of the Kaapvaal Craton. *South African Journal of Geology*, **106**, 85-97.

Interseasonal Collection and Exchange. (2007). Mean Annual Air Temperature *[on-line]*. ICA, U.K, http://www.icax.co.uk/Mean_Annual_Air_Temperature.html. Accessed on 04 December 2013.

Jones, M.Q.W. (1992a). Heat flow anomaly in Lesotho: Implications for the southern boundary of the Kaapvaal Craton. *Geophysical Research Letters*, **19**, 2031-2034.

Jones, M.Q.W. (1992b). Heat flow in South Africa. *Geological Survey of South Africa Handbook,* **14**,174 pp.

Kappelmeyer, O. and Haenel, R. (1974) Geothermics with special references to application. *Lubrecht & Cramer Ltd*. Berlin, Germany. 238 pp.

Karingithi, C.W. (2009). Chemical Geothermometers for Geothermal Exploration. *Short Course IV on Exploration for Geothermal Resources*, Lake Naivasha, Kenya, 1 – 22 November 2009.

Kent, L. (1949). The Thermal Waters of the Union of South Africa and South West Africa. *Transactions of the Geological Society of South Africa*, **52**, 231-264.

Kent, L. (1949) The thermal waters of the Union of South Africa and South West Africa. *Transactions of the Geological Society of South Africa*, **52**, 231 – 264.

Kent, L. (1969). The Thermal Waters in the Republic of South Africa. *Proceedings of Symposium II on Mineral and Thermal Waters of the World: B – Overseas Countries*, **19**, 143–146.

Kharaka, Y.K., Lico, M.S. and Law, L.M. (1982). Chemical geothermometers applied to formation waters. Gulf of Mexico and California basins. *American Association of Petroleum Geologists*, Bulletin **66**, 588.

Kharaka,Y.K. and Mariner, R.H. (1989). Chemical geothermometers and their application to formationwaters from sedimentary basins. *In*: Naeser, N.D. and McCulloh, T.H. (Eds.). Thermal History of Sedimentary Basins – Methods and Case Histories. *Springer-Verlag Incorporated*., New York, USA. 99–117.

King, L.C. (1963). The South African Scenery. *Oliver and Boyd*, London, England. 308 pp.

King, L.C. (1974). Aspects of the high Drakensberg. *South African Journal of Geology*, **56**, 128-136.

Klausen, M.B. (2009). The Lebombo monocline and associated feeder dyke swarm: Diagnostic of a successful and highly volcanic rifted margin? *Tectonophysics*, **468**, 42–62.

Kounov, A., Niedermann, S., De Wit, M.J., Viola, G., Andreoli, M., and Erzinger, J. (2007). Present denudation rates at selected sections of the South African escarpment and the elevated continental interior based on cosmogenic ^{3}He and ^{21}Ne. *South African Journal of Geology*, **110**, 235–248.

Kukkonen, I.T., Suppala, I., Sulkanen, K., Lindberg, A., Hautojärvi, A., Raiko, H. and Johansson, E. (2001). Investigations on thermal properties of rocks at test sites for final disposal of spent nuclear fuel in Finland. *In*: Särkkä, P and Eloranta, P. (Eds). Rock Mechanics – A Challenge for Society. *Swets and Zeitlinger*, Netherlands, 757-763.

Lenoir, X., Féraud, G. and Geoffroy, L. (2003). High-rate flexure of the East Greenland volcanic margin: constraints from $^{40}Ar/^{39}Ar$ dating of basaltic dykes. *Earth and Planetary Science Letters*, **214**, 515–528.

Lund, J.W. (2000). Balneological use of thermal waters in the U.S.A. *GHC Bulletin*, September, 31-34.

Matthews, P.E. and Charlesworth, E.G. (1981). National Geodynamics Project – Northern Margin of the Namaqua-Natal Mobile Belt in Natal. *University of Natal, Durban*, South Africa.

Mazor, E. and Verhagen, B.T. (1983). Dissolved ions, stable and radioactive isotopes and noble gases in the thermal waters of South Africa. *Journal of Hydrology*, **63**, 315-329.

Mazor, E. (1991). Applied Chemical and Isotopic Groundwater Hydrology. *Open University Press*. Buckingham, England. 274 pp.

McCourt, S., Armstrong, R.A., Grantham, G.H. and Thomas, R.J. (2006). Geology and evolution of the Natal belt, South Africa. *Journal of African Earth Sciences*, **46**, 71-92.

Mock, J.E. (1993). Geothermal energy – the environmentally responsible energy technology for the 90s: A federal perspective. *In*: Proc. Geothermal Energy: The Environmentally Responsible Energy Technology for the Nineties. Berkeley, California, U.S.A. 27 – 29 April 1993.

Mohammadi, Z., Bagheri, R. and Jahanshahi, R. (2010). Hydrogeochemistry and geothermometry of Changal thermal springs, Zagros region, Iran. *Geothermics*, **39**, 242–249.

Moore, A. and Blenkinsop, T. (2006). Scarp retreat versus pinned drainage divide in the formation of the Drakensberg escarpment, southern Africa. *South African Journal of Geology*, **109**, 455-456.

Moore, A., Blenkinsop, T. and Cotterill, F. (2009). Southern African topography and erosion history: plumes or plate tectonics? *Terra Nova*, **21**, 310–315.

Murakami, T. Utsunomiya, S., Yokoyama, T. and Kasama, T. (2003). Biotite dissolution processes and mechanisms in the laboratory and in nature: Early stage weathering environment and vermiculitization. *American Mineralogist*, **88**, 377–386.

Olivier, J., van Niekerk, H.J. and van der Walt, I.J. (2008). Physical and chemical characteristics of thermal springs in the Waterberg area in Limpopo Province, South Africa. *Water South Africa*, **34**, 163-174.

Özgür, N. (2003). Active geothermal systems in the rift zone of the Büyük Menderes, Western Anatolia, Turkey. *Proceedings of the European Geothermal Conference,* Szeged, Hungary, **0-5-04**.

Parkhurst, D.L. and Appelo, C.A.J. (2010). User's guide to PHREEQC (version 2.17.0.1) - a computer program for speciation, reaction-path, 1D-transport, and inverse geochemical calculations. *United States Geological Survey Water Resources Inventory*, Report 99-4259, 312 pp.

Piper, A. M. (1944). A graphic procedure in the geochemical interpretation of water analyses. *American Geophysical Union Transactions,* **25**, 914-923.

Pirlo, M.C. (2004). Hydrogeochemistry and geothermometry of thermal groundwaters from the Birdsville Track Ridge, Great Artesian Basin, South Australia. *Geothermics*, **33**, 743–774.

Pollard, D.D. and Aydin, A. (1988). Progress in understanding jointing over the past century. *Bulletin of the Geological Society of America*, **100**, 1181 – 1204.

Potts, P.J. (1987). A Handbook of Silicate Rock Analysis. *Chapman and Hall*. New York, U.S.A. 622 pp.

Price, N.J. (1966). Fault and Joint Development in Brittle and Semi-brittle Rock. *Pergamon Press*. London, England. 176 pp.

Ramsay, J.G. and Huber, M.I. (1987). The Techniques of Modern Structural Geology – Volume 2: Folds and Fractures. *Academic Press*. London, England. 391 pp.

Reeves, C.V. (1978). A failed Gondwana spreading axis in southern Africa. *Nature*, **273**, 222-223.

Reeves, C.V. (1978). A failed Gondwana spreading axis in southern Africa. *Nature*, **273**, 222-223.

Rindl, M.R. (1918). The Medicinal Springs of South Africa (supplement). *South African Journal of Science*, **15**, 217-225.

Rozanski, K., Araguas-Araguas, L. and Gonfiantini, R. (1993). Isotopic patterns in modern global precipitation. *In:* Swart, P.K. (Eds.). Climate Change in Continental Isotopic Records (Eds). *Geophysical Monograph Service*, **78**, 1– 36.

Saleh, B., Koglbauer, G., Wendland, M. and Fischer, J. (2007). Working fluids for low-temperature organic Rankine cycles. *Energy*, **32**, 1210–1221.

Sami, K., Neumand, I., Gqiba, D., De Kock, G. and Grantham, G. (2002). Groundwater Exploration in Geologically and Problematic Complex Terrain – Volume 1. *Council for Geoscience*. Pretoria, South Africa. 60pp.

Santoyo, E. and Díaz-González, L. (2010). A New Improved Proposal of the *Na/K* Geothermometer to Estimate Deep Equilibrium Temperatures and Their Uncertainties in Geothermal Systems. Proceedings *World Geothermal Congress 2010*, Bali, Indonesia, 25-29 April 2010.

Schoeller, H. (1962). Les eaux souterraines. Hydrologie dynamique et chimique. Recherche, exploitation et évaluation des resources. *Masson & Cie*. France. 642 pp.

Scholl, M.A., Shanley, J.B., Zegarra, J.P. and Coplen, T.B. (2009). The stable isotope amount effect: New insights from NEXRAD echo tops, Luquillo Mountains, Puerto Rico. *Water Resources Research*, **45**, W12407.

Schwartz, F.W. and Zhang, H. (2003). Fundamentals of Groundwater. *John Wiley & Sons*, U.S.A. 583 pp.

Svensson, P. (2000). Reshaping and Retreat of the Natal Drakensberg Escarpment, South Africa. *Gothenburg University*. Gothenburg, Sweden. 31 pp.

Taran, Y.A. and Peiffer, L. (2009). Hydrology, hydrochemistry and geothermal potential of El Chichón volcano-hydrothermal system, Mexico. *Geothermics*, **38**, 370–378

Temperley, B.N. (1975). The Welgewonden Fault Aquifer of the Central Transvaal and its Thermal Water. *South African Geological Survey*, South Africa. 22 pp.

Truesdell, A.H. (1976). Summary of Section III. Geochemical Techniques in Exploration. *In:* Proceedings of the Second United Nations Symposium on the Development and Use of Geothermal Resources. California, USA, iii–xxix.

Truesdell, A. H. and Fournier, R. O. (1976). Conditions in the deeper parts of hot spring systems of Yellowstone National Park, Wyoming. *US Geological Survey*. Open-File Report, **76-428**, 29 pp.

Truesdell, A.H., Nehring, N.L. and Frye, G.A. (1977). Steam production at The Geysers, California, comes from liquid water near the wellbottom. *Geological Society America Abstracts with Programs*, **9**, 1206.

United States Department of Energy. (2010). Geothermal Technologies Program – Hydrothermal Power Systems *[on-line]*. U.S. Department of Energy, U.S.A., http://www1.eere.energy.gov/geothermal/powerplants.html. Accessed on 24 September 2010.

Van Der Pluijm, B.A. and Marshak, S. (2004). Earth Structure. *W. W. Norton and Company Incorporated*, New York, U.S.A. 656 pp.

Verma, S.P. and Santoyo, E. (1997). New improved equations for Na/K, Na/Li and SiO2 geothermometers by outlier detection and rejection. *Journal of Volcanology and Geothermal Research*, **79**, 9–23.

Von Veh, M.W. (1994). A Structural Geology Analysis of Lineaments and Fault and Dyke Traces in the KwaZulu/Natal Provinces. *Department of Water Affairs and Forestry/Water Research Commission*. Durban, South Africa. 86 pp.

Von Veh, M.W. and Andersen, N.J.B. (1990). Normal-slip faulting in the coastal areas of northern Natal and Zululand, South Africa. *South African Journal of Geology*, **93**, 574-582.

Watkeys M. K. (2002). Development of the Lebombo rifted volcanic margin of southeast Africa. *In*: Menzies M. A., Klemperer, S. L., Ebinger, C. J. and Baker, J. (Eds.). Volcanic Rifted Margins. *Geological Society of America Special Paper*, **362**, 27-46.

Watkeys, M.K. and Sokoutis, D. (1998). Transtension in southeastern Africa associated with Gonwana break-up. *In:* Holdsworth, R.E., Strachan, R.A. and Dewey, J.F. (Eds.). Continental Transpressional and Transtensional Tectonics. *Geological Society*, London, England. Special Publications, **135**, 203-214.

Weaver, J.M.C., Talma, A.S. and Cavé, L.C. (1999). Geochemistry and Isotopes for Resource Evaluation in the Fractured Rock Aquifers of the Table Mountain Group. *Water Research Commission*, Pretoria, South Africa. Report No. 481/1/99, 298 pp.

Wernicke, B. (1985). Uniform-sense normal simple shear of the continental lithosphere. *Canadian Journal of Earth Sciences*, **22**, 108-125.

White, R.P. and McKenzie, D.P. (1989). Magmatism at rift zones: The generation of volcanic margins and flood basalts. *Journal of Geophysical Research*, **94**, 7865-7729.

Appendix A: Methods of Investigation

Appendix A1: Cumulative Rainfall Sampling

Cumulative rainfall was collected in a cumulative rainfall sampler situated at St. Cathryn's Golf Course near Kranskop. The sampler, which was constructed according to the design of Weaver *et al*. (1999), was located at an elevation of 1150m (amsl), approximately 23.5km from the Shu Shu thermal springs. At specified seasonal intervals, the two samplers (3.00l each) were emptied of the collected cumulative rainfall and placed in two 1.00l capacity polyurethane bottles; one was kept as a duplicate sample. The samples were kept in a cooler box in the field and a refrigerator prior to delivery to the laboratory.

The design of the cumulative sampler is shown overleaf in Figure A1.1.

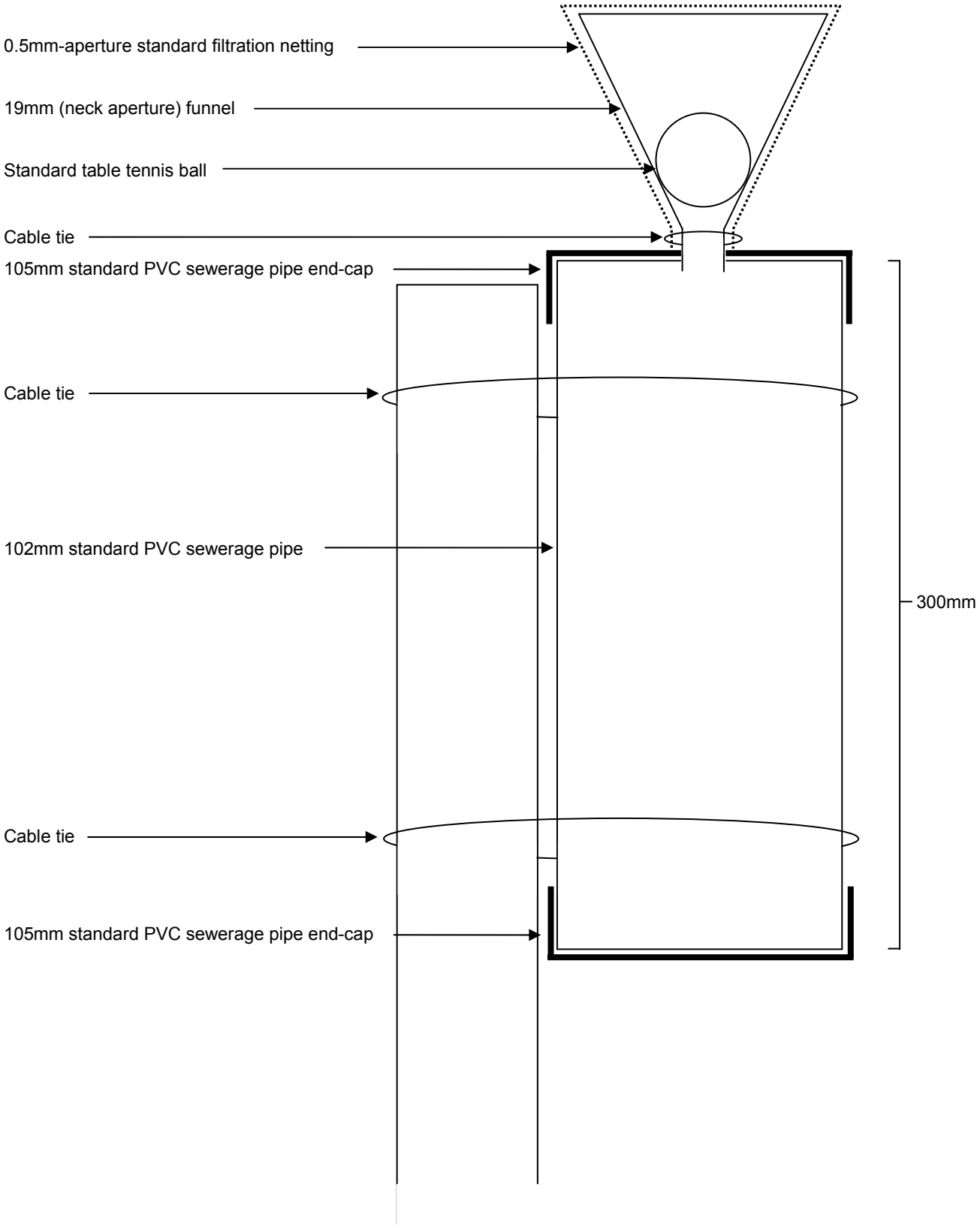

Figure A1.1: Cumulative rainfall sampler design.

Appendix A2: Water Sample Collection and Isotope Analysis

Water chemistry analysis samples were collected from the varying water sources in the field in 250ml amber bottles and were kept in a cooler box in the field and a refrigerator prior to delivery to the laboratory. Although both sets of samples remained unfiltered, cation / trace metal samples were preserved with HNO_3 to a pH of below 2. Samples were labeled according to the date, the water source and basic analysis required.

Anion samples were analysed for HCO_3^- at the SANAS-accredited Talbot and Talbot Laboratories, after being delivered within six hours of sampling, and F^-, Cl^-, NO_3^- and SO_4^{2-} using a MagIC Net ion chromatography system at the Analytical Laboratories in the UKZN Geological Sciences Department. Ion chromatography employs ion-exchange resins to isolate atomic ions based on their interaction with a specific resin. A representative sample was injected into the system such that a basic idea of anion concentrations could be attained. Consequently, a multi-element standard, which was prepared from original, individual solutions of all the anions, was used to prepare five individual standards. These standards were injected into the system; the aim of which was to formulate a calibration curve which would be used to calculate the concentrations of the anions in the various samples. A small amount of each sample was individually injected into the ion chromatography system, and once compared to the calibration curve, the concentrations of each anion (in ppm) was reported.

Cation and trace element samples were analysed at the Analytical Laboratories in the UKZN Geological Sciences Department. A Perkin-Elmer Elan 6100 inductively coupled plasma-mass spectrometer (ICP-MS) system, which was used for analysis, combines inductively coupled argon plasma detection limits with highly favourable signal-to-background ratios obtainable from mass spectroscopy, and so represents a potentially powerful method of trace element analysis (Potts, 1987). An ICP-MS system requires a set of standards, with known concentrations, to compare the water samples to, such that from the signal intensities, the concentration of each cation can be deduced. Standards of 10ppb, 20ppb, 50ppb and 100ppb were prepared such that a calibration curve could be produced, and the above process carried out. Two original multi-element standard solution, and a mercury standard solution (which have concentrations of 10ppm) were diluted and used to account for all the measurable cations; the preparation of the final standards and their concentrations shown in Table A2.1 overleaf:

Table A2.1: Standard water analysis preparation measurements.

Final Standards (ppb)	Amount of Original Standard (µl)	Amount of Stock Solution Used for Dilution (ml)
10	30	30
20	60	30
50	150	30
100	300	30

The stock solution mentioned above that was used for dilution was 5% HNO_3, and was the same agent used to dilute the various water samples. 9ml of HNO_3 were added to 1ml of sample water; the reason for such a process is to lower the sample concentration to a range that is measurable for the ICP-MS system. The final concentrations of the standards were calculated using the following formula:

$$Final\ Concentration = \frac{B}{A}.\frac{D}{C} \qquad \text{Eq. (A2.1)}$$

Where:

A – density (g/ml) of multi-element standard

B – original concentration (µg/ml)

C – mass (mg) of multi-element standard used

D – volume dilution (g)

Note that all unknowns were analysed twice, and the results averaged. The cation-anion balance for each sample, and the analytical error / measurement of uncertainty for each sample (where available) are included in Appendix H: Hydrogeochemistry of the Shu Shu Thermal Springs and Surrounds.

Water samples, which would later be required for isotope analysis, were collected in the field according to the methods set out by Mazor (1991), however with certain exceptions. 1.00l capacity polyurethane bottles were used for collection and consequent storage of $\delta^{18}O$ and $\delta^{2}H$ water samples, which were kept in a cooler box in the field and a refrigerator prior to delivery to the laboratory. A similar methodology was followed when sampling for tritium, however 2.00l capacity polyurethane bottles were used for collection and consequent storage of ^{13}C water samples

Sample analysis was kindly undertaken by Ithemba Laboratories, situated in the province of Gauteng.

The equipment utilized in the analysis of stable isotopes (^{18}O and ^{2}H) consisted of a PDZ Europa GEO 20-20 gas mass-spectrometer connected to various secondary sample preparation devices (Butler *et al.*, 2010). According to Butler *et al.* (2010), a PDZ water equilibration system (WES) is employed in dual inlet mode for the analysis of hydrogen and oxygen isotopes in water samples. Butler *et al.* (2010) state that laboratory standards, which are calibrated against international reference materials, are analysed with each of the samples – this results in an analytical precision estimated at 0.1‰ for oxygen and 0.5‰ for hydrogen. Consequently, analytical results are typically reported in the following common delta notation:

$$\delta^{18}O(‰) = \left[\frac{\left(\frac{\delta^{18}O}{\delta^{18}O}\right)_{\text{sample}}}{\left(\frac{\delta^{18}O}{\delta^{18}O}\right)_{\text{standard}}} - 1 \right] x\ 1000 \qquad \text{Eq. (A.2.2)}$$

These results are then presented in per mil deviation relative to a known standard – the standard mean ocean water (SMOW) for $\delta^{18}O$ and $\delta^{2}D$ is used here.

The samples submitted for radioactive isotope analysis (^{3}H) were distilled and enriched by electrolysis, whereby the cell consists of two concentric metal tubes (nodes) which are isolated from each other (Butler *et al.*, 2010). 500ml of water, which had been combined with sodium hydroxide ($NaOH_3$), was introduced into the cell and a direct current of 10 – 20 amperes passed through; after several days the electrolyte volume is reduced approximately 25 times so that a corresponding tritium enrichment factor of 20 is achieved (Butler *et al.*, 2010). According to Butler *et al.* (2010), samples of standard, known tritium values are run in one cell in each batch of samples to confirm the enrichment that has been attained.

Liquid scintillation counting is accomplished by preparing the samples by directly distilling the enriched water sample from the now highly concentrated electrolyte (Butler *et al.*, 2010). Butler *et al.* (2010) state that 10ml of this distilled water sample is mixed with 11ml of Ultima Gold in a vial in the analyser and counted in two or three cycles of 4 hours – this results in detection limits of 0.2TU for enriched samples.

Appendix A3: Rock Geochemistry

Samples of the various lithological units outcropping at Shu Shu thermal springs were collected according to a number of simple field rules. Specimens ranging from one fist to four fists in size were dislodged from fine-grained and coarse-grained rock types respectively, as such volumes of rock are required for geochemical analysis. Furthermore, an attempt was made to collect relatively fresh samples devoid of significant weathering or

alteration products, however when such a preference could not be achieved, considerably larger specimens were dislodged so that enough fresh rock could later be cut from the sample in the laboratory. Specimens were placed in polyurethane sample bags with the exterior of the bag being labeled with a unique sample code, along with the locality and perceived rock type.

Once in the laboratory, a rock saw (with a diamond-encrusted blade) was used to cut off any remaining weathering or alteration product, and the sample scaled down to a size deemed suitable by a laboratory technician. The remaining sample pieces were placed in an ultrasonic cleaner for one minute and then washed with tap water, at which point they were oven-dried at a temperature of 110°C for 10 – 60 minutes. A rock crusher was used to reduce the sample blocks to chip size, however a stringent cleaning sequence was employed from this point forward to ensure no contamination of the samples took place. After each crush, the sample-collecting tray was rinsed with tap water and dried, while the crusher was taken apart and cleaned with a steel brush and vacuum cleaner. Finally, the jaws of the rock crusher were cleaned with acetone.

The sample chips were subsequently cone and quartered down to a size fraction of between 80g and 160g, such that a smaller, random, representative sample was attained. This final sample portion was placed in a carbon steel rock mill and reduced to a fine powder; a requirement for geochemical analysis. After each sample, the milling vessel and rings were wiped-out with paper towel, brushed-off with a fine-haired paintbrush and cleaned with acetone. Finally, the rubber seal was removed, washed with tap water, dried with paper towel and repositioned. The fine powder was placed in a sealable plastic bag and labeled accordingly.

X-ray fluorescence was the chosen technique employed to determine both the major and minor, and trace element geochemistry of the samples. Essentially, from powder form, the techniques according to Potts (1987) and Hutchison (1974) were followed in order to accomplish the afore-mentioned task. To allow for the determination of major and minor element concentrations, a small proportion of the sample was infused into a glass disc, however, owing to the low concentration of trace elements expected to occur in the sample, small ‘pellets’ were required for analysis. A quantity of 8.0g – 9.0g of the milled sample material was weighed out in an agate pestle, to which 0.6ml of mowiol 4-88 was added. An agate pestle was used to press and mix the sample and fluid such all of the powder contained an equal amount of moisture. The ‘wetted’ material was placed inside a steel apparatus and 6 – 7 tons of pressure was added, using a hydraulic jack, so that a pellet,

approximately 3.5cm in diameter was formed. The pellet was labeled with the original sample code and placed in a drying oven, set at 105°C, to dry and harden.

Once preparation had been completed, all element concentrations were determined through the use of a Philips PW 1410 wavelength dispersive X-ray fluorescence spectrometer. A lithium tetraborate flux was used in a sample to flux ratio of approximately 1 : 4, whilst LOI was determined at a temperature of 1050°C. Note that in accordance with Govindaraju (1994), certified reference materials were used as calibration standards throughout all analyses.

Petrographical thin sections were prepared in the School of Geological Sciences at the University of KwaZulu-Natal's Westville Campus. Hand specimens, which had been collected and orientated in the field, were cut in two in the laboratory through the use of a diamond-encrusted saw blade in an approximate north – south orientation. Once a suitable face had been cut, a sliver of rock was removed from the hand specimen and glued onto a glass slide plate through the use of clear epoxy resin. After each slide had been cured on a hot plate, the thickness of the rock sliver was reduced to manageable dimensions. Finally, after the rock sliver had been ground down to 30µm in thickness, it was subjected to a rough polish, however cover slips were not employed. The thin sections were viewed through the use of a transmitting light microscope, under both plane-polarised and cross-polarised conditions, in the Department of Geological Sciences at the University of KwaZulu-Natal's Westville Campus.

Appendix A4: Field Mapping

Field mapping was undertaken at the Shu Shu thermal springs through the identification of important outcrop localities which were deemed to exhibit the elemental geological features of the study area. These localities typically include lithological contacts, variations in petrology or mineralogy, intrusive features and primary or secondary tectonic structures. The localities were assigned a number based upon their proximity relative to the nearest previously detailed locality, with these important outcrops typically grouped into sets of two or three and labeled accordingly. Locality numbers do not appear to be consecutive as two periods of mapping were completed, and as such seasonal variations had to be accommodated for. The exact position of each locality was recorded with a GPS device, whereby decimal degrees were utilised as the preferred units of measurement. Figure A4.1, which illustrates the positions of the important outcrops (from the first period of field mapping) with respects to the Shu Shu thermal springs, is included overleaf.

At each locality, a concise description of the lithology was recorded, detailing the colour, grain size and probable mineral composition of the rock type/s. Furthermore, the structures and features evident at the locality were briefly described, and if considered important, digital photographs were taken thereof. Finally, the identified lithology and contacts (where applicable) were drawn on an orthophoto of the study area, such that a basic geological map was created.

On arrival of an important joint / vein pavement, detailed outcrop mapping was undertaken by firstly measuring the length and bearing / strike of the outcrop boundaries and recording it in map format. Subsequently, the size and dip and strike of the various structures within the outcrop boundaries were recorded (using the right-hand rule) and plotted on the diagram. Finally, the diagrams were annotated with a north-arrow, scale bar and legend.

The detailed outcrop maps were then scanned at a resolution of 300 dots per inch into .tiff format, such that they could be opened in ESRI ArcMap™ 9.3.1 (a digital GIS program) as a layer (.lyr) data source. The outcrop boundaries and relevant structures were subsequently digitized using a number of themes (.shp files) and then annotated according to their respective bearing / dip and strike values. Finally, the outcrop diagrams were exported as JPEG images owing to the inherent versatility of this format.

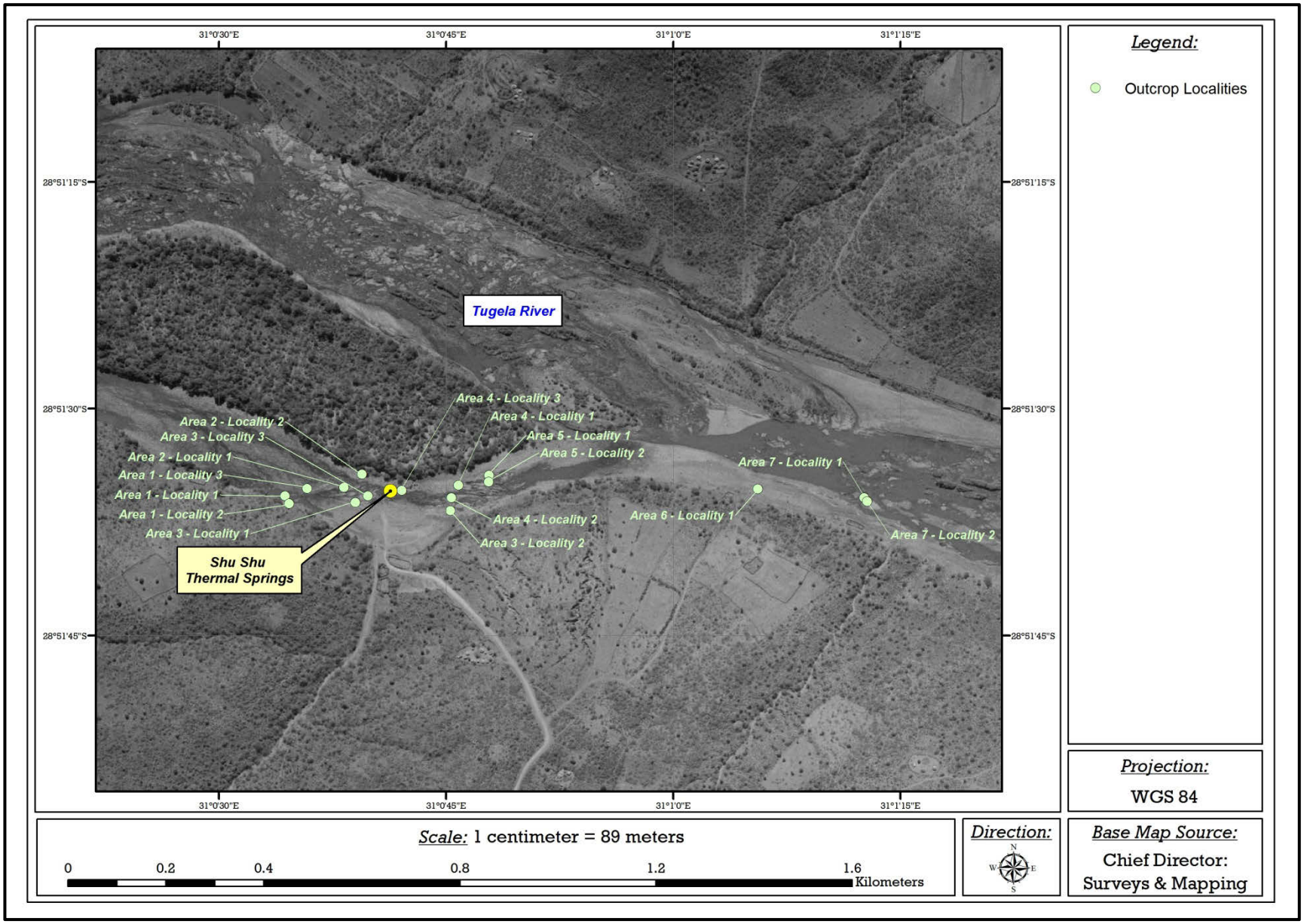

Figure A4.1: Outcrop locality map – general (1st mapping period)

The stereograph program, Stereo32 ©, was used to plot the various joint and vein readings taken at each outcrop mapping locality that are illustrated on the afore-mentioned outcrop diagrams. As joints and veins represent planar data, the readings were plotted as poles-to-planes, under equal area, lower hemisphere specifications; the resultant plots were then positioned along-side their associated outcrop diagram, as is seen in Appendix D3: Outcrop Locality Maps.

Appendix A5: Geophysical Investigation

The geophysical investigation of the Shu Shu thermal springs was sub-divided into two separate components and completed with the aid of three different apparatuses. The initial investigation was undertaken in an attempt to identify the principle zones around the thermal springs that may act as pathways for groundwater movement such that they could be studied in further detail. This part of the investigation was deemed 'Phase 1' and was completed through the use of a Geometrics © Proton Magnetometer and an ABEM © Very Low Frequency (VLF) WADI. Readers are referred to Breiner (1973) and ABEM Geophysics (1991) respectively for further information regarding these two geophysical exploration techniques.

Proton magnetometers and VLF devices are typically employed in unison to identify fractures zones that are traversed over, and so are most efficiently utilized when two operators are available. The operator using the VLF device (WADI) selects a starting position in the field and marks this locality on the ground, whilst GPS coordinates are also taken. Before commencing the traverse, this operator selects an approximate 3-dimensional end-point so that one can maintain one's bearing / orientation, as geophysical traverses must be linear. As can be seen on Figure A5.1 overleaf, which shows the WADI interface, a suitable frequency is selected / scanned for depending on one's locality in the world by selecting ↑ ; a value of 19.7kHz was utilized as part of this study. Once a suitable frequency is attained, and an appropriate traverse number / profile selected, the tilt angle (degrees) for the traverse starting point is recorded within the apparatus by selecting > . Once the first tilt angle has been recorded, the operator walks 10 metres in the selected orientation (toward the 3-dimensional end-point), at which point another marker (dot) is laid down. 10 metres is the standard value utilized when using the WADI VLF, and although it can be altered, it is the default distance value typically employed for this type of geophysical investigation. The second tilt angle is recorded by the operator on the apparatus, at which point the process is repeated until the end-point is reached and the operator

is satisfied with the length of the traverse. To avoid confusion, a secondary mark (such as a line) is laid down at the first and last geophysical point, such that the traverse is clearly delineated. The completion of the traverse denotes what is typically referred to as 'WADI forward' with respects to the geophysical readings. This process described above is then repeated, along the self-same traverse, in the opposite direction (180° shift); this is then typically known as 'WADI reverse' with respect to the attained geophysical readings. The reason as to why the traverse is walked and recorded twice is due to the fact that the chosen frequency (19.7kHz) is often stronger in one direction, and so readings are typically more accurate in this direction.

Figure A5.1: ABEM WADI VLF user interface.

The operator using the proton magnetometer commences their traverse at the already-defined starting point once the WADI VLF operator has moved sufficiently along their traverse (interference from the two apparatuses may result in incorrect readings). As can be seen on Figure A5.2 overleaf, which shows the proton magnetometer interface, the field strength (in nano Tesla) for the traverse starting point is recorded in a field note book as '0m' after a value has been attained by selecting 'Read'. The proton magnetometer operator then moves half the

distance to the second geophysical point marked by the WADI VLF operator, in the same orientation, and records the field strength as '5m'. This process is repeated along the traverse, such that readings are taken every 5m, both at the marked geophysical points and halfway in between them, until the traverse-end is reached.

Figure A5.2: Proton Magnetometer user interface.

The raw data attained from both of these geophysical investigation methods are best analysed when plotted on an X-Y graph, with both series shown on one graph; this allows for combination analysis with the data sets potentially supporting each other. The traverse distance, typically in metres, is shown on the X-axis, and the WADI VLF (in tilt angle) and Proton Magnetometer (in nano Tesla) readings shown on separate Y-axis. Such a practice, of showing the raw data in a graphical format, typically allows for the recognition of any anomalies – these are identifiable by a sudden increase or decrease (or both) in readings over a short distance, whereby they deviate from what is typically considered as the mean. The amplitude and period of the anomalies typically will result from different geological features; the identification of which can be made through experience and comparison to 'standard', published data and shapes. However, for the purposes of this investigation, the anomalies were assumed to represent zones by which

groundwater may move, and so when marked on an ortho-photograph of the study area, allowed for identification of the potential groundwater movement pathways toward the Shu Shu thermal springs.

Note that the geophysical data acquired from this study is included as Appendix E.

Appendix A6: Photogeology

Photogeological analysis was undertaken at the Shu Shu thermal springs through the identification of structural lineaments from aerial photography of the study area. The study area is defined here as a 63km^2 region (7km north-south x 9km east-west) centered on the Shu Shu thermal springs. ESRI ArcMap^{TM} 9.3.1 was utilised to delineate the study area as a .shp file; this was then layered upon a set of digital orthophotographs with the geographical codes 2831 CC (06 + 07 + 11 + 12) and 2331 DD (10 + 15). Once the map had been annotated with a scale bar and north arrow, an A2 size (420mm x 694mm) print-out was produced; this diagram had a scale of 10mm = 182m. Clear, plastic film, of similar dimensions, was overlaid upon the orthophotograph image and temporarily fixed in place along the northern border. A fine-tip, water soluble projector pen was then utilised to delineate both inferred and possible air-photograph lineaments as identified and suspected by the author. This process was aided through employing an A3-size (420mm x 297), 10mm = 91m scaled colour aerial photograph obtained from Google Earth 2010 ©. Figure A6.1, which illustrates the delineated lineaments drawn on the clear plastic film as identified from the underlying ortho-photograph image, is included overleaf.

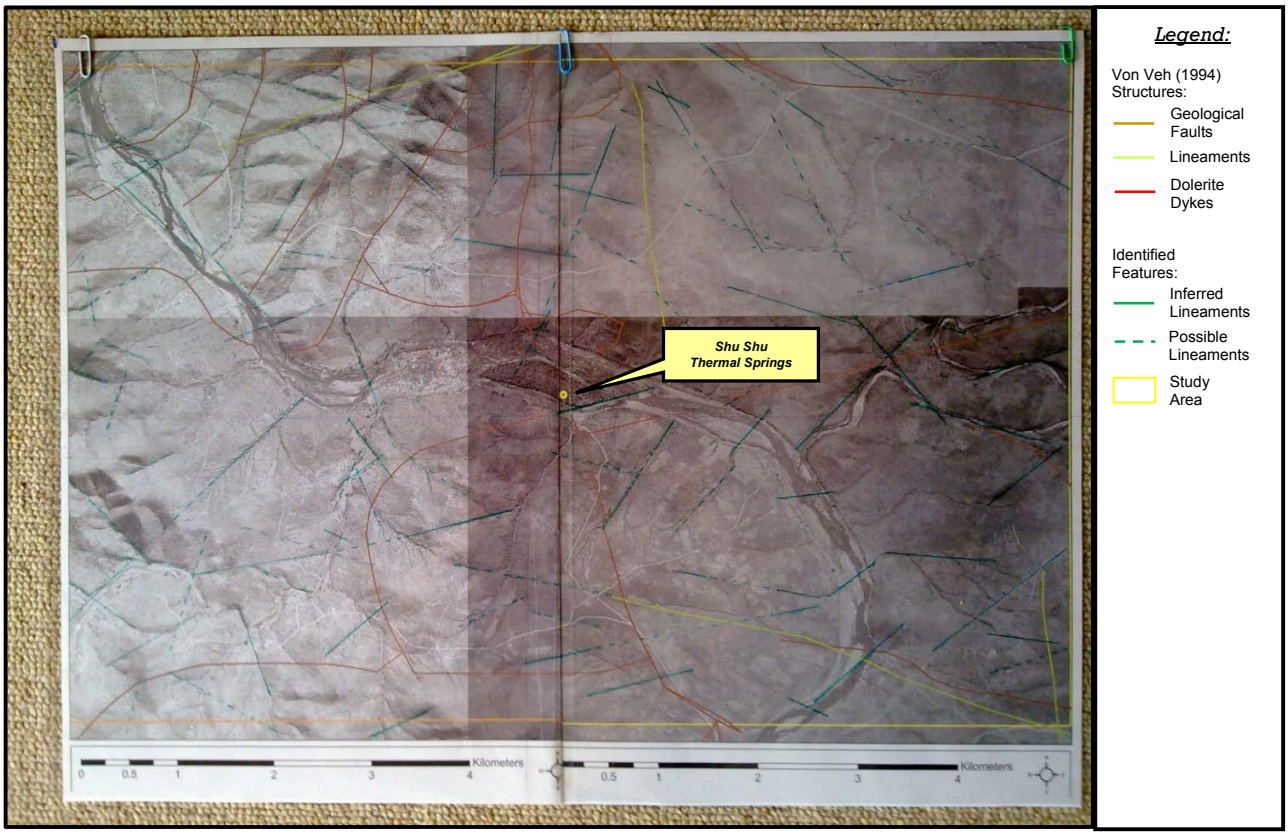

Figure A6.1: Shu Shu thermal springs ortho-photograph image with identified lineaments.

The original ortho-photograph imagery of the Shu Shu thermal springs was once again opened in ESRI ArcMap™ 9.3.1 as a base map and saved as a project (.mxd) file. Through the process of visual inspection, the inferred and possible lineaments delineated on the clear plastic film were digitized as separate theme (.shp) files and consequently over-laid onto the ortho-photograph imagery. This was undertaken by ticking each lineament on the clear plastic film as each new lineament was digitized as part of the employed theme file. The pre-existing dolerite dyke, fault and lineament shape files, as originally identified by Von Veh (1994), were too over-laid onto the base map. Once converted to the layout view, the 'lineament map' was annotated with a legend, scale bar and north arrow, and source and projection information, added.

Appendix A7: Saturation Indices

Saturation indices were calculated using PHREEQC *for Windows* Version 2.17.0.1™; a hydrogeochemical transport model that allows for forward and inverse modeling (Parkhurst and

Appelo, 2010). The aqueous model defined by *phreeqc.dat*, used here, allows for the speciation calculation and saturation state of groundwater relative to a set of minerals.

Once PHREEQC has been opened, the 'Input' tab under the default interface is selected to allow for the entering of required physical water characteristics and major element / compound concentrations. 'Title' and 'Solution' information is entered to define the project and model run. After the 'units' have been defined (ppm or mg/l are set as the default and are used here), the critical data, including the pH and temperature of the water, as well as the basic determinant concentrations, are entered. These parameters are required for a realistic hydrogeochemical transport model to be run. Note that when compound concentrations are entered, as for HCO_3, SO_4 and NO_3, these define the concentrations of chemical symbol, followed the valence states (in parathensis). Other input values, including those of 'pe', 'density' and 'redox', can be entered to increase the accuracy of the model, however for the saturation indices calculated as part of this exercise, values changed by an average of approximately 0.01. If, as in the case of the models run as part of this exercise, a 'redox' value is not entered, then the input 'pe' value will be the default. When a 'pe' value is not entered, once again as for this exercise, the default 'pe' value is 4.0 (Parkhurst and Appelo, 2010). Figure A7.1, which illustrates the entered data under the 'Input' tab, is shown overleaf.

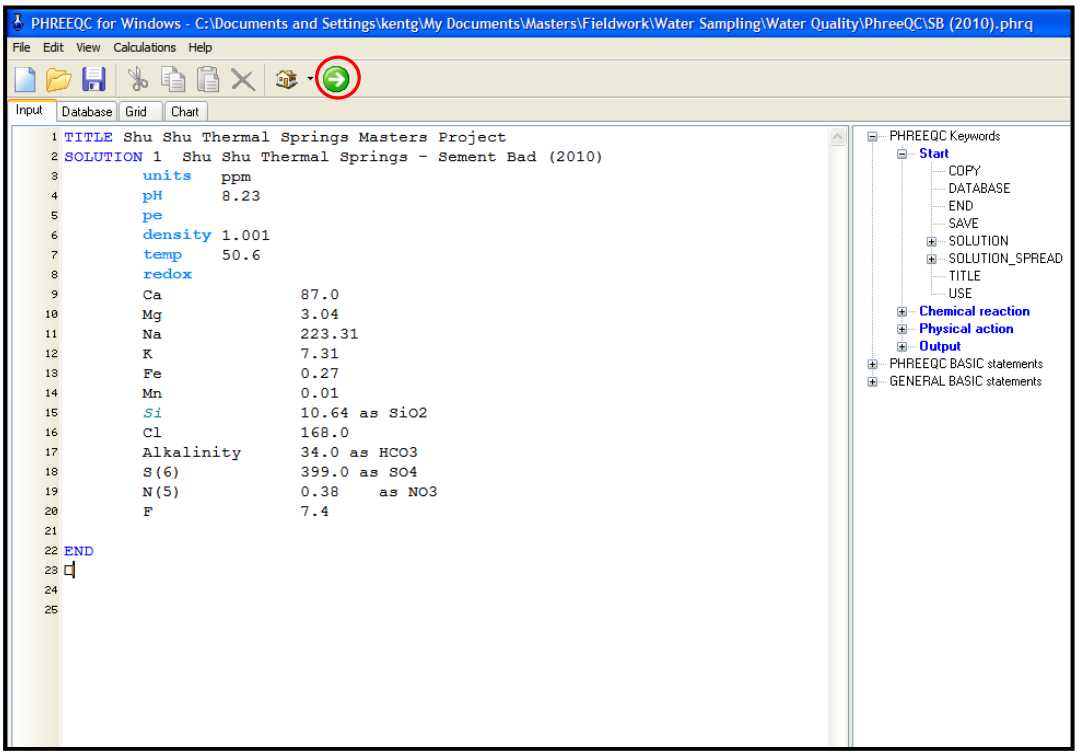

Figure A7.1: PHREEQC 'Input' interface with 'Calculate' button ringed.

Once the 'Input' data has been entered, the 'Calculate' button, as shown above, is selected, and the hydrogeochemical model is run. A 'Progress' window details the 'Input' and 'Output' files, as well as the time taken to run the model. Acceptance of this exercise results in the 'Output' tab being illustrated, with associated data shown. Once PHREEQC has read the database and input data, the 'Solution Composition', 'Description of Solution', 'Distribution of Species' and 'Saturation Indices' are calculated / detailed. As this exercise is centered on the 'Saturation Indices', this interface is shown hereafter as Figure A7.2. The saturation indices, the log value of the ion activity product (IAP) and the log value of the solubility constant (KT) is determined for each mineral and included in the final section. Mineral types include a default set based upon the entered determinants, and can be specified / altered.

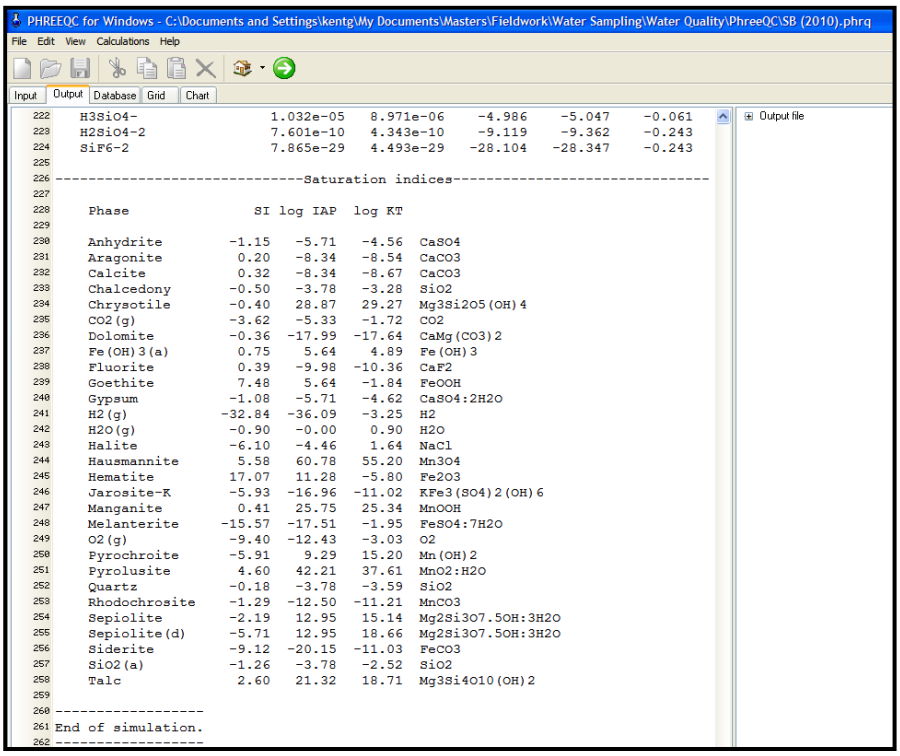

Figure A7.2: PHREEQC 'Output' interface illustrating calculated saturation indices.

Appendix B: Theories on the Formation of Thermal Spring Source Features

Appendix B1: Lebombo 'Monocline'

Watkeys (2002) and Klausen (2009) state how the formation of the Lebombo 'monocline' should be likened to rifting along the east coast of Greenland (Du Toit, 1929), however Watkeys (2002) argues against the plume / triple junction theory. Rather, he proposed that upwelling of anomalously hot sublithospheric mantle occurred across a broad zone, which was possibly induced through subduction processes along the western coast of Gondwana, resulted in the preserved pattern observable today. Furthermore however, as there is evidence of tectonic activity 70 Ma before the originally proposed plume, Watkeys (2002) states that the notion of a triple junction, as ascribed to a plume, is an oversimplification. Although elements of a 120° triple junction are observed (Fahrig, 1987), field evidence suggests that they did not develop synchronously.

Rather the initial magmatism of the Lebombo event occurred along the pre-existing, east-northeast orientated Limpopo trend / zone of weakness, whilst the later intrusion of the west-northwest orientated Okavango dyke swarm represents the first time that a new trend developed in the region (Watkeys, 2002). This fracture pattern is ascribed to 'plume power' with dilation of this dyke swarm ultimately resulting in movement along the Agulhas-Falkland Fracture Zone, which resulted in the formation of the north – south orientated Lebombo 'monocline' (Watkeys, 2002). Watkeys (2002) states that this ultimately returned the fracturing to the original site of volcanism, which resulted in the appearance of the 120° triple junction. Further extension along the Lebombo, which involved the intrusion of the Rooi Rand dyke swarm, resulted in the monoclinal flexing and faulting pattern observed (Watkeys, 2002). Despite the intrusion of the Rooi Rand dyke swarm, Watkeys (2002) argues that full continental separation did not take place (likely due to the short-lived nature of the thermal upwelling event), and so infers a failed rifted margin, or more specifically, a doubly rifted margin, as the Lebombo was involved in the Karoo event, and the later Cretaceous break-up of Gondwana.

Klausen's (2009) arguments of a successfully rifted margin and the formation of a triple junction in relation to the Lebombo 'monocline' are based upon available field observations which correlate to that which is observed within the Tertiary Igneous Province along the North Atlantic coast of Greenland (Du Toit, 1929). Detailed mapping of numerous basaltic flows and dykes within the Lebombo region allowed for the preparation of a geological cross-section that is compatible with, and highlights a tectonomagmatic resemblance to, the relatively narrow East Greenland margin (Klausen, 2009). Further evidence is sought from the relative inclinations of the mapped basaltic flow and dyke planes across the Lebombo

'monocline', which are consistent with syn-emplacement tilting in accordance with those observations drawn by Lenoir *et al*. (2003) regarding the East Greenland margin, and which likely formed within an initial east – west orientated pull-apart graben. Klausen (2009) continues by stating that due to this observed similarity between field relationships, the formation mode of the Lebombo 'monocline' can be further likened to that of the East Greenland margin, where early tectonic extension was overwhelmed by dyke intrusion that may have been laterally fed by a central magma chamber. The conclusion can thus, according to Klausen (2009), be drawn that the Lebombo 'monocline' is part of a successfully rifted margin, which furthermore belongs to a distinct class of highly volcanic and relatively narrow margins. Indeed this class of margin only forms proximal to classic triple rift systems, with Klausen (2009) arguing that the Lebombo volcanic rifted margin converted to the Lebombo-Mwenezi-Okavango triple rift system within approximately 1 million years – 3 million years, where increased magma production sustained a magmatic manner of extension.

Appendix B2: Great South African Escarpment

Numerous authors have typically championed two possible theories to explain the observed unusual elevation gain and topographical character relating to the Great South African Escarpment, although a third has recently been proposed. According to Moore *et al*. (2009), recent attempts to account for the elevated nature of the interior plateau have generally focused upon a mantle plume theory. Burke and Gunnell (2008) employed the term 'polygenetic landform' to describe the African erosion surface, whereby the presence of this topographic anomaly was attributed to a Large Low Shear Velocity Province at the Core-Mantle Boundary which is thought to have generated plumes under the African plate. It was postulated that this resulted in shallow convection and the thermal modification of the upper mantle when the African plate was stationary during the mid- to late-Tertiary (Burke and Gunnell, 2008), and hence the uplift which resulted in the interior plateau elevations observed today.

However, other authors argue for Mesozoic elevation gain which hence infers that deep mantle processes associated with the breakup of Gondwana were the source of buoyancy for plateau uplift (De Wit, 2007). This theory was furthered upon by Flowers and Schoene (2010), who identified unroofing during Mesozoic times through (U-Th)/He thermochronometry. It was postulated that such unroofing may very well have resulted from Mesozoic elevation gain, however Cretaceous unroofing post-dates significant ~183 Ma volcanism along the Lebombo 'monocline' (Flowers and Schoene, 2010). Rather, the

determined unroofing times overlap with the formation of the ~132 Ma Etendeka-Parana Large Igneous Province (LIP), which was associated with final Gondwana breakup in the south Atlantic (Flowers and Schoene, 2010). Flowers and Schoene (2010) conclude by stating that whilst a Cenozoic uplift period cannot be discounted, should it have occurred, it post-dated the most important phase of post-Palaeozoic denudation along the eastern margin of the interior plateau. Consequently, due to the overlap of Mesozoic unroofing with LIP magmatism, continental rifting and the intrusion of numerous kimberlite pipes, deep mantle processes were identified as the cause of buoyancy which resulted in the rise of the southern African plateau.

Recently, and in agreement with other authors, Moore *et al*. (2009) have identified a disparity between the expected topographic features when a deep mantle plume model is invoked, and those that are actually observed across southern Africa. Moore *et al*. (2009) continue by detailing a variation in areas of high ground across the escarpment, whilst stating that the observed, approximately coast-parallel drainage pattern in southern Africa differs from the dome and radial drainage pattern that would be expected should a plume have been in existence. Rather, and in accordance with these findings, Du Toit (1933) and King (1963) ascribe the observed drainage divides to axes of epeirogenic uplift. From the coast inland, Moore *et al*. (2009) designate these flexures as the Escarpment Axis (which pertains to this study), the Etosha-Griqualand-Transvaal (EGT) Axis and the Ovambo-Kalahari-Zimbabwe (OKZ) Axis. Moore and Blenkinsop (2006) state that the Escarpment Axis has been well-modeled as a line of isostatic flexure which is related to the erosion of the coastal plain that occurred subsequent to the breakup of Gondwana. King (1963) and Moore and Blenkinsop (2006) elaborate on this in detailing how uplift along the Escarpment Axis was initiated by the opening of the Atlantic and Indian Oceans at ~126 Ma, although the timing of uplift along all three flexures coincides with episodes of alkaline volcanism across southern Africa. Brown *et al*. (1990) state that this uplift period is reflected by a major Early Cretaceous erosional event, which is marked, in particular, along the margins of southern Africa. Such erosion of the coastal plain has continued and has resulted in the progressive inland migration of the isostatic flexure (Gilchrist and Summerfield, 1991), with the Great South African Escarpment in its present position reportedly attributable to this process.

That the Great South African Escarpment owes its origins to the actions of erosion and denudation is clear and beyond contestation, with only the reason as to the observed, unusual elevations of the interior plateau questionable. Kounov *et al*. (2007) concluded from their investigation that local variations in both lithology and climate typically control the resulting patterns of present denudation across different landforms. Indeed the latter factor

has likely varied considerably since the original uplift period of the interior plateau, although it cannot be confirmed whether this is responsible for the fact that denudation rates presently, and over the last few hundred thousand years, have typically been an order of magnitude lower than what they were during the Cretaceous, as estimated from apatite fission track analysis (Kounov *et al*., 2007). The former factor, of lithology, has also partly controlled denudation rates, as according to Svensson (2000), the location of numerous basaltic layers within the lower, warmer and more humid areas (particularly in western KwaZulu-Natal), has resulted in increased weathering and hence the undermining of the Great South African Escarpment, hence causing further inland retreat.

Appendix C: Geological Cross-Sections

Appendix C - Geological Cross Sections

North - South Cross Section from A - B Through the Shu Shu Thermal Springs Depicting Geological Units, Tectonic & Petrological Contacts and Structures

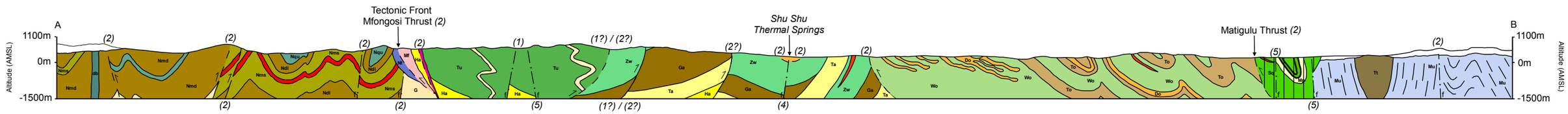

North-West - South-East Cross Section from C - D Through the Shu Shu Thermal Springs Depicting Geological Units, Tectonic & Petrological Contacts and Structures

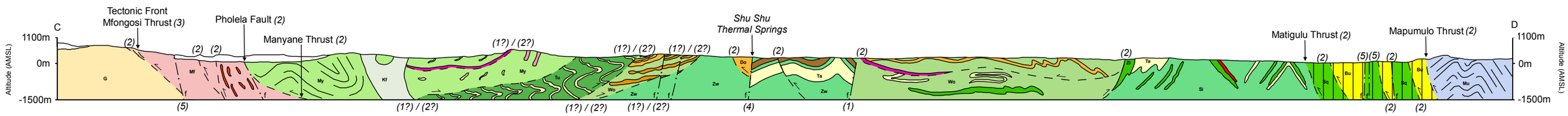

Geological Symbols:

- Geological Contact
- Thrust
- Fault (f)
- 1 Sense of Movement

Geological Legend:

- Cover Rocks (Palaeozoic to Tertiary)
- db — Meta-Dolerite Sheets & Dykes

MOBILE BELT

Mapumulo Group
- Tt — Tutini (Tt) — Diorite
- Mu — Undifferentiated (Mu) — Gneisses, migmatites aplites & pegmatites

Mapumulo Thrust

Matigulu Group (*Steep Belt*)
- Mp — Mpisi (Mp) — Gneisses
- Sq — Sequembi (Sq) — Gneisses & quartzite
- Bu — Buhleni (Bu) — Gneisses

Geological Legend Continued:

MOBILE BELT CONTINUED

Tugela Group

Tugela Nappe
- Kf — Kotongweni (Kf) — Tonalite
- My — Manyane (My) — Gneiss sheets
- Tu — Tuma (Tu) — Amphibolites, meta-volcanics & gneisses

Tuma Thrust

Mandleni Nappe
- Wo — Wosi (Wo) — Amphibolites & quartzite
- To — Thondweni (To) — Gneiss
- Du — Dulumbe (Du) — Gneisses
- Do — Dondwana (Do) — Gneiss

Mandleni Thrust

Madidima Nappe
- Zw, Si — Zwaneni (Zw) Silambo (Si) — Amphibolites & quartzite
- Ga — Gazeni (Ga) — Gneisses & schists
- Ta — Thaweni (Ta) — Gneiss

Madidima Thrust

Nkomo Nappe
- Ha — Halambu (Ha) — Gneiss

MOBILE BELT CONTINUED

Nkomo Thrust

Mfongosi Group
- Mf — Differentiated (Mf) — Schists

NORTHERN FORELAND

Ntingwe Group
- Nt — Dlolwana (Nt) — Conglomerates & breccias

Nsuze Group
- Nma Nqu — Mankene (Nma) Qudeni (Nqu) — Basaltic lavas
- Nms — Msukane (Nms) — Phyllites & schists
- Nmd Ndl — Mdlelanga (Nmd) Dlabe (Ndl) — Conglomerates & phyllites

Pre-Nsuze Post Nondweni Granitoid Gneiss
- G — Undifferentiated (G) — Gneisses & granitoids

DEFORMED METABASIC - ULTRABASIC COMPLEXES
- gb — Gabbros & pyroxenites
- Se — Serpentinites & schists

Principal Structure Orientations:

(1) Northwest - Southeast
(2) East-northeast - West-southwest
(3) North - South
(4) North-northeast - South-southwest
(5) West-southwest - East-northeast
(6) East-southeast - West-northwest
(?) Unconfirmed

Scale:

0 1.5 3 6 9 12 15 18 21 24 27 30 33 Kilometres

Vertical Exaggeration: None

Geological Map Source: Matthews and Charlesworth (1981)

Appendix D: Maps

Legend:

Rock Sampling Points

Title:

Appendix D1: Rock Sample Localities

Projection:

WGS 84

Scale:

0 75 150 300 450 600 750 900 Metres

Direction:

N W E S

Base Map Source:

Chief Director: Surveys & Mapping

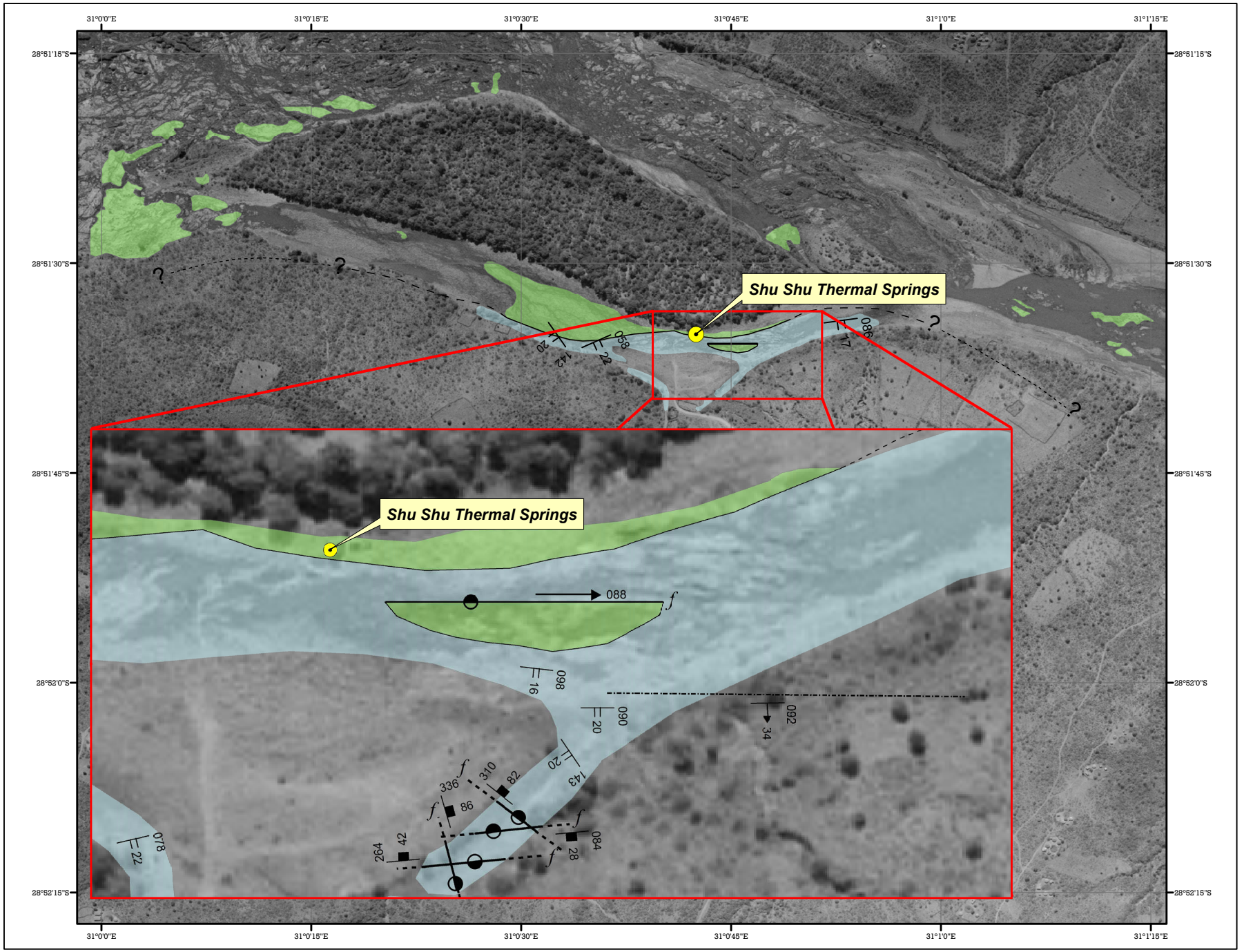

Legend:

Rock Types

- Gneiss
- Amphibolite
- Approximate Outcrop Boundary

Geological Symbols

- Contact - Observed
- Contact - Inferred
- Contact - Uncertain
- ? Contact - Unknown
- Fault - Observed
- Fault - Inferred
- Shear Zone - Observed
- *f* Fault
- Fault - Downthrow Marker
- 310 82 Dip/Strike - Fault
- 092 34 Dip/Strike - Shear Zone
- 078 22 Dip/Strike - Cleavage
- Orientations

Title:

Appendix D2: Geological Map

Projection:

WGS 84

Scale:

0 0.25 0.5 1 1.5 2 Kilometres

Direction:

N W E S

Base Map Source:

Chief Director: Surveys & Mapping

31°0'0"E

31°0'15"E

28°51'15"S

28°51'30"S

Area 8 - Locality 2

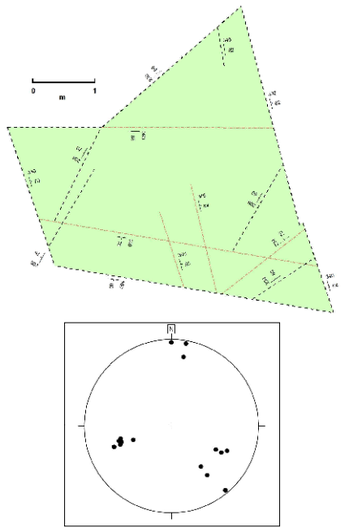

Area 9 - Locality 1

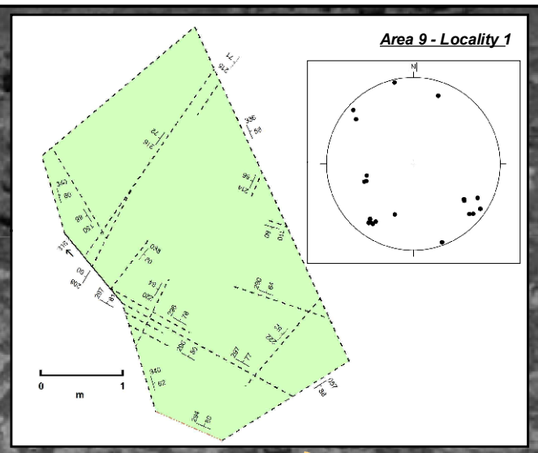

Area 9 - Locality 2

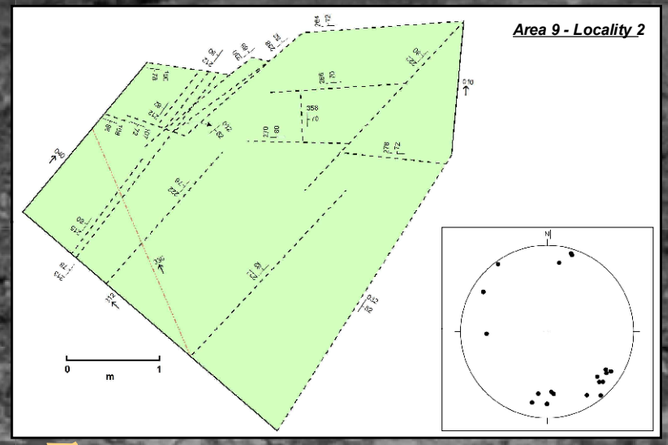

Shu Shu Thermal Springs - 815m

Area 8 - Locality 1

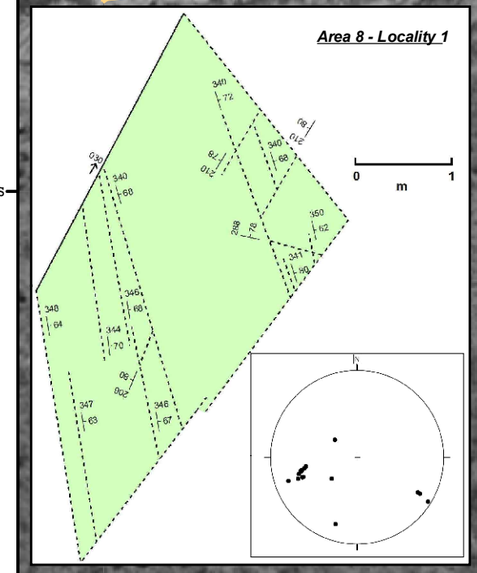

Area 8 - Locality 3

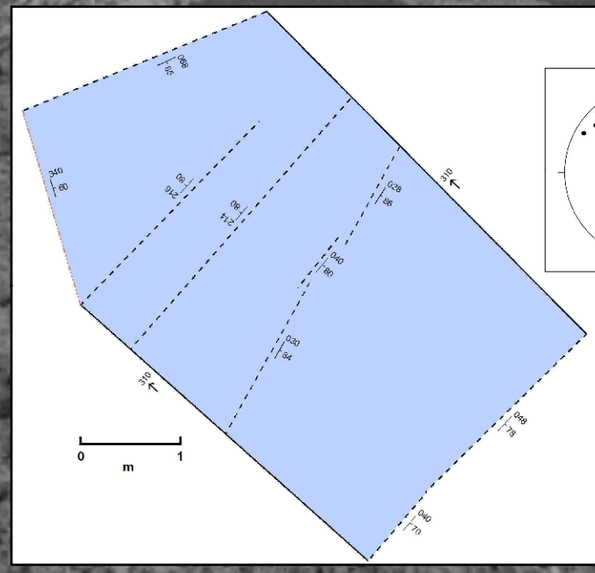

Area 9 - Locality 3

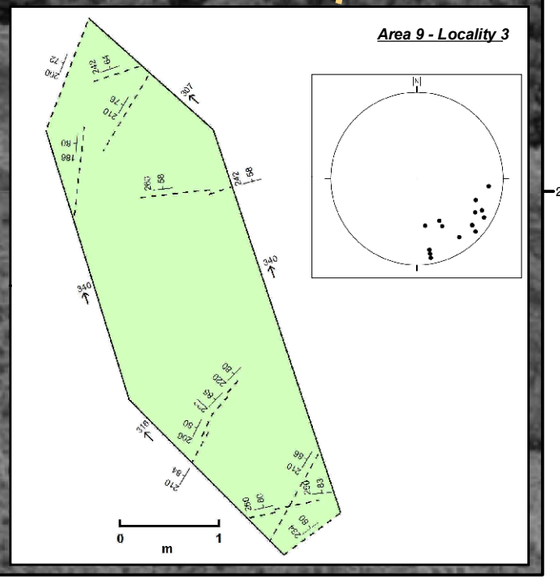

Legend:

Base Map

- Outcrop Localities
- Locality - Map Markers

Outcrop Locality Maps

- Gneiss
- Amphibolite
- Orientations
- Outcrop Boundaries
- Joints
- Veins
- 041/80 Dip/Strike - Joints & Veins

Title:

Appendix D3: Outcrop Locality Map - Western Area

Projection:

WGS 84

Scale:

0 0.1 0.2 0.4 0.6 0.8 Kilometers

Direction:

N W E S

Base Map Source:

Chief Director: Surveys & Mapping

31°0'30"E

31°0'45"E

28°51'30"S

28°51'45"S

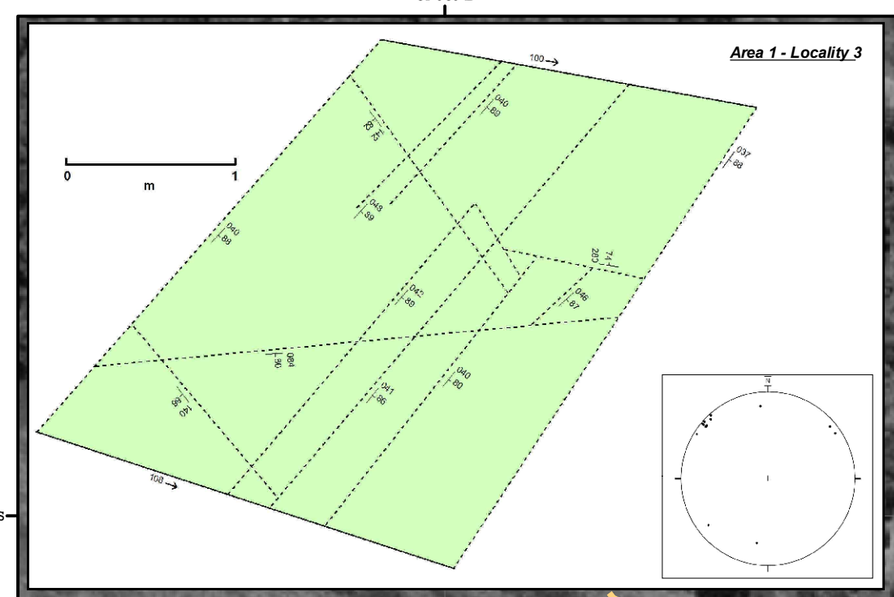

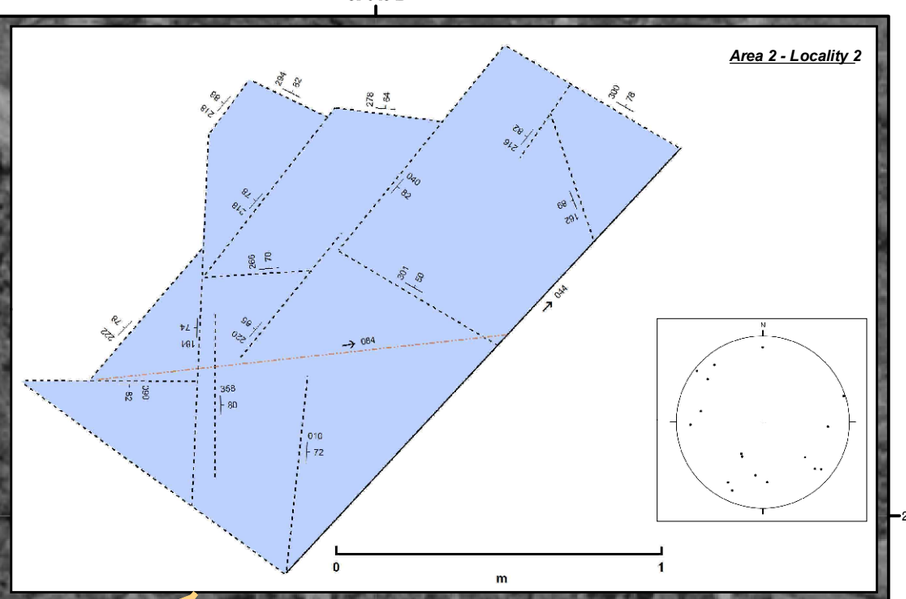

Shu Shu Thermal Springs

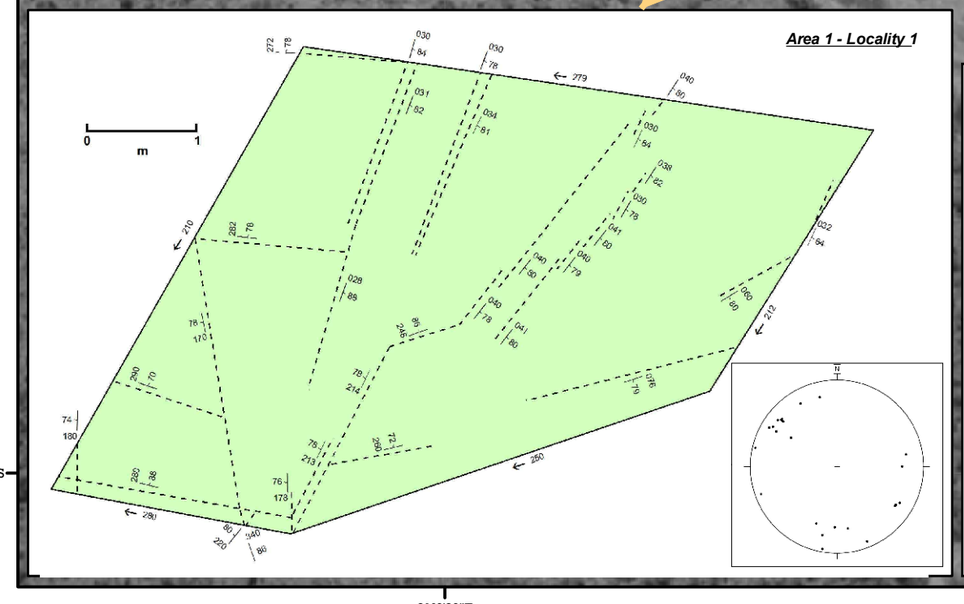

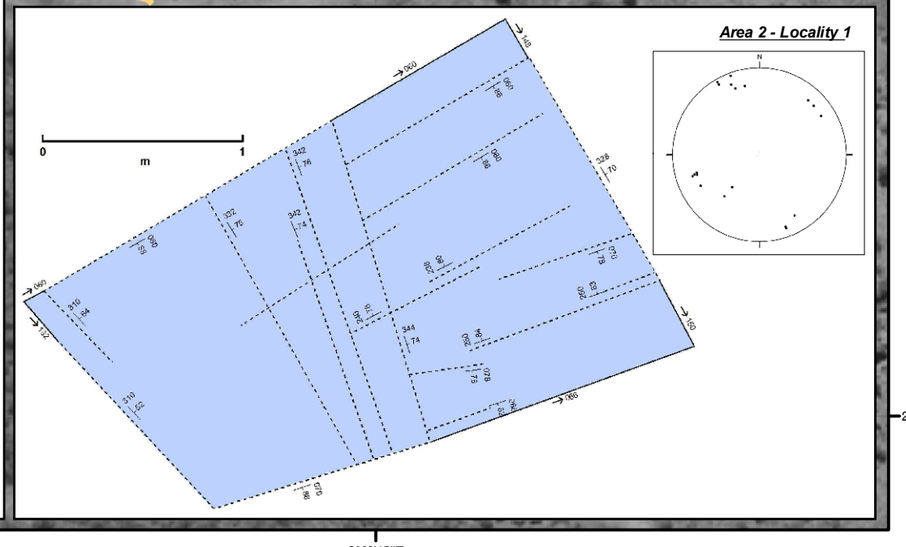

Legend:

Base Map

- Outcrop Localities
- Locality - Map Markers

Outcrop Locality Maps

- Gneiss
- Amphibolite
- Orientations
- Outcrop Boundaries
- Joints
- Veins
- 041/80 Dip/Strike - Joints & Veins

Title:

Appendix D3: Outcrop Locality Map - Central Area West

Projection:

WGS 84

Scale:

0 0.1 0.2 0.4 0.6 0.8 Kilometres

Direction:

N W E S

Base Map Source:

Chief Director: Surveys & Mapping

31°0'30"E

31°0'45"E

28°51'30"S

28°51'45"S

Area 3 - Locality 2

Area 4 - Locality 1

Shu Shu Thermal Springs

Area 3 - Locality 1

Area 4 - Locality 2

Legend:

Base Map

- Outcrop Localities
- Locality - Map Markers

Outcrop Locality Maps

- Gneiss
- Amphibolite
- Orientations
- Outcrop Boundaries
- Joints
- Veins
- Dip/Strike - Joints & Veins

Title:
Appendix D3: Outcrop Locality Map - Central Area East

Projection:
WGS 84

Scale:
0 0.1 0.2 0.4 0.6 0.8 Kilometres

Direction:
N W E S

Base Map Source:
Chief Director: Surveys & Mapping

31°0'45"E 31°1'0"E 31°1'15"E

28°51'30"S

28°51'45"S

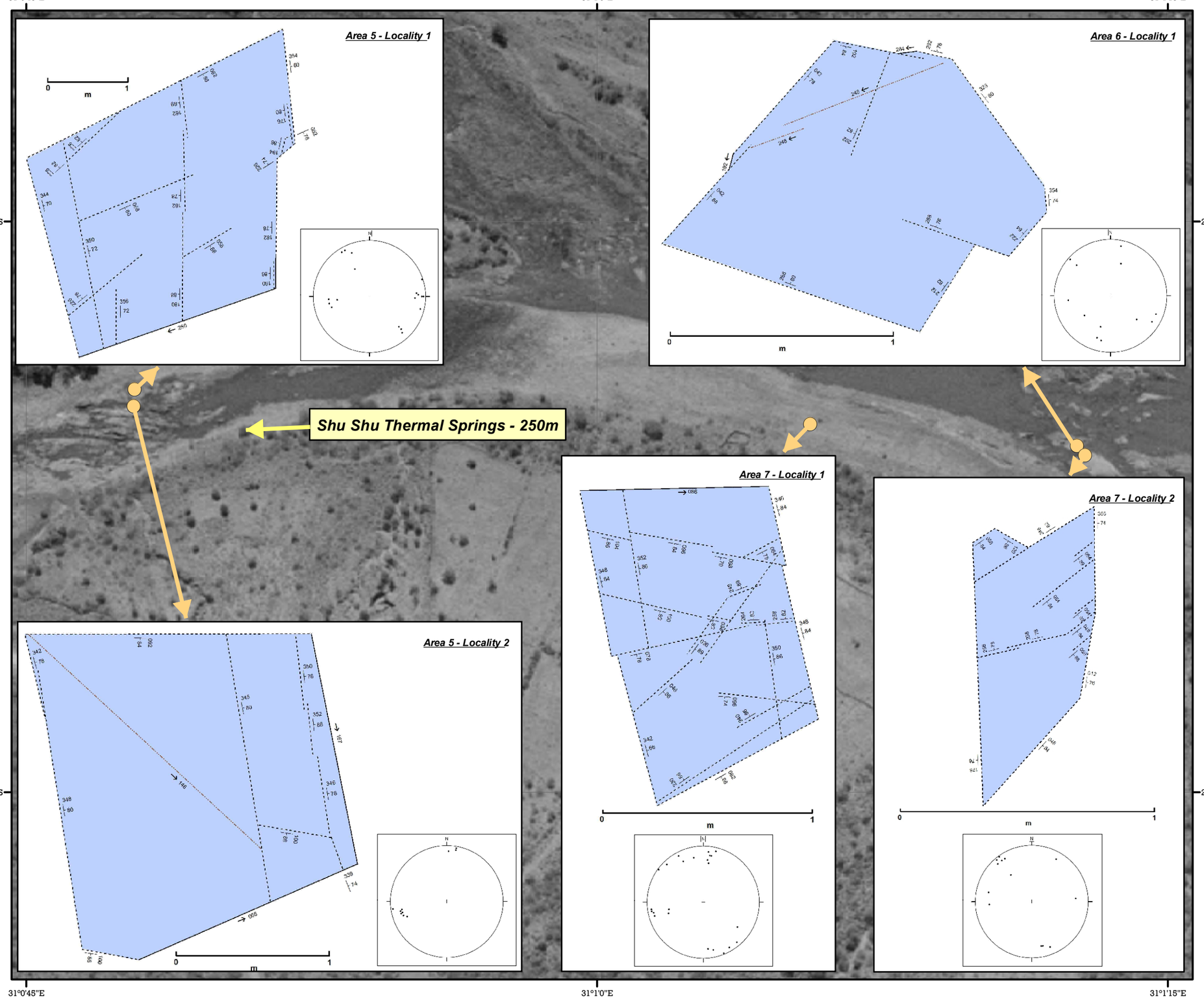

Legend:

Base Map

- Outcrop Localities
- Locality - Map Markers

Outcrop Locality Maps

- Gneiss
- Amphibolite
- Orientations
- Outcrop Boundaries
- Joints
- Veins
- 041/80 Dip/Strike - Joints & Veins

Title:
Appendix D3: Outcrop Locality Map - Eastern Area

Projection:
WGS 84

Scale:
0 0.1 0.2 0.4 0.6 0.8 Kilometres

Direction:
N W E S

Base Map Source:
Chief Director: Surveys & Mapping

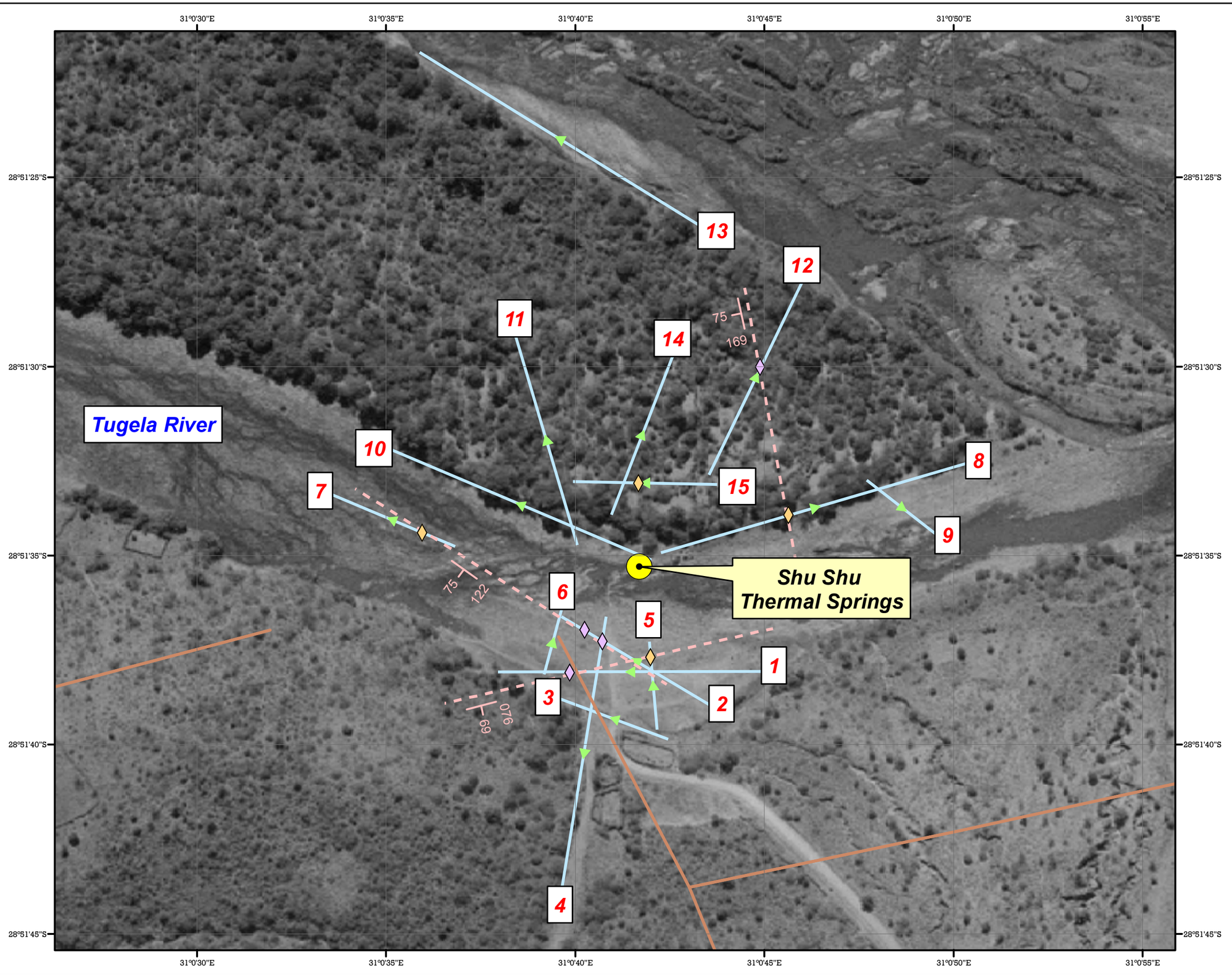

Legend:

Von Veh (1994) Structures

- Dolerite Dykes
- Lineaments
- Geological Faults

Identified Features

- Orientated Geophysical Traverses
- 5 — Geophysical Traverse Number
- Inferred Fracture Zone Anomalies
- Possible Fracture Zone Anomalies
- Probable Structures
- 75 / 169 — Dip/Strike - Structures

Title:

Appendix D4: Geophysical Investigation Map

Projection:

WGS 84

Scale:

0 0.1 0.2 0.4 0.6 0.8 Kilometres

Direction:

N W E S

Base Map Source:

Chief Director: Surveys & Mapping

30°58'30"E 30°59'15"E 31°0'0"E 31°0'45"E 31°1'30"E 31°2'15"E 31°3'0"E

28°49'30"S
28°50'15"S
28°51'0"S
28°51'45"S
28°52'30"S
28°53'15"S

Shu Shu Thermal Springs

Tugela River

Legend:

Von Veh (1994) Structures
- Dolerite Dykes
- Lineaments
- Geological Faults

Identified Features
- Inferred Lineaments
- Possible Lineaments
- Study Area

Title:

Appendix D5: Photogeological Lineament Analysis Map

Projection:

WGS 84

Scale:

0 0.5 1 2 3 4 5 6 7 8 9 Kilometres

Direction:

N W E S

Base Map Source:

Chief Director: Surveys & Mapping

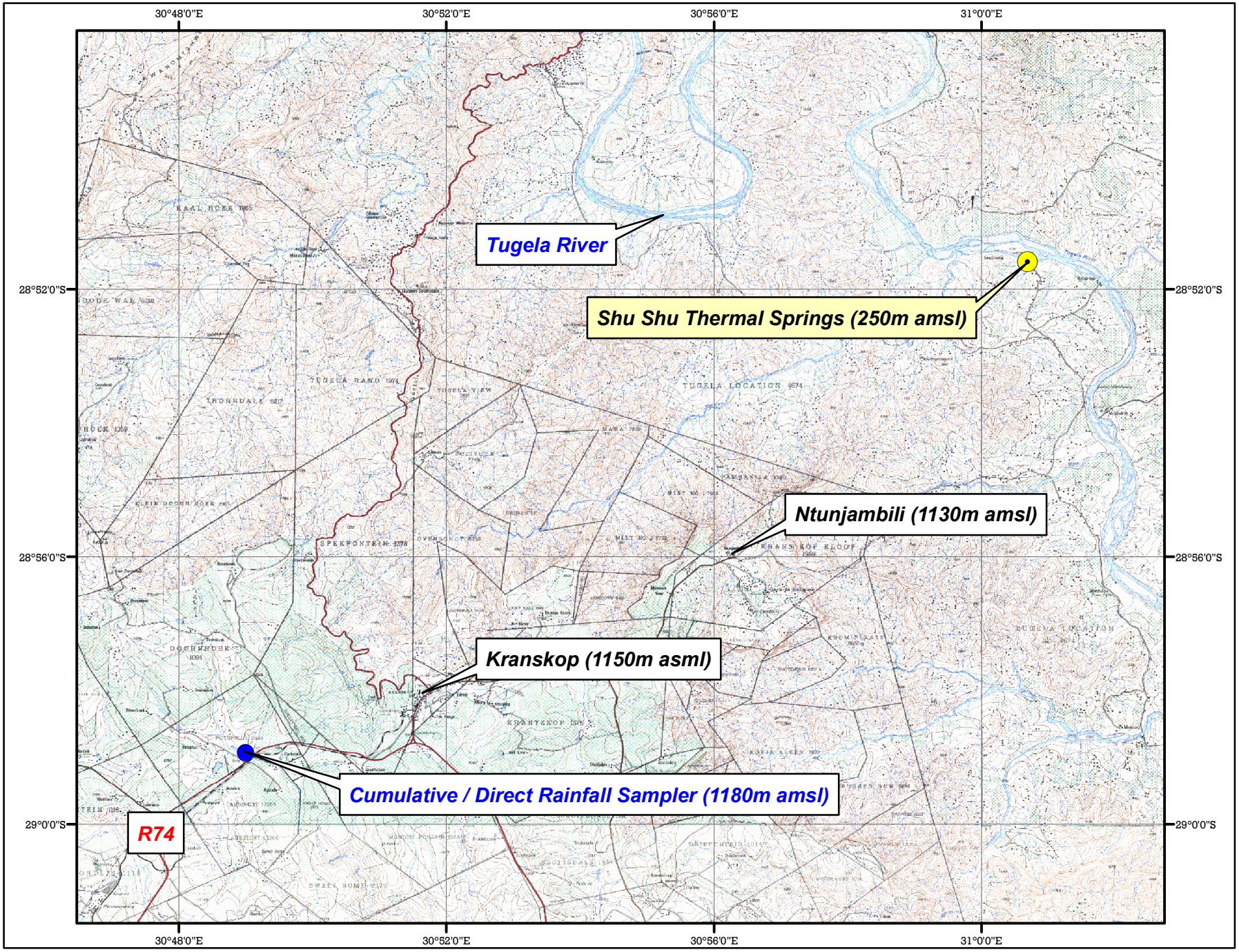

Legend:

- Rainfall Sampling Points

Title:

Appendix D6: Rainfall Sampler Locality

Projection:

WGS 84

Scale:

0 2.5 5 10 15 20 25 Kilometres

Direction:

N W E S

Base Map Source:

Chief Director: Surveys & Mapping

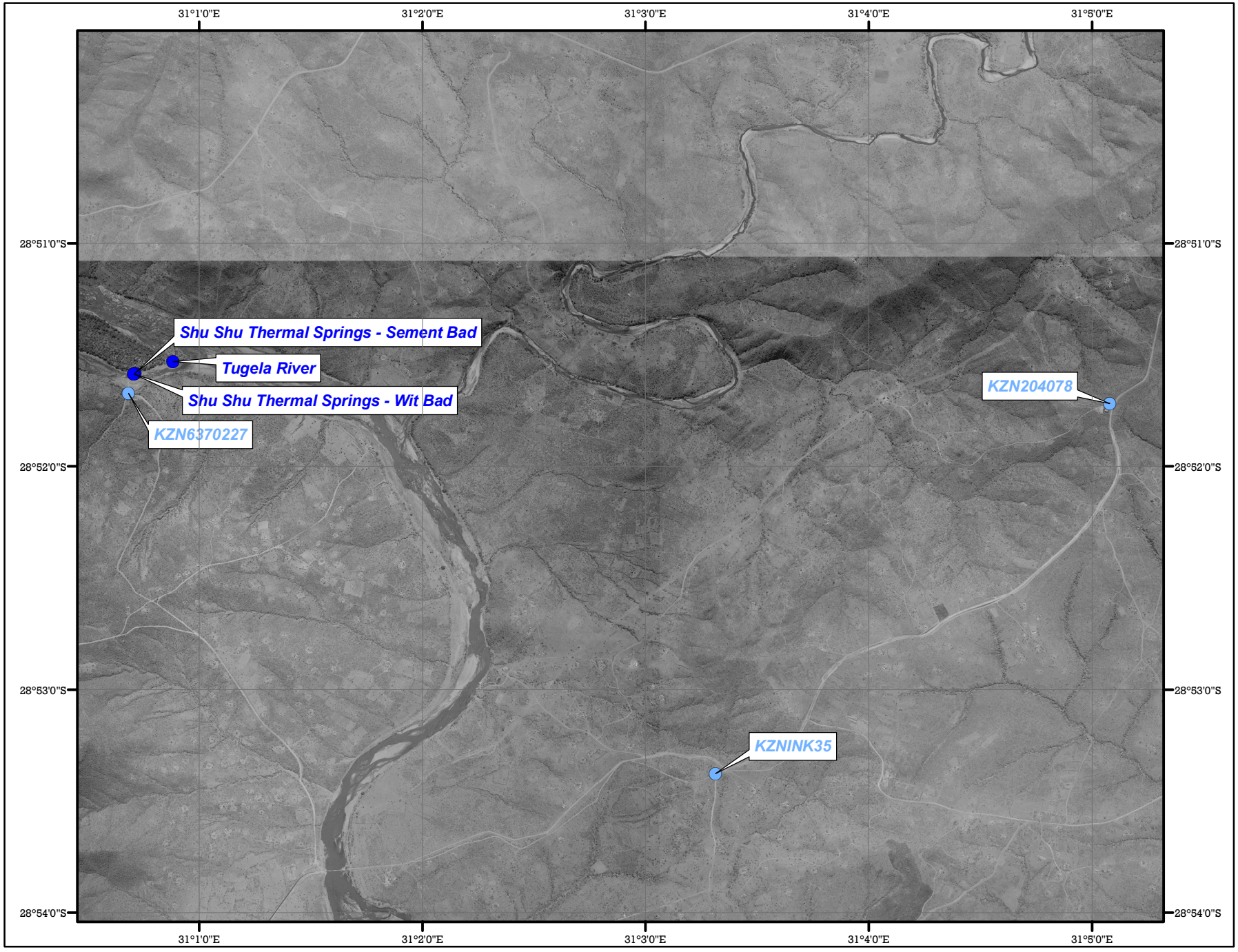

Legend:

- Surface Water Sampling Points
- Groundwater Sampling Points

Title:
Appendix D7: Water Sample Localities

Projection:
WGS 84

Scale:
0 0.5 1 2 3 4 5 6 7 8 Kilometres

Direction:
N W E S

Base Map Source:
Chief Director: Surveys & Mapping

Appendix E: Geophysical Data Graphs and Information

Appendix E1 – Geophysical Data Graphs

As per Appendix D4, the use of the ABEM WADI VLF device and the Proton Magnetometer allowed for the creation of a geophysical data graph per traverse undertaken. The fifteen geophysical graphs are included overleaf, and have been annotated as per their identified structure anomalies.

Appendix E2 – Geophysical Data Information

The details pertaining to the identified structure anomalies are included below in Table E2.1.

Table E2.1: Pertinent structure anomaly details.

Traverse Number	Structure Anomaly	Structure Type	Apparent Dip	True Dip	Approximate Dip Direction
T 1	Yes	Inferred Fracture Zone	71	70	East
T 2	Yes	Inferred Fracture Zone	76	75	North-West
T 3	No	-	-	-	-
T 4	Yes	Inferred Fracture Zone	83	82	South-Southwest
T 5	Yes	Possible Fracturing	69	69	South-Southeast
T 6	No	-	-	-	-
T 7	Yes	Possible Fracturing	76	75	West-Northwest
T 8	Yes	Possible Fracturing	77	76	West-Southwest
T 9	No	-	-	-	-
T 10	No	-	-	-	-
T 11	No	-	-	-	-
T 12	Yes	Inferred Fracture Zone	74	73	South-Southwest
T 13	No	-	-	-	-
T 14	No	-	-	-	-
T 15	Yes	Possible Fracturing	44	44	East

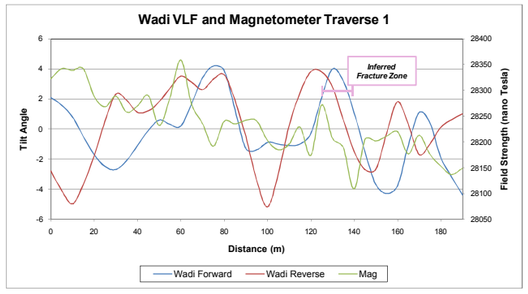
Wadi VLF and Magnetometer Traverse 1
Inferred Fracture Zone
Tilt Angle
Field Strength (nano Tesla)
Distance (m)
Wadi Forward
Wadi Reverse
Mag

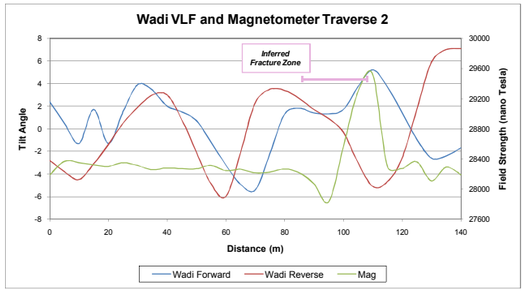
Wadi VLF and Magnetometer Traverse 2
Inferred Fracture Zone
Tilt Angle
Field Strength (nano Tesla)
Distance (m)
Wadi Forward
Wadi Reverse
Mag

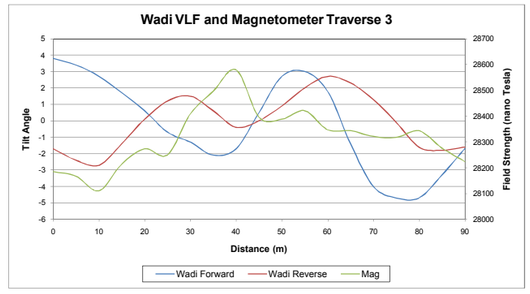
Wadi VLF and Magnetometer Traverse 3
Tilt Angle
Field Strength (nano Tesla)
Distance (m)
Wadi Forward
Wadi Reverse
Mag

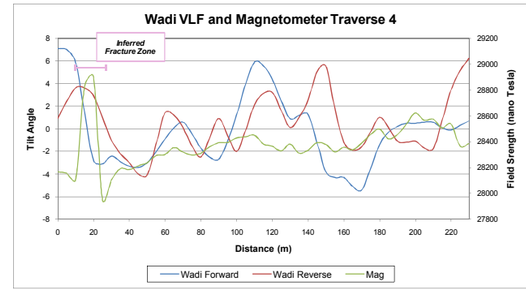
Wadi VLF and Magnetometer Traverse 4
Inferred Fracture Zone
Tilt Angle
Field Strength (nano Tesla)
Distance (m)
Wadi Forward
Wadi Reverse
Mag

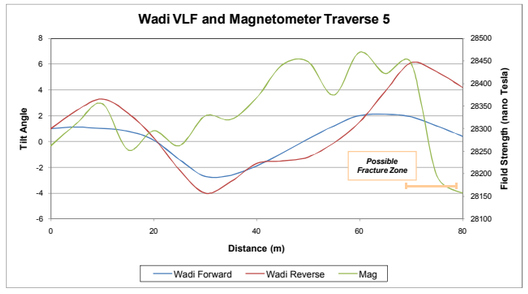
Wadi VLF and Magnetometer Traverse 5
Possible Fracture Zone
Tilt Angle
Field Strength (nano Tesla)
Distance (m)
Wadi Forward
Wadi Reverse
Mag

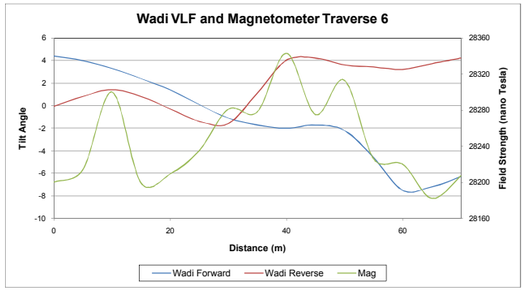
Wadi VLF and Magnetometer Traverse 6
Tilt Angle
Field Strength (nano Tesla)
Distance (m)
Wadi Forward
Wadi Reverse
Mag

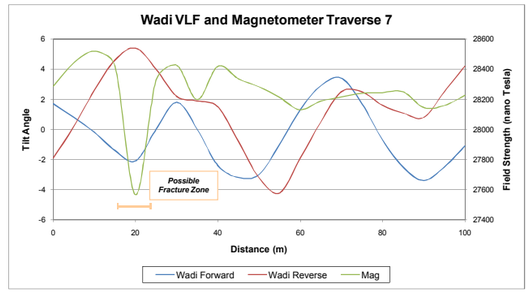
Wadi VLF and Magnetometer Traverse 7
Possible Fracture Zone
Tilt Angle
Field Strength (nano Tesla)
Distance (m)
Wadi Forward
Wadi Reverse
Mag

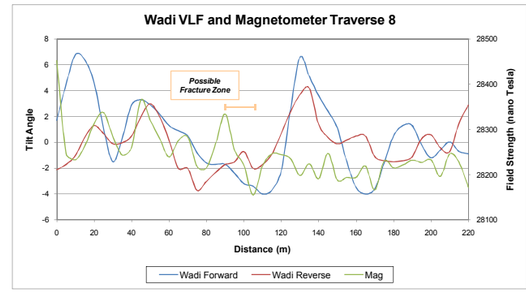
Wadi VLF and Magnetometer Traverse 8
Possible Fracture Zone
Tilt Angle
Field Strength (nano Tesla)
Distance (m)
Wadi Forward
Wadi Reverse
Mag

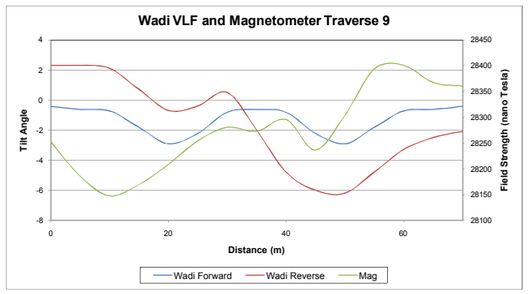
Wadi VLF and Magnetometer Traverse 9
Tilt Angle
Field Strength (nano Tesla)
Distance (m)
Wadi Forward
Wadi Reverse
Mag

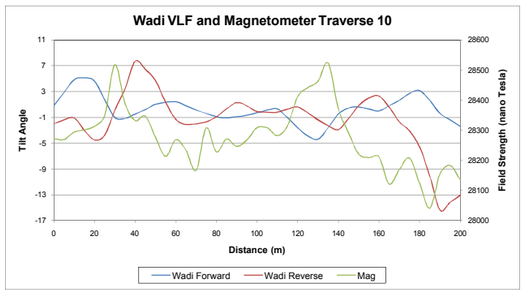
Wadi VLF and Magnetometer Traverse 10
Tilt Angle
Field Strength (nano Tesla)
Distance (m)
Wadi Forward
Wadi Reverse
Mag

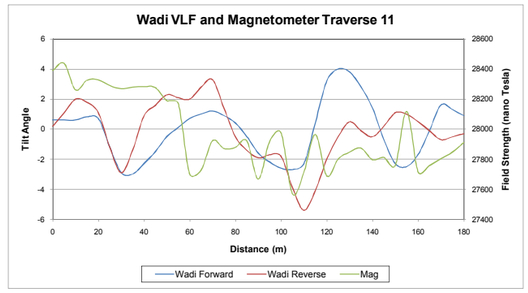
Wadi VLF and Magnetometer Traverse 11
Tilt Angle
Field Strength (nano Tesla)
Distance (m)
Wadi Forward
Wadi Reverse
Mag

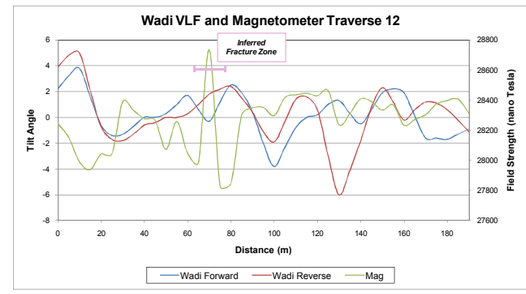
Wadi VLF and Magnetometer Traverse 12
Inferred Fracture Zone
Tilt Angle
Field Strength (nano Tesla)
Distance (m)
Wadi Forward
Wadi Reverse
Mag

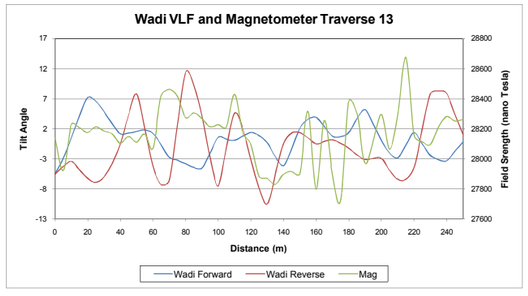
Wadi VLF and Magnetometer Traverse 13
Tilt Angle
Field Strength (nano Tesla)
Distance (m)
Wadi Forward
Wadi Reverse
Mag

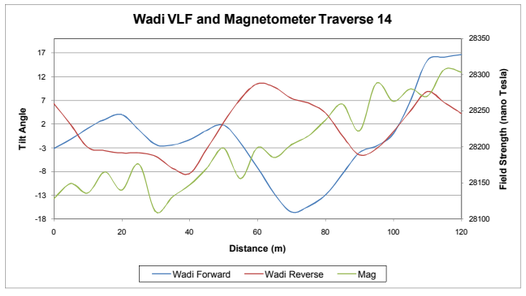
Wadi VLF and Magnetometer Traverse 14
Tilt Angle
Field Strength (nano Tesla)
Distance (m)
Wadi Forward
Wadi Reverse
Mag

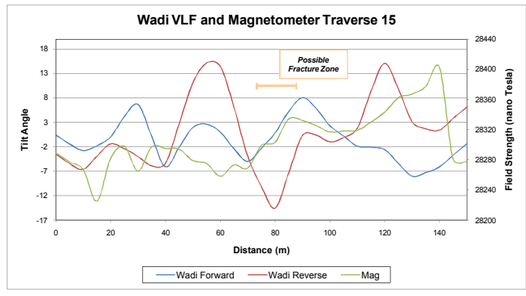
Wadi VLF and Magnetometer Traverse 15
Possible Fracture Zone
Tilt Angle
Field Strength (nano Tesla)
Distance (m)
Wadi Forward
Wadi Reverse
Mag

Appendix F: Additional Local Geology Information

Appendix F1: Theoretical (Norm-Determined) Mineral Assemblage

Table F1.1 and Table F1.2 below and overleaf highlight the proposed mineral assemblage of the collected rock samples according to the MesoNorm and CataNorm respectively, in accordance with the mesozone and catazone respectively. The EpiNorm, representing the epizone, was not used as such conditions are not considered representative of the temperature and pressure conditions that prevailed during the accretion and uplift tectonics which resulted in the formation of the Natal Mobile Province. The Norms are used only as an initial assessment, and it is acknowledged that these programs utilize only the bulk (geo-) chemical composition of the rock.

Table F1.1: MesoNorm-determined mineral composition of sampled rock types.

Rock Type	Sampling Date	Sample Code	Units	Quartz	Albite	Anorthite	Orthoclase	Hematite
Hornblende Gneiss	2010-07-04	KGB01	wt %	36.51	32.69	14.66	8.08	4.18
Biotite-Hornblende Gneiss	2010-07-04	KGB02	wt %	43.99	25.75	17.33	7.88	2.64
Amphibolite	2010-07-04	KGB03	wt %	9.36	34.81	20.05	9.75	11.25

Table F1.1 (Continued): MesoNorm-determined mineral composition of sampled rock types.

Rock Type	Sampling Date	Sample Code	Units	Biotite	Apatite	Ilmenite	Amphibole	Corundum
Hornblende Gneiss	2010-07-04	KGB01	wt %	2.45	0.33	0.37	0.00	0.73
Biotite-Hornblende Gneiss	2010-07-04	KGB02	wt %	1.99	0.19	0.22	0.00	0.08
Amphibolite	2010-07-04	KGB03	wt %	0.00	0.28	0.46	2.07	0.00

Table F1.2: CataNorm-determined mineral composition of sampled rock types.

Rock Type	Sampling Date	Sample Code	Units	Quartz	Albite	Anorthite	Orthoclase	Hematite	Hydrous Minerals
Hornblende Gneiss	2010-07-04	KGB01	wt %	33.63	35.34	14.96	9.94	2.97	1.72
Biotite-Hornblende Gneiss	2010-07-04	KGB02	wt %	41.07	27.97	17.77	9.44	1.89	1.36
Amphibolite	2010-07-04	KGB03	wt %	12.49	37.73	28.26	4.53	8.02	2.42

Table F1.2 (Continued): CataNorm-determined mineral composition of sampled rock types.

Rock Type	Sampling Date	Sample Code	Units	Apatite	Ilmenite	Diopside	Corundum	Titanite	Rutile
Hornblende Gneiss	2010-07-04	KGB01	wt %	0.30	0.06	0.00	0.84	0.00	0.25
Biotite-Hornblende Gneiss	2010-07-04	KGB02	wt %	0.17	0.12	0.00	0.11	0.00	0.11
Amphibolite	2010-07-04	KGB03	wt %	0.26	0.34	5.44	0.00	0.52	0.00

Due to the metamorphic grade implied by the gneiss and amphibolite samples collected in the vicinity of the Shu Shu thermal springs, it is inferred that the CataNorm-determined mineralogy possibly more accurately reflects the bulk mineral composition of the rock types. However, as the determined mineral composition of the samples is based solely on a quantitative assessment of the available geochemical data, a variation on that which is observed undoubtedly exists.

Appendix F2: Thin-Section Descriptions

The hornblende gneiss sample (KGB-01) is dominated by various feldspar minerals, to ~55% by modal abundance. Average crystal size is approximately 60µm – 100µm, whilst crystal boundaries are subhedral (see Figure F2.1 overleaf). An albite to anorthite solid solution series is observed, as is twinned microcline, with these minerals typically forming the 'groundmass' of the rock. Semi-isolated occurrences of quartz (~35%), which are 40µm – 50µm in size, display subhedral crystal boundaries, within the feldspar 'groundmass'. Subordinate amounts (~8%) of hornblende, whose crystals are approximately 50µm in diameter, are observed, with crystal boundary shapes typically subhedral to anhedral. The accessory minerals, which comprise just 2% of the rock, appear to be dominated by titanite in thin-section, and pyrite as the opaque portion, which was identified in hand specimen. The minerals display a weak to moderate alignment of minerals, and as well-developed banding is absent, a gneissic fabric appears to dominate. Furthermore, due to their size and shape, the feldspar minerals and quartz appear as subequant. Consequently, in accordance with principle mineral types, this metamorphic rock can best be labeled as a hornblende gneiss.

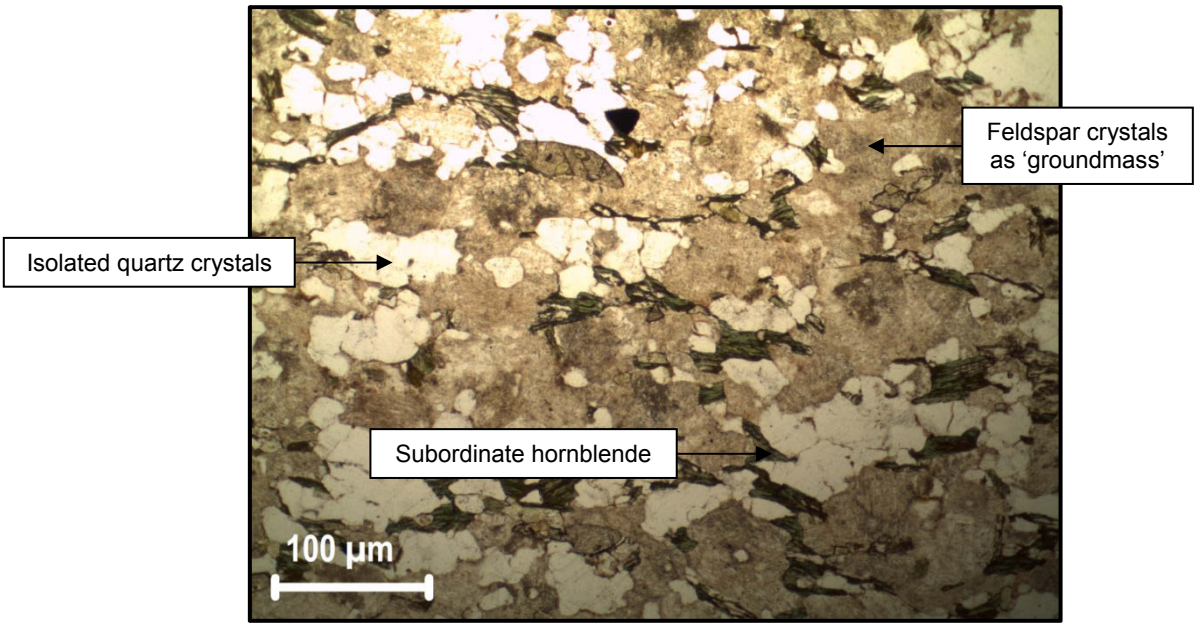

Figure F2.1: Sample KGB 01 photomicrograph – hornblende gneiss.

Sample KGB-02, identified in the field as a gneiss, contains elevated amounts of quartz (~55% modal composition), as is visible in thin section (see Figure F2.2 overleaf). Average crystal size is estimated at 50µm – 70µm, whilst crystal boundaries are subhedral to anhedral. Numerous feldspar minerals comprise a quarter of the rock, with subhedral to anhedral crystal boundaries common, whilst most crystals vary between 40µm – 60µm in size. Cross-hatched microcline is observed, as is untwined orthoclase, whilst a solid solution between albite and anorthite, comprising plagioclase, appears to be in existence. Biotite and hornblende are approximately subequal in their modal abundances, which is set at ~8%, with both displaying subhedral crystal boundaries. Hornblende crystals are typically only 20µm – 40µm in size at maximum, however they are interstitial and mainly surround quartz.

Furthermore, these crystals are needle-like in form, however they are subordinate. Biotite crystals, which likely originated due to the replacement of hornblende (Gevers, 1942), are typically larger, indeed varying from 80 µm – 100µm, although such a size range is due to their elongate yet parallel form. In close association with these two minerals occurs epidote and titanite, comprising approximately 4% of the rock by modal abundance. Opaques, which likely include pyrite as identified in hand specimen, appear spatially related to biotite and hornblende in this rock. A typical gneissose structure and associated layering is certainly evident, likely due to the moderately developed alignment of biotite, however in general it is not extremely well-developed. Compositional banding is apparent in thin section, and as such, and in accordance with principle mineral types, this metamorphic rock can best be termed as a biotite-hornblende gneiss.

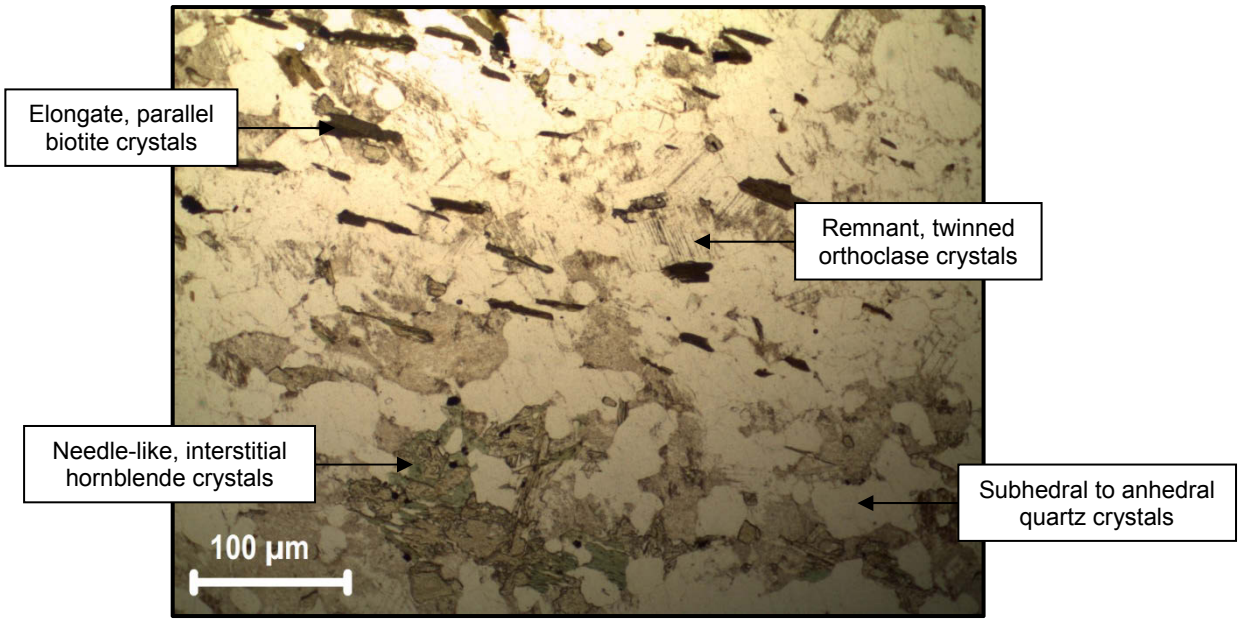

Figure F2.2: Sample KGB 02 photomicrograph – biotite-hornblende gneiss.

The amphibolite sample, which was labeled as sample KGB-03, is dominated by hornblende, indeed up to ~40% modal abundance, as is visible in thin section. Average crystal size is approximately at 80µm – 100µm, whilst crystal boundaries exhibit a subhedral shape (see Figure F2.3 overleaf). In accordance with the findings of Gevers (1942), crystals take on an elongate form hence their apparent increased size, whilst pronounced parallelism is observed. Hornblende appears to have been partly saussuritised, leading to the production of epidote-clinozoisite; this is noted as comprising approximately 40% of the rock. Crystal size appears much smaller, indeed only ~10µm at maximum, with crystal boundaries displaying a subhedral to euhedral shape. Limited amounts of remnant, twinned plagioclase feldspar are seen, as are occasional hornblende crystals within the epidote-clinozoisite bands, which take on the appearance of mineral aggregates. Subordinate amounts (~15%) of quartz, whose crystals vary between 30µm – 40µm in size, are observed, with crystal boundaries strictly subhedral. This mineral appears as lenses within the epidote-clinozoisite, whilst an apparent 'groundmass' aptly describes its form when surrounding hornblende. The accessory minerals, which comprise approximately 5%, appear to be dominated by titanite, as observed once again, and pyrite as part of the opaque portion, which was seen in hand specimen.

A very strong alignment of minerals is seen in thin section, particularly hornblende and epidote-clinozoisite. This leads to a classification of distinct planar anisotropy with respects to texture, whilst an amphibolites-grade facies is inferred from available pressure and temperature data (Bisnath *et al*., 2008). Consequently, in accordance with principle mineral

types, this metamorphic rock can best be described as an epidote-clinozoisite hornblende amphibolite.

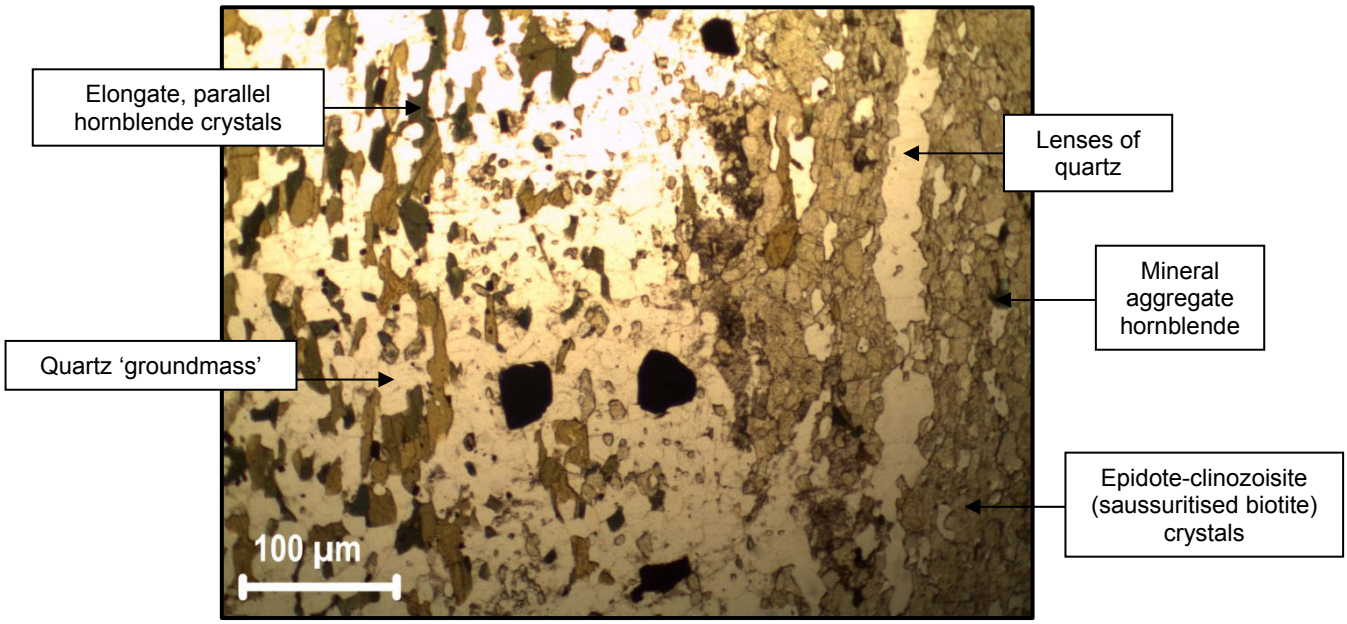

Figure F2.3: Sample KGB 03 photomicrograph – epidote-clinozoisite hornblende amphibolite.

Appendix G: Additional Tectonic Evolution Information

Appendix G1: Theories on the Formation of Joints

According to Van Der Pluijm and Marshak (2004), joints originate at mechanical defects in the rock; the most common of which are Griffith cracks. The types of joints which form are dependent upon the magnitude and orientation of the three principle orthogonal stress axes, σ_1 (maximum), σ_2 (intermediate) and σ_3 (minimum), in relation to σ_t, the tensile strength of the rock. A simple generalized single joint forms when $(\sigma_1 - \sigma_3) < 4\sigma_t$, such that it develops parallel to σ_1 and perpendicular to σ_3 (Pollard and Aydin, 1988) (see Figure G1.1 below). Under these circumstances, an extension joint will form with dilation along the joint, forcing the rough rock surfaces apart such that the joint may fill with a fluid, thereby producing a vein. If $(\sigma_1 - \sigma_3) > 4\sigma_t$, then a set of smooth-surfaced conjugate joints will form, whereby two joints of different orientations form simultaneously (Pollard and Aydin, 1988). In such an instance, the acute angle between the joints is bisected by the maximum principle stress axis; these joints form as shear joints (see Figure G1.1 below).

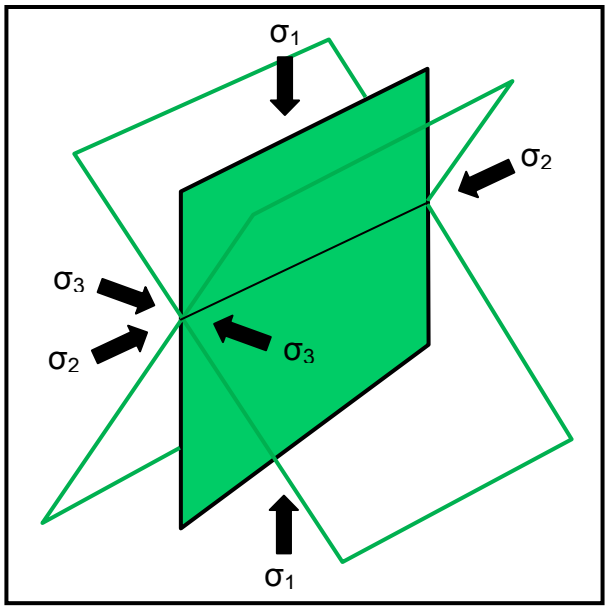

Figure G1.1: Formation of single extension joint (black) and conjugate shear joints (green). Note that the line of intersection of the conjugate joints is the orientation of σ_2.

Price (1966) states that after much field investigation, it has been established that systematic joints often exhibit well-defined relationships to brittle features (faults). Consequently, it can be said that when faulting is related to joint formation, regional joints will develop in the country rock as a result of the stress field that was responsible for the generation of the fault itself (Van Der Pluijm and Marshak, 2004). As faults are usually inclined to the remote σ_1 direction, Van Der Pluijm and Marshak (2004) state that the joints that form as a result of the stress field will not be parallel to the fault, however will attain a similar orientation, although

with varying dips. It can hence be inferred that joints, in similar orientations to those of the faults located in the region surrounding the Shu Shu thermal springs, will be in evidence.

Furthermore however, Price (1966) and Ramsay and Huber (1987) state that joints will form in country rock in response to tectonic forces which resulted in the ductile deformation (folding) of a region, should it have occurred. The 'axial cross' reference system is subsequently employed by Price (1966) and Ramsay and Huber (1987) to detail the various possible orientations of these fold-related joints. As can be seen in Figure G1.2 hereafter, this system delineates the three orthogonal directions as a, b and c, with the bedding at each locality typically defining the ab plane, the c-axis as normal and the b-axis as parallel to the fold axis (Ramsay and Huber, 1987). Ramsay and Huber (1987) state that while the a- and c-axes vary around the fold, the b-axis remains constant. Typically, there are four types of major joint sets that may develop as a result of folding, with two of these likely to be found on the limbs of the fold (Price, 1966).

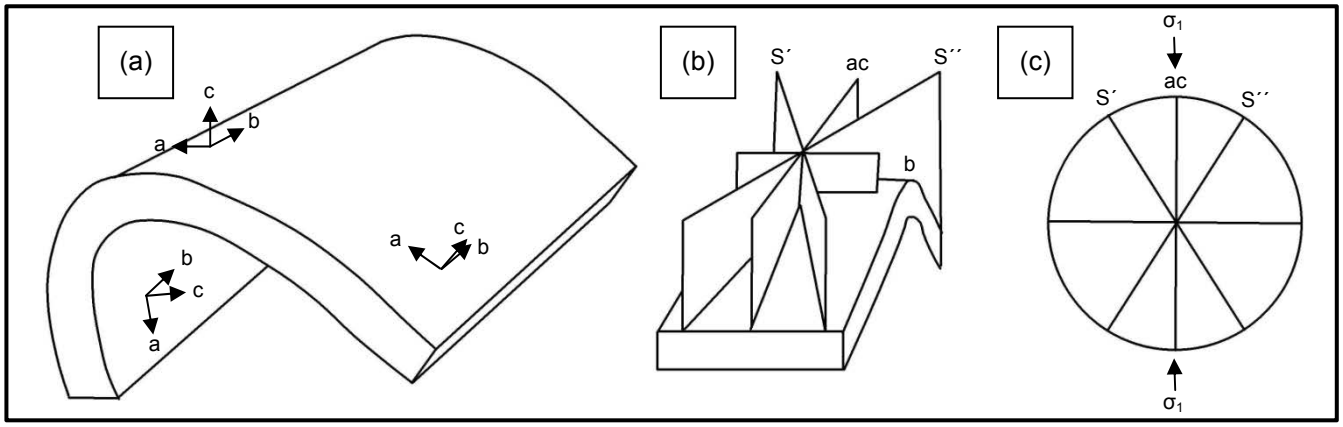

Figure G1.2: (a) Depiction of the 'axial cross' reference system employed for joints associated with a fold (redrawn after Ramsay and Huber, 1987) (b) Conjugate shear (S´, S´´) and extension ac joints in relation to a fold and (c) Stereographic illustration of these joints (both redrawn after Price, 1966).

Appendix G2: Tectonic Evolution of the Shu Shu Thermal Springs Region

The earliest known deformation events / structural controls on the formation of the various structures in the region surrounding the Shu Shu thermal springs have been partly detailed previously. Von Veh (1994), Sami *et al*. (2002) and Watkeys (2002) detail the effects of regional basement control across north-eastern southern Africa – the relationship thereof with the development of the Lebombo 'monocline' and the break-up of Gondwana is focused upon by the latter. Watkeys (2002) makes reference to an east-northeasterly orientated zone of weakness (Limpopo Mobile Belt) situated to the north of the Kaapvaal Craton; the orientation of which is consistent with the Murchison Lineament and the Barberton Hinge, the Tugela Fault and the Lilani-Matigulu Shear Zone. Watkeys (2002) states further that this

east-northeast alignment is consistent with a strong fabric which developed as an important fracture direction during the Proterozoic, as is evidenced by the east-northeasterly orientated fractures evident in the basement upon which the sediments of the Karoo Supergoup were deposited in this region. This control on the formation of structures in the region surrounding the Shu Shu thermal springs is significant mainly as it provided a zone of weakness that could be exploited through reactivation during tectonic processes operating during the Proterozoic and Phanerozoic.

McCourt *et al*. (2006), and to a lesser extent Cornell *et al*. (2006), recognized and defined the two principle post-accretionary deformation events to have affected the Tugela Terrane of the Natal Metamorphic Province as it was uplifted and emplaced onto the Kaapvaal Craton. As previously detailed, early-stage syn-emplacement deformation occurred as a result of northeast – southwest orientated convergence characterized in the Tugela Terrane by north-east verging, recumbent and assymetrical folds that are transposed along southerly (south-westerly) dipping, geometrically-related, thrust faults and ductile (sinistral transcurrent) shear zones (McCourt *et al*., 2006; Cornell *et al*., 2006). According to McCourt *et al*. (2006), subsequent, late-stage deformation was responsible for the formation of north to northwesterly verging overthrust folds and associated faults. As is detailed by Van Der Pluijm and Marshak (2004), such regional tectonics will give rise to shallow to moderately dipping contractional faults, with reverse movement, that may contain several ramps and flats, yet do not necessarily have uniform dips. Although the characteristics of fold-thrust belts are typically dependent upon the mechanical stratigraphy of the region, the resultant thrust traces tend to be roughly parallel whilst faults are typically orientated perpendicular to main thrust direction (Van Der Pluijm and Marshak, 2004).

Fold features infer that the region surrounding the Shu Shu thermal springs underwent oblate strain during the formation of the Tugela Terrane. This is evidenced by numerous competent veins which intruded the amphibolites (prior to deformation) in an orientation initially parallel to the Z-axis, such that during pure shear, both fold and boudin structures formed. Figure G2.1 (a) and (c), which follow overleaf, illustrate the structures and their orientations in relation to Figure G2.2 (b), the X-, Y- and Z-axes.

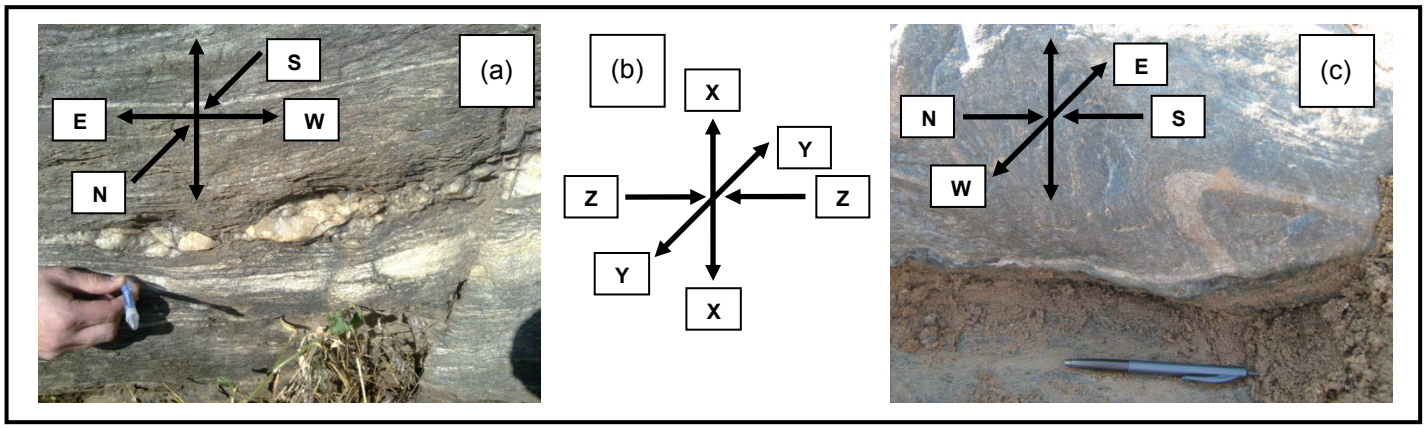

Figure G2.1: (a) East – west orientated vein boudinaging (b) Orientation of X-, Y- and Z-axes in relation to (c) North – south orientated D_3 S-fold parasitic fold. Pen for scale in (a) and (c) is pointing toward the north.

An apparent hiatus of ~ 800 Ma separates the Proterozoic and Phanerozoic deformation events which controlled the formation of the structures in the region surrounding the Shu Shu thermal springs. These Phanerozoic events are essentially confined to a southern African perspective of Gondwana break-up, and are best detailed in the context of Watkeys' (2002) 5-stage model. Stage 1, which occurred between 180 Ma – 175 Ma, incorporates the fracturing associated with the formation of the Karoo Igneous Province, whereby the earliest volcanics were erupted through the previously detailed west-southwest – east-northeast orientated zone of reactivation associated with strong basement control (Watkeys, 2002). According to Watkeys (2002), this event was followed by the intrusion of the Okavango and Olifants River dyke swarms which trend in a west-northwest – east-southeast and north-east – south-west orientation respectively. Although the former stretches from the Mwenezi Igneous Province across southern Zimbabwe, and the latter from northern end of the Lebombo 'monocline' (Watkeys, 2002), they are centered well north of the Shu Shu thermal springs.

Movement along the Agulhas-Falkland Fracture Zone, which likely resulted in the Lebombo undergoing east – west extension (Watkeys and Sokoutis, 1998), denotes the fourth structural event within Stage 1 to have possibly affected the region around the Shu Shu thermal springs. Continued extension associated with the normal faulting pattern observed in the region resulted in the intrusion of the north – south orientated Rooi Rand dyke swarm, only after which did the faulted monoclinal structure of the Lebombo become fully developed (Watkeys, 2002). However, this east – west extension also resulted in the formation of strike-slip faults, which are orientated east-northeast – west-southwest, as is detailed by Cox (1992). This orientation coincides with that observed in the basement, and as such, a degree of reactivation is likely.

Stage 2 of Watkeys' (2002) 5-stage model does not coincide with any further deformation events that may have resulted in the formation of structures in the region around the Shu Shu thermal springs, however Stage 3, which occurred between 155 Ma – 135 Ma, does. Watkeys (2002) states that dextral strike-slip movement along the Davie Fracture Zone split Gondwana in two plates, and it is thought that this may have reactivated the pre-existing west-southwest – east-northeast and north – south fractures – these would have been reactivated as normal faults (Von Veh, 1994). North – south orientated micro faults were observed to the south-west of the Shu Shu thermal springs, as is seen below in Figure G2.2, having formed in association with the Lebombo 'monocline', and then possibly having been reactivated during the early Cretaceous.

Figure G2.2: North – south orientated micro normal faults in amphibolite. Pen for scale is pointing toward the north.

Stage 4 of Watkeys' (2002) 5-stage model, which occurred between 135 Ma – 115 Ma, likely represents the most recent deformation event which may have resulted in structure formation in the region around the Shu Shu thermal springs. This stage was marked by the two principle trans-Gondwana fracture systems linking and thus enabling East- and West-Gondwana to drift apart, whilst the Falklands Plateau was extracted from the Natal Valley (Watkeys, 2002). This event lead to the formation of strike-slip coast-parallel faults, in a north-northeast – south-southwest orientation (Von Veh and Andersen, 1990), as well as normal faults orientated east-northeast – west-southwest. Reactivation of any existing fractures in these orientations may have occurred. Stage 5 was characterized by the strike-slip of the Falklands Plateau past the Agulhas Bank between 115 Ma – 90 Ma, however as Watkeys (2002) states, only evidence of minor faulting has been observed.

Appendix H: Hydrogeochemistry of the Shu Shu Thermal Springs and Surrounds

Appendix H1: Additional Water Quality Data

The cation-anion balances and the analytical errors / measurements of uncertainty pertaining to the analysed groundwater and surface water samples are included in Table H1.1 to Table H1.6. Note that the original water quality results are included in Table 3.7 to Table 3.10 on Page 36 to Page 39.

Table H1.1: Cation-anion balances – groundwater.

Sample Name	Sampling Date	Sample Code	Units	Cation-Anion Balance	
				Cation	Anion
Shu Shu Thermal Springs – Sement Bad	2010-07-05	SB / 2010	meq/l	14.60	14.00
Shu Shu Thermal Springs – Wit Bad	2010-07-05	WB / 2010	meq/l	12.51	13.88
BH KZN6370227	2010-07-05	BH 1 / 2010	meq/l	14.09	14.60
BH KZN204078	2011-04-28	BH 2 / Late Summer	meq/l	14.06	10.27
BH KZNINK35	2011-04-28	BH 3 / Late Summer	meq/l	30.68	21.66
Shu Shu Thermal Springs – Sement Bad	2011-06-13	SB / 2011	meq/l	15.46	23.90
Shu Shu Thermal Springs – Wit Bad	2011-06-13	WB / 2011	meq/l	14.83	8.37
BH KZN6370227	2011-06-13	BH 1 / 2011	meq/l	14.34	12.25
BH KZN204078	2011-08-25	BH 2 / Late Winter	meq/l	13.59	10.46
BH KZNINK35	2011-08-25	BH 3 / Late Winter	meq/l	29.10	21.87

Table H1.2: Cation-anion balances – surface water.

Sample Name	Sampling Date	Sample Code	Units	Cation-Anion Balance	
				Cation	Anion
Tugela River	2010-07-05	TR / 2010	meq/l	6.50	2.30
Tugela River	2011-06-13	TR / 2011	meq/l	2.57	2.01

Table H1.3: Major and minor determinant analytical errors / measurements of uncertainty – groundwater.

Sample Name	Sampling Date	Sample Code	Na^+		Ca^{2+}		K^+		Mg^{2+}		Si^{4+}	
			mg/l	%	mg/l	%	mg/l	%	mg/l	%	mg/l	%
Shu Shu Thermal Springs – Sement Bad	2010-07-05	SB / 2010	na		0.031	0.036	na		na		na	
Shu Shu Thermal Springs – Wit Bad	2010-07-05	WB / 2010	na		0.031	0.051	na		na		na	
BH KZN6370227	2010-07-05	BH 1 / 2010	na		0.031	0.044	na		na		na	
BH KZN204078	2011-04-28	BH 2 / Late Summer	10.071	8.027	0.033	0.053	0.388	2.497	0.738	1.193	3.696	32.731
BH KZNINK35	2011-04-28	BH 3 / Late Summer	5.282	2.262	0.033	0.023	2.635	9.988	12.615	8.109	0.035	0.299
Shu Shu Thermal Springs – Sement Bad	2011-06-13	SB / 2011	7.024	2.707	0.033	0.057	0.225	2.770	0.015	0.483	0.059	0.176
Shu Shu Thermal Springs – Wit Bad	2011-06-13	WB / 2011	6.331	2.457	0.033	0.054	0.054	0.666	0.028	0.792	0.875	2.585
BH KZN6370227	2011-06-13	BH 1 / 2011	2.962	1.318	0.033	0.057	0.054	0.687	0.035	0.211	1.006	5.559
BH KZN204078	2011-08-25	BH 2 / Late Winter	0.671	0.567	0.033	0.057	0.085	0.573	0.03	0.049	0.044	2.641
BH KZNINK35	2011-08-25	BH 3 / Late Winter	2.663	1.233	0.033	0.026	0.266	1.064	1.771	1.165	0.015	0.636

na – not available as it was not supplied by the laboratory, despite attempts to retrieve this data

Table H1.3 (continued): Major and minor determinant analytical errors / measurements of uncertainty – groundwater.

Sample Name	Sampling Date	Sample Code	HCO_3^-		SO_4^{2-}		Cl^-		F^-		NO_3^-	
			mg/l	%	mg/l	%	mg/l	%	mg/l	%	mg/l	%
Shu Shu Thermal Springs – Sement Bad	2010-07-05	SB / 2010	0.030	0.088	0.051	0.013	0.031	0.018	0.002	0.027	0.002	0.526
Shu Shu Thermal Springs – Wit Bad	2010-07-05	WB / 2010	0.030	0.075	0.051	0.013	0.031	0.019	0.002	0.028	0.002	0.588
BH KZN6370227	2010-07-05	BH 1 / 2010	0.030	0.049	0.051	0.013	0.031	0.018	0.002	0.032	0.002	0.556
BH KZN204078	2011-04-28	BH 2 / Late Summer	0.030	0.007	0.051	0.218	0.035	0.037	0.002	0.159	0.002	6.667
BH KZNINK35	2011-04-28	BH 3 / Late Summer	0.030	0.007	0.051	0.030	0.035	0.009	0.002	0.308	0.002	0.005
Shu Shu Thermal Springs – Sement Bad	2011-06-13	SB / 2011	0.030	0.068	na		na		na		na	
Shu Shu Thermal Springs – Wit Bad	2011-06-13	WB / 2011	0.030	0.082	na		na		na		na	
BH KZN6370227	2011-06-13	BH 1 / 2011	0.030	0.015	na		na		na		na	
BH KZN204078	2011-08-25	BH 2 / Late Winter	0.030	0.007	na		na		na		na	
BH KZNINK35	2011-08-25	BH 3 / Late Winter	0.030	0.007	a		a		a		na	

na – not available as it was not supplied by the laboratory, despite attempts to retrieve this data

Table H1.4: Trace element determinant analytical errors / measurements of uncertainty – groundwater.

Sample Name	Sampling Date	Sample Code	Sr		Fe		Li		Al		Ba	
			µg/l	%	µg/l	%	µg/l	%	µg/l	%	µg/l	%
Shu Shu Thermal Springs – Sement Bad	2010-07-05	SB / 2010	na		na		na		na		na	
Shu Shu Thermal Springs – Wit Bad	2010-07-05	WB / 2010	na		na		na		na		na	
BH KZN6370227	2010-07-05	BH 1 / 2010	na		na		na		na		na	
BH KZN204078	2011-04-28	BH 2 / Late Summer	19	2.762	212	2.524	0	0.000	1	33.333	4	2.260
BH KZNINK35	2011-04-28	BH 3 / Late Summer	53	0.457	58	11.395	1	6.667	1	16.667	1	1.351
Shu Shu Thermal Springs – Sement Bad	2011-06-13	SB / 2011	45	1.186	4	1.379	1	0.725	1	3.571	0.059	0.176
Shu Shu Thermal Springs – Wit Bad	2011-06-13	WB / 2011	54	1.448	4	1.176	2	1.471	1	2.083	0.875	2.585
BH KZN6370227	2011-06-13	BH 1 / 2011	34	1.169	11	0.308	2	2.410	1	3.571	1.006	5.559
BH KZN204078	2011-08-25	BH 2 / Late Winter	7	0.936	4	0.667	0	0.000	2	25.000	2	1.130
BH KZNINK35	2011-08-25	BH 3 / Late Winter	118	0.923	6	1.091	0	0.000	1	11.111	0	0.000

na – not available as it was not supplied by the laboratory, despite attempts to retrieve this data

Table H1.4 (continued): Trace element analytical errors / measurements of uncertainty – groundwater.

Sample Name	Sampling Date	Sample Code	Cs		Mn		Zn		Se	
			µg/l	%	µg/l	%	µg/l	%	µg/l	%
Shu Shu Thermal Springs – Sement Bad	2010-07-05	SB / 2010	na		na		na		na	
Shu Shu Thermal Springs – Wit Bad	2010-07-05	WB / 2010	na		na		na		na	
BH KZN6370227	2010-07-05	BH 1 / 2010	na		na		na		na	
BH KZN204078	2011-04-28	BH 2 / Late Summer	0	0.000	0	0.000	20	0.325	0	0.000
BH KZNINK35	2011-04-28	BH 3 / Late Summer	0	0.000	1	3.448	134	4.509	1	9.091
Shu Shu Thermal Springs – Sement Bad	2011-06-13	SB / 2011	0	0.000	0	0.000	0	0.000	0	0.000
Shu Shu Thermal Springs – Wit Bad	2011-06-13	WB / 2011	0	0.000	0	0.000	0	0.000	1	20.000
BH KZN6370227	2011-06-13	BH 1 / 2011	0	0.000	1	1.220	5	0.816	1	33.333
BH KZN204078	2011-08-25	BH 2 / Late Winter	0	0.000	1	0.588	1	0.588	0	0.000
BH KZNINK35	2011-08-25	BH 3 / Late Winter	0	0.000	0	0.000	0	0.000	1	8.333

na – not available as it was not supplied by the laboratory, despite attempts to retrieve this data

Table H1.4 (continued): Trace element analytical errors / measurements of uncertainty – groundwater.

Sample Name	Sampling Date	Sample Code	Cr		Ni		Cu		Mo		As	
			µg/l	%	µg/l	%	µg/l	%	µg/l	%	µg/l	%
Shu Shu Thermal Springs – Sement Bad	2010-07-05	SB / 2010	na		na		na		na		na	
Shu Shu Thermal Springs – Wit Bad	2010-07-05	WB / 2010	na		na		na		na		na	
BH KZN6370227	2010-07-05	BH 1 / 2010	na		na		na		na		na	
BH KZN204078	2011-04-28	BH 2 / Late Summer	1	5.882	1	5.263	0	0.000	0	0.000	0	0.000
BH KZNINK35	2011-04-28	BH 3 / Late Summer	1	3.846	0	0.000	0	0.000	0	0.000	0	0.000
Shu Shu Thermal Springs – Sement Bad	2011-06-13	SB / 2011	0	0.000	0	0.000	0	0.000	0	0.000	0	0.000
Shu Shu Thermal Springs – Wit Bad	2011-06-13	WB / 2011	0	0.000	0	0.000	0	0.000	0	0.000	0	0.000
BH KZN6370227	2011-06-13	BH 1 / 2011	0	0.000	0	0.000	0	0.000	0	0.000	0	0.000
BH KZN204078	2011-08-25	BH 2 / Late Winter	1	5.263	0	0.000	0	0.000	0	0.000	0	0.000
BH KZNINK35	2011-08-25	BH 3 / Late Winter	1	4.167	0	0.000	0	0.000	0	0.000	0	0.000

na – not available as it was not supplied by the laboratory, despite attempts to retrieve this data

Table H1.4 (continued): Trace element analytical errors / measurements of uncertainty – groundwater.

Sample Name	Sampling Date	Sample Code	Hg		Ag		Cd		Co		Pb	
			µg/l	%	µg/l	%	µg/l	%	µg/l	%	µg/l	%
Shu Shu Thermal Springs – Sement Bad	2010-07-05	SB / 2010	na		na		na		na		na	
Shu Shu Thermal Springs – Wit Bad	2010-07-05	WB / 2010	na		na		na		na		na	
BH KZN6370227	2010-07-05	BH 1 / 2010	na		na		na		na		na	
BH KZN204078	2011-04-28	BH 2 / Late Summer	0	0.000	0	0.000	0	0.000	0	0.000	0	0.000
BH KZNINK35	2011-04-28	BH 3 / Late Summer	0	0.000	0	0.000	0	0.000	0	0.000	0	0.000
Shu Shu Thermal Springs – Sement Bad	2011-06-13	SB / 2011	0	0.000	0	0.000	0	0.000	0	0.000	0	0.000
Shu Shu Thermal Springs – Wit Bad	2011-06-13	WB / 2011	0	0.000	0	0.000	0	0.000	0	0.000	0	0.000
BH KZN6370227	2011-06-13	BH 1 / 2011	0	0.000	0	0.000	0	0.000	0	0.000	0	0.000
BH KZN204078	2011-08-25	BH 2 / Late Winter	0	0.000	0	0.000	0	0.000	0	0.000	0	0.000
BH KZNINK35	2011-08-25	BH 3 / Late Winter	0	0.000	0	0.000	0	0.000	0	0.000	0	0.000

na – not available as it was not supplied by the laboratory, despite attempts to retrieve this data

Table H1.5: Major and minor determinant analytical errors / measurements of uncertainty – surface water.

Sample Name	Sampling Date	Sample Code	Na^+		Ca^{2+}		K^+		Mg^{2+}		Si^{4+}	
			mg/l	%	mg/l	%	mg/l	%	mg/l	%	mg/l	%
Tugela River	2010-07-05	TR / 2010	na		0.031	0.182	na		na		na	
Tugela River	2011-06-13	TR / 2011	0.394	2.050	0.033	0.220	0.016	0.938	0.138	1.299	0.775	10.580

na – not available as it was not supplied by the laboratory, despite attempts to retrieve this data

Table H1.5 (continued): Major and minor determinant analytical errors / measurements of uncertainty – surface water.

Sample Name	Sampling Date	Sample Code	HCO_3^-		SO_4^{2-}		Cl^-		F^-		NO_3^-	
			mg/l	%	mg/l	%	mg/l	%	mg/l	%	mg/l	%
Tugela River	2010-07-05	TR / 2010	0.031	0.031	0.051	0.364	0.031	0.258	0.002	0.909	0.002	0.513
Tugela River	2011-06-13	TR / 2011	0.033	0.035	na		na		na		na	

na – not available as it was not supplied by the laboratory, despite attempts to retrieve this data

Table H1.6: Trace element determinant analytical errors / measurements of uncertainty – surface water.

Sample Name	Sampling Date	Sample Code	Sr		Fe		Li		Al		Ba	
			µg/l	%	µg/l	%	µg/l	%	µg/l	%	µg/l	%
Tugela River	2010-07-05	TR / 2010	na		na		na		na		na	
Tugela River	2011-06-13	TR / 2011	2	1.538	10	3.268	0	0.000	24	4.263	1	1.087

na – not available as it was not supplied by the laboratory, despite attempts to retrieve this data

Table H1.6 (continued): Trace element analytical errors / measurements of uncertainty – surface water.

Sample Name	Sampling Date	Sample Code	Cs		Mn		Zn		Se	
			µg/l	%	µg/l	%	µg/l	%	µg/l	%
Tugela River	2010-07-05	TR / 2010	na		na		na		na	
Tugela River	2011-06-13	TR / 2011	0	0.000	0	0.000	0	0.000	1	100.000

na – not available as it was not supplied by the laboratory, despite attempts to retrieve this data

Table H1.6 (continued): Trace element analytical errors / measurements of uncertainty – surface water.

Sample Name	Sampling Date	Sample Code	Cr		Ni		Cu		Mo		As	
			µg/l	%	µg/l	%	µg/l	%	µg/l	%	µg/l	%
Tugela River	2010-07-05	TR / 2010	na		na		na		na		na	
Tugela River	2011-06-13	TR / 2011	0	0.000	0	0.000	0	0.000	0	0.000	0	0.000

na – not available as it was not supplied by the laboratory, despite attempts to retrieve this data

Table H1.6 (continued): Trace element analytical errors / measurements of uncertainty – groundwater.

Sample Name	Sampling Date	Sample Code	Hg		Ag		Cd		Co		Pb	
			µg/l	%	µg/l	%	µg/l	%	µg/l	%	µg/l	%
Tugela River	2010-07-05	TR / 2010	na		na		na		na		na	
Tugela River	2011-06-13	TR / 2011	0	0.000	0	0.000	0	0.000	0	0.000	0	0.000

na – not available as it was not supplied by the laboratory, despite attempts to retrieve this data

Appendix H2: Shu Shu Thermal Springs Hydrochemistry

Gevers (1942) and Kent (1949) directly attribute the hydrochemistry of thermal spring waters to the geological units in which the groundwater circulates, before it surfaces. This is in accordance with Freeze and Cherry (1979), who state that once water comes into contact with a mineral, dissolution will commence and indeed continue until equilibrium conditions are attained, or until the mineral is totally dissolved. However, the solubility of a particular mineral is affected by such attributes as temperature, pressure and pH, all of which are highly variable in thermal spring waters. An assessment of the major and minor oxide and trace element analysis results of the rock samples collected as part of this study support this notion. Dissolution of particularly plagioclase, hornblende and (saussuritised) biotite, through amphibolite and gneiss leaching, accounts for the majority of the dissolved constituents found in the thermal spring samples. Na-plagioclase, in the form of albite, which has been identified in thin section analysis, is proposed as the principle source of Na, as it is particularly susceptible to dissolution in near-neutral waters (Huang and Kiang, 1972).

Huang and Kiang (1972) state that the dissolution of Ca-plagioclase occurs more readily under acidic conditions, and as thermal groundwaters in these units are typically basic, this accounts for the comparatively reduced amounts of Ca measured in the thermal spring samples. Furthermore, this variation in the concentrations of Na and Ca (approximately three to four times) may also be attributable to the removal of Ca from groundwater through adsorption and / or cation exchange on to the surface of clay minerals (Chae *et al*., 2006). Si and Al too likely owe their origin chiefly to plagioclase dissolution, with the former having a greater dissolvability irrespective of which end-member the plagioclase is aligned with (Huang and Kiang, 1972). Murakami *et al*. (2003) infer biotite as a principle source of K, however as biotite likely originated through the replacement of hornblende (Gevers, 1942), it remains a certainty that leaching of the latter mineral, where still present, accounts for a proportion of the dissolved solid content in the Shu Shu thermal spring waters. Finally, in accordance with Gevers (1942), Cl concentrations are attributable to salt carried inland from the sea and precipitated by rain, with many meteoric-origin thermal springs known to contain NaCl. However, it is possible that the dissolution of either hornblende, or of secondary alteration minerals along fractures in the rock, may too partly account for the measured Cl levels.

The noticeably elevated concentrations of certain determinants are of particular interest in thermal spring waters. SO_4 concentrations in the Shu Shu thermal spring waters, which are the highest amongst the various cations and anions analysed for, likely cannot be attributed

to the dissolution of plagioclase, hornblende or biotite, but rather their origin can be sought from pyrite, which is prevalent in the amphibolites and gneisses in the region. Gevers (1942) states that dissemination of pyrite, under reducing conditions, results in the formation of H_2S (and likely some SO_4), however this is oxidized at shallow depths, which ultimately allows for the elevated concentrations of SO_4 in the Shu Shu thermal waters.

Kent (1949) states that F is a common constituent in South African thermal spring waters, however the concentrations thereof typically vary considerably. Owing to its presence at increased concentrations in numerous boreholes across South Africa, Kent (1949) states that F cannot be assumed to indicate water of juvenile origin. It is however, proposed that the levels of F measured in this study are attributable to the dissolution of biotite, with Chae *et al*. (2006) recording highly elevated concentrations of F from the leaching of basement rocks. Concentrations are time-dependent however, as F saturation typically varies as a function of Ca accumulation attained through the dissolution of Ca-plagioclase, which was observed in thin-section (Chae *et al*., 2006). Elevated Sr levels, at concentrations exceeding 3.00 mg/l, were expected in the Shu Shu thermal spring waters, given the concentration of this element in the rock samples and its known, inherent solubility. Bau *et al*. (2004) suggest the dissolution of plagioclase as the likely principle source of Sr, although the Sr isotope ratio may vary considerably depending upon the presence of specific accessory minerals.

The relatively elevated concentrations of some metals are possibly unexpected, given the alkalinity of the water sources. However, the water surfacing in the thermal springs is acidic at depth (as detailed), and hence this accounts for the dissolution and mobilisation of such metals. Concentrations have remained elevated, as the increase in pH occurs at shallow depths, where pressures are insufficient to rapidly result in precipitation out of the water.

Appendix H3: Shallow Groundwater Hydrochemistry

The hydrochemical signature of the water intercepted by shallow boreholes is also typically due to dissolution of various minerals along the flow-path of the circulating groundwater. Such an origin accounts for the dissolved constituents present in the groundwater sampled from the shallow boreholes in the region surrounding the Shu Shu thermal springs. Kent (1949) states that a close compositional relationship typically exists between thermal spring waters and groundwaters sampled from boreholes located in the same geological formation, with any variation on the part of the former attributed to different lithologies at depth from whence the thermal waters are sourced. Rather however, it is suggested that the observed variations can be attributed to a variation in pressure and temperature along the flow-path of

the thermal waters, with such attributes already detailed as having an effect on the dissolvability and mobility of numerous elements. Furthermore, it is believed that as the samples of the shallow, cold groundwater were collected through anthropogenic means, namely from frequently used, drilled boreholes, this may account for a degree of variation across the late summer and late winter results. Indeed it is likely that the highly elevated NO_3 levels measured at BH 3 in late summer are attributable to anthropogenic surface water contamination of the groundwater, whilst the difference in Mg and Zn concentrations are thought to have arisen as a result of the poor state of the steel casing and Mono-T handpumps through which the sampled water passed.

The similarity observed between the isotopic signature, physical water parameters and hydrochemical signature of the Shu Shu thermal springs samples, and those samples collected from BH 1, clearly confirms a common origin. Invariably then, the hydrogeological processes that account for the thermal springs water quality, through the dissolution and leaching of prevalent minerals, too account for the dissolved constituent concentrations measured in the groundwater sampled from BH 1. However a lower T.D.S. value, obtained through an apparent dilution of certain anion levels, and a temperature typically half that of the thermal springs, defines the existence of an applicable hydrogeological process. Indeed the variations observed, particularly in the levels of Si, Cl, SO_4 and F in the Shu Shu thermal springs samples, are likely attributable to the same process, namely the intermixing of deep, thermal groundwater with shallow, cold groundwater. The possibility of intermixing, through the addition of cold groundwater to thermal waters, will act to alter the prevailing temperature and pressure conditions, and consequently saturation states, and through the addition of water displaying a variable hydrochemical signature, likely accounts for the non-uniform thermal spring water quality that would otherwise be expected in a hydrogeological system of this type.

Appendix H4: Geothermal Indicator Elements

An assessment of trace element concentrations, when incorporated into comparative ratios, allows for a further evaluation of the geothermal system. Such ratios are included in Table H4.1, where it can be seen that the thermal waters sampled from the Sement Bad represent a slightly more dominant geothermal component, however variations are in evidence when Sr, Mg and Al concentrations are incorporated into ratios.

Table H4.1: Groundwater trace element concentration ratios.

Sample Name	Sampling Date	Sample Code	Li:Na	Na:K	Li:Mg	Cs:Na	Sr:Mg	Al:Na
Shu Shu Thermal Springs – Sement Bad	2010-07-05	SB / 2010	0.000613	30.548564	0.045066	0.000081	1.108553	0.000157
Shu Shu Thermal Springs – Wit Bad	2010-07-05	WB / 2010	0.000611	30.438700	0.044681	0.000078	1.101773	0.000218
BH KZN6370227	2010-07-05	BH 1 / 2010	0.000580	29.108639	0.017917	0.000018	0.458611	0.000346
BH KZN204078	2011-04-28	BH 2 / Late Summer	0.000072	8.074003	0.000145	0.000000	0.011122	0.000008
BH KZNINK35	2011-04-28	BH 3 / Late Summer	0.000064	8.851024	0.000096	0.000000	0.074573	0.000026
Shu Shu Thermal Springs – Sement Bad	2011-06-13	SB / 2011	0.000532	31.997534	0.039093	0.000066	1.056091	0.000570
Shu Shu Thermal Springs – Wit Bad	2011-06-13	WB / 2011	0.000528	31.731527	0.043730	0.000066	1.219614	0.000186
BH KZN6370227	2011-06-13	BH 1 / 2011	0.000369	28.587786	0.005000	0.000089	0.175241	0.000125
BH KZN204078	2011-08-25	BH 2 / Late Winter	0.000085	7.966330	0.000163	0.000017	0.012202	0.000068
BH KZNINK35	2011-08-25	BH 3 / Late Winter	0.000074	8.632947	0.000105	0.000009	0.084119	0.000042